Post-tensioned Horizontal Connections Typically Used For Precast Concrete Load-bearing Shear Wall Panels

by

Robin L. Hutchinson

A Thesis

Presented to the University of Manitoba

in Partial Fulfillment of the

Requirements for the Degree of

Master of Science in Civil Engineering

Winnipeg, Manitoba

January, 1990

ISBN 0-315-63348-4

POST-TENSIONED HORIZONTAL CONNECTIONS TYPICALLY USED FOR PRECAST CONCRETE LOAD-BEARING SHEAR WALL PANELS

BY

ROBIN L. HUTCHINSON

A thesis submitted to the Faculty of Graduate Studies of the University of Manitoba in partial fulfillment of the requirements of the degree of

MASTER OF SCIENCE

I hereby declare that I am the sole author of this thesis.

I authorize the University of Manitoba to lend and/or reproduce this thesis, in whole or in part, by photocopying or by other means at the request of other institutions or individuals for the purpose of scholarly research.

Robin L. Hutchinson

The University of Manitoba requires that all persons using or photocopying this thesis give their signatures, their addresses, and the date of use.

ABSTRACT

Precast load-bearing shear wall panels are used extensively for high-rise construction because of the ease and speed of assembly, and the high quality of the precast panels. The connections between panels are extremely important since they affect both the speed of erection and the overall integrity of the structure. This thesis presents the results of a research program conducted to investigate the behavior and capacity of post-tensioned horizontal connections for precast load-bearing shear wall panels subjected to static shear loading.

Nine prototype specimens with three different connection configurations were tested. The first two configurations modelled the connections of the interior shear walls which support the hollow-core floor slab. Post-tensioning was included in the second connection configuration and not in the first. The third configuration consisted of post-tensioned connections without hollow-core slab. Two different levels of load normal to the connection were used to determine the effects of dead load.

Failure was characterized mainly by slip along the connection and top panel interface surfaces. At high levels of normal load and shear load, cracking occured in the hollow-core floor slab.

A comparison of the behavior and capacity of the different connection configurations indicated that an increase in load normal to the connection increases the shear capacity. The effect of post-tensioning is to increase the load normal to the connection. For connections supporting hollow-core slab at high levels of normal load and shear load, the maximum shear capacity of the connection may be

controlled by the shear capacity of the hollow-core slab.

The shear capacity of connections supporting hollow-core slab continued to decrease with the propogation of cracks in the hollow-core. The ultimate limit state is represented by complete cracking of the hollow-core.

Rational mathematical models were developed to predict the shear capacity of the connections at the maximum and ultimate limit states. These models were found to be in good agreement with the experimental results.

ACKNOWLEDGEMENTS

This study was carried out under the direct supervision of Dr. S.H. Rizkalla, Department of Civil Engineering, University of Manitoba. The author wishes to express her sincere gratitude to Dr. Rizkalla for his valuable advice, and for his continued guidance, encouragement and support throughout the investigation.

The author also wishes to thank Mr. S. Heuvel, P.Eng., former Manager of Engineering at Con-Force Structures Limited, Winnipeg, Manitoba and Mr. M. Lau, P.Eng., Manager of Engineering at Con-Force Structures Ltd. for their helpful advice and for supplying all of the precast components of the test specimens. Financial support provided by Con-Force Structures Ltd., the National Sciences and Engineering Research Council of Canada, and the Prestressed Concrete Institute is also greatly appreciated.

The author is very grateful to Mr. Moray McVey for his continued and tireless assistance during the laboratory experimental program. Special thanks is also extended to Mr. Ed Lemke, Mr. Marty Green, Mr. Steve Meyerhoff, and Mr. Brian Turnbull for their assistance in the laboratory. The author would also like to thank Mr. Dong for his assistance in the analysis stage of the investigation.

TABLE OF CONTENTS

LIST OF TABLES

LIST OF FIGURES

LIST OF SYMBOLS

A_c	=	cross-sectional area of interface
A_{c1}	=	area of the hollow-core in contact with the drypack, mm^2
A_{c2}	=	area of the concrete fill in contact with the drypack, mm^2
A_{cu}	=	hollow-core area at ultimate, mm^2
C	=	filled core factor
E_i	=	modulus of elasticity of connection component i, MPa
f_{c1}'	=	compressive strength of hollow-core slab at time of testing, MPa
f_{c2}'	=	compressive strength of concrete fill at time of testing, MPa
f_{t1}	=	tensile strength of hollow-core slab, MPa
f_{t2}	=	tensile strength of concrete fill, MPa
F_{t1}	=	magnified tensile capacity of hollow-core slab due to applied load normal to connection, MPa
F_{t2}	=	magnified tensile capacity of concrete fill due to applied load normal to connection, MPa
F_{tu}	=	magnified tensile capacity of hollow-core slab at ultimate due to applied load normal to connection, MPa
k	=	fraction of load through concrete fill
k_1	=	equivalent spring constant of hollow-core "column"
k_2	=	equivalent spring constant of concrete fill "column"
M	=	moment due to eccentricity of applied shear load, Nmm
N	=	applied load normal to the connection, N
t	=	thickness of connection, including drypack, hollow-core or concrete fill, and bearing pads, mm
t_i	=	thickness of component i of connection
v	=	shear stress, MPa
V	=	applied shear load, N

V_f	=	shear friction resistance, N
V_h	=	nominal shear capacity of hollow-core slab, N
V_{hu}	=	nominal shear capacity of hollow-core slab at ultimate, N
V_{pc}	=	nominal shear capacity of partially cracked hollow-core, N
V_u	=	shear friction resistance at ultimate, N
λ	=	concrete density factor
μ	=	coefficient of friction
μ_e	=	effective coefficient of friction
σ_n	=	normal load applied to the wall panel, MPa
σ_{n1}	=	applied normal load distributed to hollow-core in contact with drypack, MPa
σ_{n2}	=	applied normal load distributed to concrete fill in contact with drypack, MPa

CHAPTER 1

INTRODUCTION

1.1 GENERAL

The use of precast concrete load-bearing shear wall panels for high-rise construction has increased substantially in the past decade. The foremost advantages of precasting are the high quality control possible with off-site fabrication of structural elements, and the ease and speed of assembly at the erection site. In addition, precast construction is seldom interrupted by adverse weather conditions.

Shear wall load-bearing panel systems are currently a popular method of precast construction. The large panel building system consists of load-bearing shear walls in the longitudinal and transverse directions. The shear walls of the elevator shaft and stair wells resist lateral loads in the longitudinal direction, while the interior shear walls resist lateral loads in the transverse direction, as shown in Figure 1.1.

The major difference between the longitudinal and transverse shear walls is the type of horizontal connection between the panels. The transverse interior shear walls support the hollow-core floor slabs at the horizontal connection, while the longitudinal shear walls are parallel to the hollow-core slabs, as shown in Figure 1.2.

The required strength and dimensional tolerance of the precast wall panels can be easily achieved in the controlled environment of a factory. The structural integrity and economy of a precast panel building depends on detailing and design of the connections between precast panels. A well designed simple connection normally minimizes the construction time, requires minimal falsework, and maintains the overall integrity of the structure.

A recent innovation in horizontal connections for load-bearing shear wall panels is the use of vertical post-tensioning tendons. The gap between panels, which is necessary for proper alignment, is filled with a drypack grout while the panels are temporarily braced. After the erection of several stories, the tendons, extending from the base of the structure to the current story, are post-tensioned and the temporary braces are removed.

The post-tensioned connection, with or without hollow-core floor slab, has not been examined for a thorough understanding of its behavior under the various limit states. The available literature has very little information applicable to this type of connection. Therefore, this research program was undertaken to provide the necessary information on the behavior and capacity of post-tensioned connections for precast load-bearing shear wall panels.

1.2 OBJECTIVE

The primary objective of this research is to investigate the behavior of post-tensioned connections for precast concrete load-bearing shear wall panels subjected to static shear loading. The interior shear wall panel connections, which support the hollow-core floor slab, will also be considered.

The scope of the investigation includes development of rational mathematical models to predict the behavior and capacity of these connections at various limit states. The maximum shear capacity and the ultimate shear capacity based on the proposed mathematical models will be compared with test results.

1.3 SCOPE

Nine prototype wall panel specimens were tested in this research program. The nine specimens included three different joint configurations. The first category consists of three post-tensioned specimens without hollow-core slab. The second and third categories each consist of three specimens with hollow-core slab, and are tested with and without post-tensioning, respectively. Two different levels of load normal to the connection were used to investigate the effects of dead load.

A review of the relevant literature related to the shear capacity of horizontal post-tensioned connections is presented in Chapter 2.

The experimental program undertaken is described in detail in Chapter 3. Included in this chapter are descriptions of the test specimens, material specifications, test set-up and testing sequence.

The test results from the experimental program are summarized in Chapter 4. Detailed test results are presented in a separate technical report [1].

In Chapter 5, the effects of the presence of post-tensioning tendons, the presence of hollow-core slab, and the level of load normal to the connection are presented. Based on test results and observations made during the testing of specimens, rational mathematical models are developed to predict the maximum and ultimate limit state shear capacities. The reliability of the models is established by comparison of the model predictions with the test results.

Conclusions and recommendations based on this research program are made in Chapter 6.

CHAPTER 2

LITERATURE REVIEW

2.1 INTRODUCTION

During the past decade, the use of precast load-bearing shear wall panels for high-rise construction has increased substantially. The major advantages of precast construction are the high level of quality control possible with off-site manufacturing, the ease and speed of assembly at the construction site, and the minimal interruption due to adverse weather conditions. Precast wall panel construction is particularly well suited for hotel and apartment buildings where there is repetition between storeys and good thermal and acoustical barriers are required.

With the high quality of the precast members assured, attention is directed toward the behavior and capacity of the connections which tie the precast members together. It is widely agreed in the literature, that an extremely important component of precast large panel buildings is the connection between precast members [1,4,8]. Precast panel connections are regions of high stress concentration and without adequate design to transfer the forces through these connections, the full capacity of the precast panels cannot be utilized.

Of particular interest, are the horizontal connections which transfer vertical and horizontal forces between load-bearing wall panels and "upon which the ultimate stability of the structure is dependent" [3]. The horizontal connections must provide adequate strength, continuity, and ductility when the shear wall is subjected to bending moments and shear forces, as shown in Figure 2.1.

The horizontal connections are typically reinforced with some combination of continuity bars, mechanical shear connectors, and/or post-tensioning. The gap between wall panels, necessary for alignment purposes, is filled with a drypack grout.

In a previous study conducted at the University of Manitoba [4], it was shown that the ultimate shear capacity of a plain surface connection may be determined by the sum of the contributions from (1) the shear friction resistance, (2) the shear resistance of the continuity reinforcement and (3) the shear resistance of the mechanical connectors. However, no information is available regarding the contribution of post-tensioning strands to the ultimate resistance of the connection.

Since the intermediate shear wall panels of the structure support the hollow-core slab of the floor system, the effect of the presence of the hollow-core slab must also be considered. Several tests have been conducted in Europe to study the shear capacity of horizontal connections with hollow-core. However, the European connection details are quite different in comparison to those used in North America, as shown in Figures 2.2 a) and 2.2 b), and therefore their findings are not applicable to North American practice [8,9,10]. Testing of North American or "American type" horizontal joints with hollow-core slab, shown in Figure 2.2 a), is very limited.

The North American type of horizontal joints with hollow-core have been tested mainly for their vertical load carrying capacity, and to a lesser extent, for their shear capacity under monotonic and reversed cyclic load. Since the vertical loading on a horizontal connection may have some effect on the shear capacity of the connection, both the vertical and shear loading studies will be reviewed in this Chapter.

This chapter will review and summarize the present state of knowledge regarding the design and behavior of post-tensioned horizontal connections which include hollow-core slab and are typically detailed according to the current North American practice.

2.2 SHEAR FRICTION RESISTANCE

The shear friction theory may be used to predict the shear resistance provided by the various interfaces of horizontal connections. The classical shear friction model could be expressed as:

$$V_f = \mu \sigma_n A_c \tag{2.1}$$

where V_f = shear friction resistance of interface

μ = friction coefficient for interface

σ_n = compressive stress normal to interface

A_c = cross-sectional area of interface

Design of horizontal connections according to the Canadian Prestressed Concrete Institute (CPCI) Handbook [5] and the ACI Building Code [6] is based on the classical shear friction model given above. The difference between the two codes is mainly the magnitude of the coefficient of friction.

The Prestressed Concrete Institute (PCI) Design Handbook [7] requires the use of an effective coefficient of friction, μ_e, which is expressed in terms of the shear stress, v, and the concrete density factor, λ, as follows:

$$\mu_e = (6.895\lambda^2\mu)/v \qquad (2.2)$$

where λ = 1.0 for normal density concrete

λ = 0.75 for structural low density concrete

The values of the coefficients of friction recommended by the codes are given in Table 2.1.

2.3 INTERIOR HORIZONTAL CONNECTIONS

2.3.1 Vertical Loads

The distribution of vertical load through the components of the interior horizontal connection may affect the shear capacity of the connection. Although the actual state of stress due to the vertical load is very complex [8], it is generally accepted that the connection may be modelled as three separate "columns" transferring the vertical load [11,12], as shown in Figure 2.3.

The Prestressed Concrete Institute [11] recommends three methods for the design of horizontal connections for vertical loads. Based on more recent experimental work, Hanson and Johal [12] propose another design method. However, since the purpose of these design methods is to determine the strength of the connection under vertical loading, most of these methods may only be used to consider the distribution of vertical loads at the ultimate limit state.

The first PCI method [11] is based on the ultimate strength of the concrete fill and the stress-deformation characteristics of the concrete fill and the bearing pads. This method may be used to find the ultimate strength of the connection.

The second PCI method [11] is based on an elastic analysis of the connection and a stress distribution under service load conditions. This method may be used to determine the distribution of the vertical load through the connection components at load levels lower than the ultimate vertical load, for the purpose of relating the distributed vertical stress to the shear capacity of the connection.

Based on a uniform strain distribution, the second PCI method distributes the vertical load based on the relative stiffness of the connection components, as shown in Figure 2.3, using the following expressions:

$$\sigma_{n1} = (2b_1 + b_2)\ \sigma_n\ /\ (2b_1 + b_2k_2/k_1) \qquad (2.3\ a)$$

$$\sigma_{n2} = \sigma_{n1}\ (k_2/k_1) \qquad (2.3\ b)$$

where σ_{n1} = vertical load distributed across "column" 1, hollow-core slab portion of connection

σ_{n2} = vertical load distributed across "column" 2, concrete fill portion of connection

σ_n = vertical average stress applied normal to connection

b_1 = width of "column" 1

b_2 = width of "column" 2

k_1 = equivalent spring constant of "column" 1

k_2 = equivalent spring constant of "column" 2

with k_1 = $(\Sigma t_i)\ /\ (\Sigma t_i/E_i)$, i = 1 to 4

and k_2 = $(\Sigma t_i)\ /\ (\Sigma t_i/E_i)$, i = 4 to 5

t_i = thickness of component i of current "column"

E_i = modulus of elasticity of component i

i = 1, for the bearing pad

i = 2, for the hollow-core

i = 3, for the concrete fill in the cores of the hollow-core

i = 4, for the drypack

i = 5, for the concrete fill between the hollow-core slabs

If the modulus of elasticity of the drypack, concrete fill, or hollow-core is not known, the following expression recommended by the Canadian Standards Association [9], or any other rational method, may be used:

$$E = 5000 \sqrt{f_c'}$$

where f_c' = compressive strength of concrete

The third method recommended by the PCI is based on empirical data from tests conducted by the Danish Structural Research Center, and others [11]. The connections tested, unlike those used in North America, had an open gap under the floor slabs which suggests a bearing pad stiffness of zero. In addition, the empirical equation resulting from these tests is applicable only when the strength of the concrete fill is comparable to the strength of the wall panels [11].

Based on the results of 23 full-scale tests of North American type horizontal connections, Hanson and Johal developed design equations for interior and exterior connections with and without concrete fill [12]. The expressions proposed by Hanson and Johal also distribute the vertical load to three "columns" in the connection. However, the factor used to distribute the vertical load is based on the compressive strength of the concrete fill and the expressions are applicable to the distribution of the vertical load at the ultimate limit state only.

2.3.2 Shear Load

Harris and Abboud [9] tested a total of 16 scale models of interior North American type horizontal connections under monotonic and reversed cyclic shear load. A scale of 3/32 was used for these models. The level of load applied normal to the connection was very low, between zero and 2 MPa. There was an "unavoidable eccentricity"[8] of the applied shear load as shown on the diagram of the test model in Figure 2.4.

Several of the models were tested with an overturning moment applied, as shown in Figure 2.4. The total compressive normal stress in these models, considering the effects of the overturning moment, was still less than 2MPa.

During the tests with monotonically applied shear load, there was a slight increase in slip with increasing shear load up to 95% of the ultimate shear load. At this level of shear load, there was a significant increase in the amount of slip with a relatively small increase in shear load.

In both the monotonic and reversed cyclic tests, slip occured on either the drypack to top panel interface or on the concrete fill to bottom panel interface. Failure of the connection models was sudden and was characterized by splitting of the hollow-core floor slab adjacent to the vertical reinforcement.

Harris and Abboud, made no effort to separate the contributions of the various connection components in the total shear capacity of the connection [9]. However, they calculated the shear friction coefficients of their connection models, as shown in Figure 2.5.

Hanson examined the load versus slip response of interior North American type horizontal connections subjected to repeated reversals of shear load along the joint [14]. A total of 10 full-scale connections were tested, with connection lengths of 600 and 1200 mm. The level of load normal to the connection was varied between 3.5 and 21 MPa. The coefficients of friction obtained in this research project were extremely low, from 0.2 to 0.4, as shown in Figure 2.5.

CHAPTER 3

EXPERIMENTAL PROCEDURE

3.1 INTRODUCTION

This experimental program is designed to investigate the shear behavior and shear capacity, at various limit states, of typical post-tensioned connections for precast load-bearing shear walls. The program also considers the presence of the hollow-core slab of the floor system at the connection. In addition, two levels of load normal to the connection, which simulate the effect of gravity, are included in this investigation.

This chapter describes, in detail, all the parameters, test specimens, instrumentation, and the test set-up used in this experimental program.

3.2 TEST SPECIMENS

A total of nine specimens were tested in this experimental program. Two different types of specimens were investigated. The first group was designed to simulate the shear wall at the elevator shaft. The second group was designed to simulate the intermediate shear wall of a high-rise building supporting the hollow-core floor slabs. For each category, the presence of the post-tensioned prestressing was investigated and two levels of load normal to the connection were considered.

In this program, the first digit of the specimen mark represents the specimen number. The following two characters of each specimen mark indicate the particular variation of parameters chosen for each specimen as follows:

HD: Hollow-core with Drypack only

HP: Hollow-core and Post-tensioning

PD: Post-tensioning and Drypack, without hollow-core

The last digit of the specimen mark represents the level of the load normal to the connection. Two load levels were considered, 4 MPa and 8 MPa, which are representative of two levels within a 32 story high-rise structure. A connection subjected to a 4MPa load normal to the connection represents the load at the top floors of a 32 story structure while a connection loaded with an 8 MPa load simulates the gravity load in the lower floors of the structure.

The following is an example of a specimen mark used in this experimental program:

3 HD 8

specimen number 3

Hollow-core slab with Drypack only

8 MPa load normal to the connection

A detailed description of all tested specimens is given in Table 3.1.

3.3 DESCRIPTION OF SPECIMENS

3.3.1 Precast Wall Panels

All of the panels used in this experimental program were cast by Con-Force Structures Limited of Winnipeg, Manitoba. The dimensions for all panels were identical as shown in Figure 3.1. Each panel had an overall length of 1750 mm, a connection length of 1200 mm and a 500 mm deep corbel portion for the purpose of loading the connection in direct shear. At the connection, the wall panel was 830 mm wide with a typical interior wall thickness of 150 mm. The thickness of the panel was increased to 200 mm at the corbel to avoid premature failure of the panel before the connection.

Two post-tensioning ducts were included in those panels which were to be used for post-tensioned specimens. The ducts were located 900 mm apart on the 1200 mm connection length, as shown in Figure 3.2. These semi-rigid deformed galvanized ducts were elliptical in shape with radii of 32 mm and 57 mm.

To form a continuous duct, the duct in the bottom panel was coupled with the duct in the top panel. The ducts were coupled inside pockets in the top panel as normally detailed for actual structures. The small tapered pocket used in the test specimens is shown in Figure 3.3.

The post-tensioning anchorage detail, shown in Figure 3.4, consisted of a 12.7 mm thick steel plate, two 15.9 mm diameter Nelson studs 150 mm in length, and a 10M spiral with six turns.

3.3.2 Panel Reinforcement

Reinforcement of the panel, as shown in Figure 3.5, was identical for all specimens. The shapes and sizes of the bars used are shown in Figure 3.6. The sizes of the closed stirrup ties were 10M with a nominal yield strength of 300 MPa while all other bars were 20M with a nominal yield strength of 400 MPa.

3.3.3 Connection Configurations

The three connection configurations tested in this experimental program are shown in Figure 3.7. The hollow-core slab of the floor system used in the "HD" and "HP" connections series is shown in Figures 3.7 a) and 3.7 b). The "HP" and "PD" connections series were post-tensioned as shown in Figures 3.7 b) and 3.7 c). Both of these parameters will be discussed in detail in this section.

The precast hollow-core floor slab was produced by Con-Force Structures Limited. The slab is 200 mm deep, 1200 mm wide, and is cut to the desired length of span after casting. The span of the floor slab in actual structures is approximately 9000 mm. However, for the purposes of this experimental program, two 150 mm long spans were used for each test specimen. This length is representative of the length of the concrete fill normally used for hollow-core slab at the shear wall location.

At the connection, the cores of the hollow-core slab and the 50 mm gap between the two ends of the hollow-core slabs are filled with concrete as shown in Figures 3.7 a) and 3.7 b).

The hollow-core floor slab rests on a "Korolath" bearing pad on the bottom wall panel, as shown in Figures 3.7 a) and 3.7 b). The bearing pad is 50 mm wide, approximately 3 mm thick, and covers the entire 1200 mm length of the connection.

Each post-tensioned specimen in the "HP" and "PD" series had two post-tensioning ducts crossing the connection. A 12.7 mm diameter seven wire prestressing strand was used for post-tensioning of the specimen, as shown in Figures 3.7 b) and 3.7 c). The tensile force applied to each tendon was 108 kN which resulted in a prestress level of 1.2 MPa at the connection. Figures 3.7 b) and 3.7 c) also illustrate the coupling of the post-tensioning ducts in the pocket just above the connection and the grout which fills the ducts after the strands are tensioned.

All specimens in the testing program had a 20 mm gap between the top panel and the hollow-core slab or bottom panel, as shown in Figures 3.7 a), 3.7 b) and 3.7 c). This gap is normally used in actual structures for alignment purposes. The gap is packed with a drypack grout. Mix proportions of the drypack and other grouts used in this program are given in the following section.

3.4 MATERIAL SPECIFICATIONS

3.4.1 Panel Concrete

The concrete mix for the precast panels produced by Con-Force Structures Limited had the following proportions:

Coarse aggregate	884 kg/m^3
Sand	612 kg/m^3
High Early Strength Portland Cement	234 kg/m^3

Flyash	32 kg/m^3
Pozzolith	0.58 kg/m^3
Water	119 kg/m^3

To evaluate the strength of the concrete, two standard 150 mm x 300 mm concrete cylinders were cast according to CSA specifications for each precast panel.

3.4.2 Concrete Fill

The concrete fill used in this experimental program had the same mix proportions normally used in actual structures. The mix proportions are as follows:

Coarse aggregate	980 kg/m^3
Sand	920 kg/m^3
Normal Portland Cement	350 kg/m^3
Water	166 kg/m3
Water Reducing Agent	1576 mL/m^3

The strength of the grout fill concrete was evaluated at 28 days and at the day of testing. Three standard 150 mm x 300 mm cylinders were cast according to CSA specifications and three 75 mm x 75 mm x 150 mm prisms were also used.

3.4.3 Drypack Grout

The drypack grout used in this experimental program was mixed and cast by Con-Force personnel. The composition and consistency of the drypack was the same as that used in actual structures. The drypack proportions were as follows:

	by volume	by weight
Concrete sand	2 parts	2 parts
Normal Portland Cement	1 part	1 part
Water (approximate)	0.5 parts	0.2 parts

The consistency of this drypack is best described by the fact that the grout would hold its shape when compressed in the palm of the hand, as shown in Figure 3.8.

To evaluate the strength of the drypack grout, 75 mm cubes were fabricated. Two cubes were used for each specimen to evaluate the strength at the time of testing. Additional cubes were also used to evaluate the 7 and 28 days strengths of the drypack.

3.4.4 Post-tensioning Grout

The post-tensioning grout was of a liquid consistency suitable for pumping through the ducts. The same grout proportions were used as in actual structures and are as follows:

Normal Portland Cement	1300 kg/m^3
Water	584 kg/m^3
Interplast Type "N"	8 kg/m^3

Four 75 mm x 150 mm cylinders were cast for each specimen to evaluate the strength of the grout at 28 days and at the time of testing. Figure 3.9 illustrates the expansive characteristic of this grout with three cylinders that were levelled at the time of casting.

3.4.5 Concrete Sand

The concrete sand used in the concrete fill and the drypack grout had the following gradation, as determined by sieve analysis:

Sieve Size	Total Percentage Passing by Mass
10 mm	100.0
5 mm	97.3
2.5 mm	88.5
1.25 mm	76.1
630 µm	54.6
315 µm	17.2
160 µm	4.0

The preceding is in accordance with the CSA Standard CAN3-A23.1M77 [15].

3.4.6 Hollow-Core Floor Slab

The hollow-core floor slab produced by Con-Force Structures is 200 mm deep, 1200 mm wide, and is cut to the desired length of span after casting. There are six 150 mm diameter cores per 1200 mm width of hollow-core slab. The "webs" of concrete between the cores are 40 mm wide, 50 mm wide at the outer edges.

52 MPa is the design strength of the hollow-core slab recommended by Con-Force Structures.

3.4.7 Post-tensioning Strands

Seven wire, 12.7 mm diameter post-tensioning strands were used in this testing program. The strands were stressed to 60 percent of their ultimate strength to achieve a desired post-tensioning force that was 50 percent of their ultimate strength, 108 kN.

3.5 TEST SPECIMEN ASSEMBLY

3.5.1 General

The precast wall panels and hollow-core floor slabs were fabricated at Con-Force Structures and delivered to the Structures Laboratory at the University of Manitoba where the test specimens were assembled. The first stage of assembly was the positioning and grouting of the hollow-core floor slabs in the specimens which included this parameter. All specimens were then drypacked. The third stage of assembly was the tensioning of the post-tensioning strands and the grouting of the ducts in those specimens which were post-tensioned.

3.5.2 Grouting of Hollow-Core Slab

For positioning and grouting of the hollow-core slab, the bottom panel was positioned with the connection orientated horizontally. Two short pieces of hollow-core slab, 150 mm long, were positioned on top of bearing pads and allowing a 50 mm gap in between them, as shown in Figure 3.10.

A load was applied to the hollow-core producing effective stresses on the bearing pads which were similar in magnitude to the value in the long spans of hollow-core slabs in the actual structure. This load was applied by attaching threaded rods to the frame which was clamping the hollow-core slabs. The threaded rods were anchored on the bottom wall panel and tensioned by tightening the nuts on the threaded rod. On each threaded rod was a calibrated load cell used to achieve the appropriate stresses to simulate the gravity load. The hollow-core loading apparatus is shown in Figures 3.11 and 3.12.

The concrete fill was cast through the gap between the hollow-core slabs. The concrete fill flows and was tamped to fill the cores of the slabs and the gap between the two pieces of hollow-core slab. Wooden forms were used at the two ends of the hollow-core slabs as shown in Figure 3.12 immediately after casting of the concrete fill.

The test specimen and the concrete cylinders were covered with wet burlap and a polyethylene tarpaulin after casting. After seven days of moist curing, the specimen and concrete cylinders were exposed to the open air of the laboratory.

3.5.3 Drypacking

To facilitate drypacking of the connections and to avoid initiation of cracks, the bottom panel was placed in an upright position with the connection orientated vertically. For those specimens with hollow-core slab, the hollow-core clamping apparatus remained in place.

The top panel was then aligned with the bottom panel using temporary braces. For those specimens with post-tensioning ducts, the post-tensioning strands were threaded through the ducts of the top and bottom panels, as shown in Figure 3.13. The ducts were then coupled inside the small tapered pocket of the top panel by inserting the end of the bottom panel duct about 5 mm into the top panel duct.

The gap between panels, or between top panel and hollow-core, was packed with drypack grout by two employees of Con-Force Structures.

After drypacking, the specimens and the cubes for material testing were covered with wet burlap and polyethylene tarpaulins for seven days. The temporary bracing remained in place until moments before testing to eliminate premature cracking of the drypack grout.

3.5.4 Post-tensioning

When the drypack had cured for seven days, the strength of the drypack was determined before post-tensioning of the specimens.

The strands were tensioned with a hydraulic jack as shown in Figure 3.14. The tension applied to each strand was measured using a calibrated load cell located between the chuck and the panel. Figure 3.15 a) and b) show the calibrated load cell detail, and its location with respect to the specimen, respectively.

To avoid excessive tensile stresses in the drypack due to the eccentric location of the two post-tensioning cables, the post-tensioning was done in stages. One-third of the full tension force was applied to the bottom strand, then two-thirds were applied to the top strand, followed by post-tensioning the two strands to their final level.

A hand-pump was used to grout the post-tensioning ducts. A grouting tube was provided at each end of the ducts, as shown in Figure 3.15 b). The grout was pumped through the grouting tube at one end while air escaped through the tube at the other end.

The load cells on the post-tensioning strands were monitored throughout the curing of the expansive duct grout until the time of testing.

3.6 INSTRUMENTATION

3.6.1 Displacements

Relative horizontal and vertical displacements across the various interface surfaces were measured. Displacements were measured using dial gauges on side A of the specimen and linear variable differential transducers (LVDT's) on side B. At each measurement station, two instruments were used to measure horizontal and vertical relative displacement. A typical measurement station with dial gauges is shown in Figure 3.16.

The location of the measurement stations were similar on both sides of each specimen. The location of typical measurement stations for specimens with hollow-core slab on side A and B are shown in Figure 3.17. On both sides, stations 1 and 2 measured the relative displacements between hollow-core and panel across the drypack, while stations 3 and 4 measured displacement between hollow-core and panel across the bearing pad and concrete fill. LVDT stations 5 and 6 measured relative displacement between the two panels. In addition, slip was measured from hollow-core to drypack at station 7 and from drypack to panel at station 8. Stations 7 and 8 were the exception to the rule, consisting of one dial gauge each and located on side B with the LVDT stations.

For specimens without hollow-core, the instrumentation was much simpler as shown in Figure 3.18. Relative displacement was measured from panel to panel at the top and bottom of the connection on each side of the specimen.

Both the dial gauges and the LVDT's were attached to the specimen using Rawl insert plugs in 5 mm diameter holes which were approximately 40 mm deep. For the purpose of measuring relative displacement only, between two different surfaces, the holes were drilled at the same level on the different surfaces.

The stroke of the testing machine was also measured, using an LVDT with a range of ± 50 mm and an accuracy of ± 0.5 %. The ranges of the LVDT's attached to the specimen were from ± 6.4 mm to ± 25.4 mm with accuracies of ± 0.5%. The dial gauges had ranges of 10 mm to 50 mm and had accuracies of ± 0.1%.

The LVDT readings were monitored and recorded during the test with a Data Acquisition System capable of monitoring 12 channels. An IBM-PC, a printer, and a plotter were part of this system. A program was used to calibrate the LVDT's and to record the readings.

3.6.3 Testing Machine

A Baldwin 2670 kN Universal Testing Machine was used for all tests. The machine was equipped with an MTS 2310 signal amplifier, a 464 MTS data display, a Hewlett Packard 7044A X-Y plotter, and a Hewlett Packard 34702A multimeter.

3.7 TESTING PROCEDURE

3.7.1 Test Set-up

Two cranes were used to lift the specimen, with the connection orientated vertically, and move it into the testing machine. When the centreline of the connection was aligned with the centreline of the top and bottom heads of the testing machine, the specimen was levelled using a mason's level.

Between the bottom platform of the testing machine and the specimen were placed: two sheets of teflon, a steel bearing plate, and bags of quick-set plaster-of-paris. The plaster-of-paris was used to provide a uniform contact surface between the specimen and the bearing plate, while the teflon sheets prevented any restraining of the specimen in the horizontal plane.

The bottom platform of the machine was raised until it was in contact with the specimen and the vertical alignment of the specimen was then rechecked. The plaster-of-paris was allowed to set while similar layers of plaster, steel, and teflon were placed on top of the specimen.

After placement of the specimen in the testing machine, the outer edges of the specimens were post-tensioned using Dywidag bars, as shown in Figure 3.19, to prevent premature cracking of the wall panels during the test. Each pair of horizontal Dywidag bars were tensioned to a total load level of 200 kN and each pair of vertical bars was tensioned to a total load level of 340 kN. To achieve the desired level of post-tensioning, the Dywidag bars had strain gauges attached to them and had previously been individually calibrated with the Baldwin Testing Machine.

Next, the apparatus used to apply a simulated gravity load normal to the connection was positioned on the specimen. The apparatus, as shown in Figure 3.19, consisted of eight Dywidag bars and a system of four hydraulic jacks. The jacks had previously been calibrated as one unit using the Baldwin Testing Machine and an Enerpac hydraulic pump with a pressure gauge. Figure 3.20 shows the end of the normal loading apparatus containing the jacks. A system of rollers is also visible in Figure 3.20. These rollers were used on both sides of the apparatus to prevent the restraining of relative slip between panels during the test.

3.7.2 Testing Sequence

Immediately before testing, the load normal to the connection was applied and maintained at the appropriate 4 MPa or 8 MPa level with a regulator valve attached to the hydraulic pump. Initial readings for all instruments were recorded at this stage. The initial dial gauge readings were manually recorded.

Throughout the test, the LVDT readings and load levels were monitored and recorded by the Data Acquisition System. The X-Y Plotter provided a load versus slip curve of the test as well. All dial gauge readings were recorded manually.

The load was applied vertically to the connection in 100 kN increments until the maximum shear load was reached. At this point stroke control was used to determine appropriate increments between instrument readings.

The presence of cracks and their propogation during the test were recorded by felt pens on the specimen and sketches drawn on transparencies, a new transparency for each increment. Photographs of these crack patterns were also taken at the end of the test.

The test was terminated when excessive deformation had occured in the connection and the stroke was over 15 mm. The entire testing sequence was approximately 2 to 4 hours in duration.

CHAPTER 4
TEST RESULTS

4.1 INTRODUCTION

In this chapter, the experimental results for the nine specimens tested in this research program are presented. The results include the specimen material properties, the shear capacity of the connections, and displacement measurements. The measured data is presented in tabular and/or graphical form.

4.2 MATERIAL PROPERTIES

4.2.1 Panels

The average compressive strength of the concrete used for the panels, at the time of testing, is given in Table 4.1.

4.2.2 Concrete Fill

The compressive strength, at the time of testing, of the prisms cast from the concrete fill is given in Table 4.2. The equivalent standard cylinder strength of the prisms was estimated as 0.91 times the prism compressive strength [16]. The average prism compressive strength and the equivalent cylinder strength are given in Table 4.2.

4.2.3 Drypack Grout

Table 4.3 gives the average compressive strength of the drypack, at the time of testing, as determined by the 75 mm cubes. The equivalent standard cylinder compressive strength was estimated as 0.73 times the cube compressive strength [16]. The cube compressive strength and the equivalent cylinder strength are given in Table 4.3.

4.2.4 Post-tensioning Grout

The average compressive strength of the post-tensioning grout, at the time of testing, is given in Table 4.4.

4.3 TEST RESULTS

4.3.1 Shear Load

The maximum and ultimate shear loads for each of the connections tested in this program are given in Table 4.5. In this investigation, the ultimate shear load was defined as the load corresponding to a relative vertical displacement of 5 mm. Although the shear load continued to decrease with increasing slip in the connections with hollow-core slab, the 5 mm slip was chosen to be the limit based on the allowable deflection used for high-rise structures.

4.3.2 Displacement Measurements

Figures 4.1 to 4.9 give the relative vertical displacement, or slip, between panels during loading. This information is also presented in tabular form in Tables 4.6 to 4.14. For the specimens with hollow-core slab, during the initial stages of loading, the slip was not uniform over the length of the connection. Figures 4.10 to 4.14 give the distribution of the relative slip between the hollow-core slabs and the panels, along the length of the top and bottom contact surfaces of the tested connections during the initial loading stage.

The distribution of relative slip shown in Figures 4.10 to 4.14 is plotted for the initial stages of loading up to maximum only, not including the ultimate stages of loading where the distribution of slip was uniform. A plot of the distribution of slip for specimen 5HP8 is not available since specimen 5HP8 was the pilot specimen and had a slightly different instrumentation arrangement.

The measured values indicate that the slip occured at the drypack interface, with the exception of specimen 3HD8 where the slip occured between the concrete fill and the panel interfaces. The maximum measured slip was within the 10 mm range.

Detailed recorded displacement measurements at each measurement station and the corresponding stroke displacements for each specimen are given in reference [1]. The measured test data given in reference [1] are presented in graphical and tabular form.

4.3.3 Crack Patterns

The crack patterns for all specimens at ultimate are shown in Figures 4.15 to 4.23.

CHAPTER 5

DISCUSSION OF TEST RESULTS

5.1 INTRODUCTION

In this chapter, the behavior of each connection tested in this experimental program is discussed. The test results presented previously will be used to study the effect of the load normal to the connection, post-tensioning, and hollow-core slab.

The mechanisms of shear transfer for each type of connection are presented in this chapter. Rational mathematical models, developed to predict the maximum and ultimate shear capacity of the connections, are presented. The reliability of these models is established by comparison of predicted values and experimental results.

5.2 SPECIMEN BEHAVIOR

5.2.1 General

The measured loads and observed behavior of the connections tested in this program indicate that the maximum shear capacity depends mainly on the friction resistance along the interface surfaces at the connection. However, for the connections with hollow-core slab tested under high levels of normal load, cracking of the hollow-core floor slab and/or concrete fill was observed at failure.

A detailed description of the observed behavior for each specimen is given in the following sections.

5.2.2 Specimen 1HD4

Specimen 1HD4 consisted of two panels supporting hollow-core floor slab and subjected to 4 MPa load normal to the connection.

The relationship between the applied shear load and the relative slip displacement between the hollow-core and the top and bottom panels is shown in Figure 4.10. The diagram indicates that slip was initiated between the hollow-core and panels in the two corners beneath the corbel portion of each panel, as schematically shown in Figure 5.1. At a shear load of 525 kN, a significant reduction in the stiffness of the connection was observed, as indicated by the load versus slip curve given in Figure 4.1. The slip continued to increase uniformly only between the hollow-core and the top panel, as shown in Figure 4.10.

The recorded measurements, using dial gauges 7 and 8, indicate that slip occured at the interface surface between the drypack and the top panel. No slip was measured on the interface surface between the drypack and the hollow-core.

For specimen 1HD4, a maximum shear load of 550 kN was reached prior to uniform slip along the drypack and panel interface. There was a considerable increase in slip at a constant load of 535 kN, which was recorded as the ultimate load carrying capacity of this specimen.

After removal of the specimen from the testing machine, the top panel was removed to examine the interface slip surface, as shown in Figure 5.2. The observed slip surface and the load versus slip relationship suggest that no bond was present at the drypack to panel interface and that resistance to the applied load was mainly due to shear friction along the interface.

5.2.3 Specimen 2HD8

Specimen 2HD8, similar to the configuration of specimen 1HD4, included hollow-core slab. However, specimen 2HD8 was subjected to a higher constant load level of 8 MPa normal to the connection.

The applied shear load versus slip distribution relationship, shown in Figure 4.11, indicates that the slip started at the two corners of the connection beneath the corbel portion of the top and bottom panels, similar to specimen 1HD4.

A gradual reduction in the stiffness of the connection occured at a shear load level of approximately 550 kN, as shown in Figure 4.2, and continued to increase up to a maximum load of 905 kN.

Prior to the maximum shear load level, at a shear load of 895 kN, a loud cracking sound was heard and cracks became visible in the hollow-core slab. The observed crack patterns at ultimate are presented in Figure 4.16.

The cracks in the hollow-core continued to propogate, causing deterioration of the shear capacity of the connection, as indicated by the load versus slip curve shown in Figure 4.2. At the same time, slip continued between the drypack and the top panel.

5.2.4 Specimen 3HD8

Specimen 3HD8 was identical to specimen 2HD8, with hollow-core slab and a constant load level of 8 MPa normal to the connection.

The relationship between the applied shear load and slip distribution for specimen 3HD8 is shown in Figure 4.12. As in specimens 2HD8 and 1HD4, slip began at the two corners of the connection beneath the corbel portion of the panels. For specimen 3HD8, there was no significant change in the stiffness of the connection up to a maximum shear load of 885 kN.

At the maximum applied shear load level, a loud cracking sound was heard and visible cracks appeared in the hollow-core slab, as shown in Figure 4.17. Immediatedly following this, the capacity of the connection significantly decreased to 722 kN.

The slip behavior of specimen 3HD8, beyond the maximum shear load level, was different in comparison to the other specimens tested in this program. In specimen 3HD8, slip occured between the hollow-core and the bottom panel at the bearing pad and concrete fill interface surface, as shown in Figure 4.12. The slip increased at a much lower rate with a slight decrease in the resistance of the connection, as shown in Figure 4.3. When the applied shear load had decreased to 650 kN, the slip began to increase at a higher rate with a slight increase in load.

It was observed that cracks in the hollow-core did not continue beyond the measured maximum load. The behavior of this connection at ultimate suggests that the ultimate shear capacity of the connection was dependent mainly on the friction resistance of the bearing pad and concrete fill and panel interface. It should be noted that this behavior occured only in one specimen. Therefore, due to the limited data, no conclusion can be made regarding the friction resistance of this interface. Additional tests are recommended to investigate the friction resistance of the concrete fill and bearing pad interface with the panel.

5.2.5 Specimen 4HP4

Specimen 4HP4, similar to specimen 1HD4, included hollow-core slab and was subjected to a 4 MPa normal load. However, specimen 4HP4 also included post-tensioning strands which induced an additonal 1.2 MPa uniform prestressing normal to the connection.

In general, the behavior of specimen 4HP4 was similar to that of specimen 1HD4. The presence of post-tensioning increased the shear resistance capacity of specimen 4HP4. Slip started at the same two corners of the connection, beneath the corbel portion of the panel, as shown in Figure 4.13. The stiffness of the connection began to decrease prior to a maximum applied shear load of 704 kN. Following the maximum shear load, slip continued and was evenly distributed along the drypack and top panel interface.

At ultimate, the slip continued to increase considerably at a constant load of 660 kN. After 3 mm of slip, at the constant shear load of 660 kN, cracking was observed in the lower portion of the hollow-core on both sides, as shown in Figure 4.18. The cracks began on side B at the bottom core of the hollow-core which was only partially filled with concrete. These cracks, however, did not propogate along the length of the connection or affect the ultimate shear capacity of the connection.

5.2.6 Specimen 5HP8

Specimen 5HP8, like specimen 4HP4, included hollow-core slab and post-tensioning, but was subjected to a higher load level of 8 MPa normal to the connection.

Behavior of specimen 5HP8 was similar to that of specimen 2HD8, except that a higher maximum shear capacity was achieved as a result of the additonal 1.2 MPa stress due to the presence of post-tensioning normal to the connection. Slip began under the corbel portion of the top panel. A gradual reduction in the stiffness of the connection began at an applied shear load level of approximately 750 kN and continued up to a maximum shear load of 957 kN.

Prior to the maximum shear load, at a shear load of 950 kN, cracks became visible in the hollow-core slab. The observed crack patterns are presented in Figure 4.19.

The visible cracks in the hollow-core continued to propogate while the shear capacity of the connection continued to decrease. At the same time, slip occured at the drypack and top panel interface.

5.2.7 Specimen 6HP8

Specimen 6HP8 was identical to specimen 5HP8, with hollow-core and post-tensioning, and subjected to a normal load level of 8 MPa. It was tested to confirm the behavior for these types of connections.

The behavior of specimen 6HP8 was similar to that of specimens 2HD8 and 5HP8. The maximum shear capacity of specimen 6HP8 was comparable to the capacity of 5HP8 and slightly higher than the capacity of 2HD8 due to the presence of post-tensioning. Figure 4.14 shows that slip started typically in the same two corners of the connection for all the tested specimens with hollow-core. Reduction of the connection stiffness began at approximately 500 kN, as shown in Figure 4.6.

At an applied shear load of 935 kN, a loud cracking sound was heard and cracks became visible in the hollow-core. As the cracks propogated, the capacity of the connection continued to decrease. Slip continued and was evenly distributed along the drypack and panel interface.

As in specimens 2HD8 and 5HP8, the shear capacity of specimen 6HP8 was controlled by the extent of cracking in the hollow-core slab and the concrete fill. The crack patterns at ultimate are shown in Figure 4.20.

5.2.8 Specimen 7PD4

Specimen 7PD4 simulated the post-tensioned connections typically used for the elevator shaft shear walls. The connection was subjected to a 4 MPa normal load level.

Figure 4.7 illustrates the relationship between the applied shear load and the slip between the two panels. No slip occured until a shear load level of 600 kN. At 670 kN, the stiffness of the connection was reduced significantly. At a maximum shear load of 690 kN, the slip along the interface of the panel and the drypack was visible and several diagonal tension cracks occured in the drypack.

Considerable slip occured at a constant shear load of 690 kN.

The connection at ultimate is shown in Figure 4.21.

5.2.9 Specimen 8PD8

Specimen 8PD8, similar to specimen 7PD4, was post-tensioned. However, specimen 8PD8 was subjected to a higher load level of 8 MPa normal to the connection.

As indicated in Figure 4.8, slip was initiated at a shear load level of 650 kN, but did not increase significantly until 1100 kN. Slip continued to increase considerably after a maximum shear load of 1160 kN.

The connection continued to undergo extensive slip at an ultimate shear capacity of 1130 kN. The connection at ultimate is shown in Figure 4.22.

5.2.10 Specimen 9PD8

Specimen 9PD8 was identical to 8PD8, post-tensioned with drypack only and subjected to an 8 MPa load level normal to the connection.

The relationship between applied shear load and slip is shown in Figure 4.9. Slip was initiated at 400 kN, but did not increase significantly until a shear load of 1050 kN. At this point, the stiffness of the connection reduced significantly and shortly thereafter, the maximum shear load of 1157 kN was reached.

At ultimate, the slip between the drypack and the panel increased considerably at a constant shear load of 1125 kN. The connection at ultimate is shown in Figure 4.23.

5.3 BEHAVIOR OF THE CONNECTIONS SUPPORTING HOLLOW-CORE SLAB

5.3.1 General

These type of connections simulate typical connections used for the interior shear wall load-bearing panels supporting hollow-core floor slab. Two different levels of load normal to the connection were used. The effect of the load normal to the connection is discussed in the following sections.

5.3.2 Load Level of 4 MPa

The shear load versus slip response for the post-tensioned connections tested at the 4 MPa load level normal to the connection is shown in Figure 5.3. Considering the effect of an additional uniform post-tensioning stress of 1.2 MPa, both connections were subjected to a total stress of 5.2 MPa normal to the connection.

The behavior of specimen 4HP4, with hollow-core slab, was similar to that of specimen 7PD4 without hollow-core. The failure was mainly due to friction slip between the panel and the drypack. Therefore, the presence of hollow-core does not affect the behavior or the capacity of post-tensioned connections with a total stress level of 5.2 MPa normal to the connection.

5.3.2 Load Level of 8 MPa

The shear load versus slip response for the post-tensioned connections tested at the 8 MPa normal load level are shown in Figure 5.4 a). Considering the effect of post-tensioning equivalent to an additional stress of 1.2 MPa, all four connections in this category were subjected to a total of 9.2 MPa stress normal to the connection.

It was expected that the high level of load normal to the connection would enhance the friction resistance of the interface surfaces. This behavior is clearly illustrated by the high level of the shear resistance of the specimens without hollow-core slab, 8PD8 and 9PD8. However, the behavior and capacity of specimens 5HP8 and 6HP8, with hollow-core slab, was significantly different and the maximum shear capacity was lower than the capacity of specimens 8PD8 and 9PD8.

The behavior past the maximum shear load capacity was also significantly different. Specimens 8PD8 and 9PD8 maintained constant ultimate shear capacities essentially equivalent to their maximum capacities. The shear capacity of specimens 5HP8 and 6HP8 continued to decrease following the maximum shear load.

The reduction of the maximum shear capacity of the connections with hollow-core slab relative to the connections without hollow-core, at a load level of 9.2 MPa normal to the connection, could be attributed to cracking of the hollow-core and/or the concrete fill. Degradation of the shear capacity of these connections coincided with the propogation of these cracks during the test.

Two important effects of the presence of hollow-core slab at high levels of normal load are:

1. Reduced ductility of the connection, as shown in Figure 5.4a)
2. Reduced stiffness of the connection, as shown in Figure 5.4b).

5.4 EFFECT OF LOAD NORMAL TO THE CONNECTION

5.4.1 Post-tensioned Connections With Drypack Only

The effect of the load normal to the connection for post-tensioned connections without hollow-core is shown in Figure 5.5.

Increase of the load normal to the connection results in an increase in the maximum and ultimate shear capacities of the connections. The increase in the shear capacities were also approximately proportional to the increase in load normal to the connection. This behavior could be attributed to the friction resistance along the slip surface which is known to be proportional to the normal load. This behavior suggests that the shear resistance of the post-tensioned connections without hollow-core was mainly provided by the friction resistance of the drypack and panel interface.

5.4.2 Connections With Hollow-Core Slab

The effect of the load level normal to the connections with hollow-core slab, with and without post-tensioning, is shown in Figures 5.6 and 5.7, respectively.

In both figures, it is apparent that under 4 MPa, the shear capacity was proportional to the load normal to the connection. Under the higher load of 8 MPa, the increase in the maximum shear capacity was not proportional to the increase in load normal to the connection. The shape of the load versus slip curves of the connections were quite different for the two different levels of load normal to the connections.

The difference in the behavior could be attributed to the difference in the observed failure mechanisms of the connections. The load versus slip curves for the connections tested at 4 MPa load level suggest that friction resistance of the drypack and panel interface was the main failure mechanism resisting the applied shear load. The load versus slip curves for the connections tested at 8 MPa load level suggest that the maximum and ultimate shear capacities were controlled by the cracking mechanism of the hollow-core slab and/or concrete fill.

5.5 EFFECT OF POST-TENSIONING

The shear load versus slip response of specimens with hollow-core slab and subjected to a 4 MPa load level normal to the connection are shown in Figure 5.8.

The increase in the maximum and ultimate shear capacities of specimen 4HP4 are proportional to the increase in load normal to the connection with the addition of post-tensioning stresses. These results suggest that the post-tensioning effects enhance the friction resistance of the connection and may be accounted for simply by adding the effect of the applied post-tensioning stresses to the gravity load.

The shear load versus slip response of specimens with hollow-core slab and subjected to an 8 MPa load normal to the connection are shown in Figure 5.9.

The increase in maximum shear capacities for specimens 5HP8 and 6HP8 was not proportional to the increase in load normal to the connection with the addition of post-tensioning stresses. This result suggests that frictional resistance, which is usually proportional to the normal load, is not the controlling mechanism for higher levels of load normal to the connection. The observed behavior indicates that the failure is controlled by the resistance of the hollow-core slab which looks like a weak link between the two panels.

5.6 MECHANISMS OF SHEAR TRANSFER

5.6.1 General

The results of this experimental program indicate that the behavior and shear capacity of the connections are dependent on the following parameters:

1) the level of load normal to the connection including post-tensioning stresses
2) the strength of the concrete fill
3) the strength of the hollow-core slab
4) the width of hollow-core bearing on the bottom panel
5) the uncracked length of hollow-core and/or concrete fill

Based on these observations, the mechanisms of shear transfer of the connections tested in this study are summarized in the following sections.

5.6.2 Interface Shear Friction Resistance

Post-tensioned connections without hollow-core slab exhibited the same behavior and mechanism of shear transfer as the connections with hollow-core subjected to 4 MPa load normal to the connection. The applied shear load was initially resisted by friction along the panel and drypack interface. The maximum shear load, which is required to overcome frictional resistance, was accompanied by a small amount of deformation parallel to the applied load. Following the maximum load level, the ultimate shear capacity was provided mainly by the shear friction resistance along the slip surface. The behavior at ultimate was characterized by a considerable increase in slip under a constant load.

Based on the above mechanism of shear transfer across an interface, the maximum and ultimate shear capacity of the connections may be determined using the shear friction theory discussed in Chapter 2:

$$V_f = \mu \sigma_n A_c \tag{5.1}$$

where V_f = shear friction resistance, N

μ = friction coefficient for drypack-panel interface

σ_n = compressive stress normal to the connection, MPa

A_c = area of drypack-panel interface, mm^2

The friction coefficent for the drypack and panel interface may be estimated using the applied shear load and the total load applied normal to the connection. In a previous study [4], the coefficient for the drypack and panel interface was found to be 0.7 ± 0.1. Based on the measured results of this experimental program, a coefficient of friction of 0.7 was also obtained.

5.6.3 Shear Resistance of Connections with Hollow-core

For specimens with hollow-core slab, the applied shear load has to be transferred from one wall panel to the other panel through the hollow-core and the concrete fill. For the specimens subjected to a higher load level of 8 MPa normal to the connection, the capacity of the hollow-core slab was found to determine the maximum shear capacity of the connection.

A free body diagram of the typical connection supporting hollow-core slab is shown in Figure 5.10. The normal stresses on the hollow-core and concrete fill are mainly due to the applied load normal to the connection, N, and the moment due to the shear load, V, applied through an eccentricity of t/2, where t is the total thickness of the connection between panels. The applied shear load, V, is assumed to be distributed along the length of the connection as shown in Figure 5.10.

Based on the second method recommended by the PCI [11], the load applied normal to the connection is distributed across the width of the connection as shown in Figure 2.3 and using the following expressions, with $b_1 = b_2 = 50$ mm:

$$\sigma_{n1} = 3\sigma_n \ / \ (2 + k_2/k_1) \tag{5.2 a}$$

$$\sigma_{n2} = \sigma_{n1} \ k_2/k_1 \tag{5.2 b}$$

where σ_{n2} = normal load distributed to concrete fill, MPa

σ_{n1} = normal load distributed to hollow-core, MPa

σ_n = normal load applied to the wall panel, MPa

k_1 = equivalent spring constant of "column" 1

k_2 = equivalent spring constant of "column" 2 with $k_1 = (\Sigma t_i) / (\Sigma t_i/E_i)$, $i = 1$ to 4

and $k_2 = (\Sigma t_i) / (\Sigma t_i/E_i)$, $i = 4$ to 5

t_i = thickness of component i of current "column"

E_i = modulus of elasticity of component i

i = 1, for the bearing pad

i = 2, for the hollow-core

i = 3, for the concrete fill in the cores of the hollow-core

i = 4, for the drypack

i = 5, for the concrete fill between the hollow-core

Based on combination of the shear and normal stresses shown in Figures 5.10 and 2.3, the maximum principle tensile stress was determined and found to be located at the centre of the connection length. Equating the maximum tensile principle stress due to the critical combination of stresses, with the tensile strength of the concrete, the nominal shear capacity of the connection with hollow-core slab, V_h, could be predicted as follows:

$$V_h = 2/3 \, [\, A_{c1}F_{t1} + A_{c2}F_{t2} \,] \tag{5.3}$$

where V_h = nominal shear capacity of the connection with hollow-core slab, N

A_{c1} = area of the hollow-core in contact with the drypack, mm^2

A_{c2} = area of the concrete fill in contact with the drypack, mm^2

F_{t1} = magnified tensile strength of the hollow-core slab due to applied load normal to connection, MPa

F_{t2} = magnified tensile strength of concrete fill due to applied load normal to connection, MPa

with $F_{tj} = \sqrt{f_{tj}(f_{tj}+\sigma_{nj})}$

j = 1, for hollow-core slab

j = 2, for concrete fill

σ_{nj} = applied load normal to surface j, MPa based on equation (5.2)

f_{tj} = tensile strength of concrete for part j, MPa

and f_{tj} = $0.6\sqrt{f_{cj}'}$ as proposed in a previous study [17]

with f_{cj}' = compressive strength of concrete for part j, MPa

5.6.4 Prediction of the Maximum Shear Capacity

For the type of connections typically used at the elevator shaft, without hollow-core slab, the maximum shear capacity could be predicted using the shear friction mechanism proposed by equation (5.1).

For the connections typically used for the interior shear walls supporting the hollow-core slab, the maximum shear capacity could be determined based on the lesser of the capacities predicted by the shear friction model, using equation (5.1), and the nominal capacity of the hollow-core, using equation (5.3).

The maximum shear capacities predicted using the proposed models are compared with the experimental results, as shown in Figures 5.11 to 5.20 and Table 5.1.

5.6.5 Prediction of the Ultimate Shear Capacity

For the type of connections typically used at the elevator shaft, without hollow-core slab, the ultimate shear capacity could be predicted using the shear friction mechanism proposed by equation

(5.1).

For the connections typically used for the interior shear walls supporting the hollow-core slab, the ultimate shear capacity could be predicted by assuming a complete loss of bond between the hollow-core slab and the concrete fill placed in the cores. In specimens 2HD8, 3HD8, 5HP8, and 6HP8, a partial loss of bond did occur during testing as shown in Figures 4.17, 4.18, 4.20 and 4.21. For connections in actual structures, a complete loss of bond may exist due to shrinkage and/or methods used to place the concrete fill.

Prediction of the reduced shear capacity of connections with partially cracked hollow-core, V_{pc}, could be made using the model for uncracked connections given in equation (5.3). The area of hollow-core and concrete fill that remains uncracked should be used in equation (5.3) to estimate the capacity of the remaining uncracked portion of the connection, as shown in Table 5.2.

The nominal shear capacity of the hollow-core slab at ultimate, assuming a complete loss of bond, could be predicted as follows:

$$V_{hu} = 2/3 \left[A_{cu}F_{tu} + A_{c2}F_{t2} \right] \qquad (5.4)$$

where V_{hu} = nominal shear capacity of hollow-core slab at ultimate, N

A_{cu} = minimum cross-sectional area of the hollow-core at ultimate, assuming a complete loss of bond, mm^2 This cross-section is located at the centre of the hollow-core, as shown in Figure 5.21.

A_{c2} = area of concrete fill in contact with the drypack, mm^2

F_{tu} = tensile strength of hollow-core slab at ultimate, magnified due to the load normal to the connection which is applied to the reduced cross-sectional area of the hollow-core assuming a complete loss of bond, MPa

F_{t2} = magnified tensile capacity of concrete fill due to applied load normal to connection, MPa

with A_{cu} = width of contact area x Σ web thickness of the webs of the hollow-core slab

For the type of hollow-core used in this investigation,

A_{cu} = (2 x 50 mm) x (2 x 50 + 5 x 40)
A_{cu} = $A_{c1}/4$

$F_{tu} = \sqrt{f_{t1}(f_{t1}+4\sigma_{n1})}$

$F_{t2} = \sqrt{f_{t2}(f_{t2}+\sigma_{n2})}$

The above model, proposed to predict the nominal capacity of connections supporting hollow-core slab at ultimate, is based on the same principles as the model proposed to predict the maximum nominal capacity of the hollow-core. However, at ultimate, the applied shear load is assumed to be distributed only along the width of the webs of the hollow-core slab as shown in Figure 5.21. This simplified shear stress distribution is verified by a finite element model used to simulate the test specimens without concrete fill in the cores of the hollow-core slab.

To study the effects of complete loss of bond, it is recommended to test additional specimens without concrete fill in the cores of the hollow-core.

The ultimate shear capacities predicted using the proposed models are compared with the experimental results, as presented in Figures 5.12 to 5.20 and in Table 5.2.

CHAPTER 6

SUMMARY AND CONCLUSIONS

6.1 SUMMARY

The main objective of this research program is to investigate the behavior of typical post-tensioned connections for precast concrete load-bearing shear wall panels, at various limit states, under static shear loading.

Nine prototype specimens were tested in this research program. The nine specimens consisted of three different joint configurations as follows:

HD series: hollow-core slab with drypack only

HP series: hollow-core slab and post-tensioning

PD series: post-tensioning with drypack only

To investigate the effects of gravity load, two different levels of load normal to the connection were used.

6.2 CONCLUSIONS

Based on the observations made and the data obtained during this experimental program, the following conclusions may be drawn:

1. An increase in the level of load normal to the horizontal connection increases the maximum shear capacity of the connection.
2. The effect of post-tensioning may be accounted for by adding the applied post-tensioning stresses to the gravity load normal to the connection.
3. For interior horizontal connections supporting hollow-core slab,

the failure mechanism could be controlled by shear friction resistance or by the shear capacity of the hollow-core slab. At a high level of normal load, the connection capacity is typically controlled by the shear capacity of the hollow-core slab, while at a lower normal load level, the connection capacity is typically controlled by shear friction.

4. For interior horizontal connections supporting hollow-core slab at high levels of normal load, the stiffness of the connection is reduced and the ductility of the connection is reduced in comparison to the same type of connection without hollow-core slab.

5. The maximum shear capacity of the connection supporting hollow-core slab is governed by the lower magnitude of the capacity predicted by the shear friction and the shear capacity of the hollow-core slabs. The predicted values were found to be in good agreement with the test results.

6. The ultimate shear capacity of the connection supporting hollow-core slab is based on complete loss of bond between the concrete fill in the cores and the precast hollow-core slab. The predicted values were found to provide a conservative lower bound in comparison with the test results.

6.3 SUGGESTIONS FOR FURTHER RESEARCH

Based on the experience gained in this research program, the following are some recommendations for possible further research in this area:

1. Tests should be conducted to investigate the capacity of

connections without concrete fill in the cores of the hollow-core slab to simulate complete loss of the bond between the hollow-core slab and the concrete fill.

2. Additional specimens similar to specimen 3HD8 should be tested to confirm the unique slip behavior observed at the interface of the concrete fill and the panel interface.

3. The behavior of post-tensioned horizontal connections, with and without hollow-core slab, should be investigated under reversed cyclic loading.

4. Research is needed to investigate the behavior of post-tensioned connections supporting hollow-core slab under combined flexural, shear, and axial loading.

REFERENCES

1. Hutchinson, R.L., "Test Results of Post-tensioned Horizontal Connections for Precast Load-Bearing Shear Wall Panels", technical report submitted to the Dept. of Civil Engineering, University of Manitoba, January, 1990.

2. Council on Tall Buildings and Urban Habitat, Structural Design of Tall Concrete and Masonry Buildings, American Society of Civil Engineers, Vol.CB, 1978.

3. Mattock, A.H., "A Survey of Precast Wall Systems", Proceedings of a Workshop on Design of Prefabricated Concrete Buildings for Earthquake Loads, Applied Technology Council, April 27 to 29, 1981, pp.253-276.

4. Foerster, H.R., "Behavior of the Connections Typically Used in Precast Concrete Load-Bearing Shear Wall Panels", a thesis presented to the University of Manitoba in partial fulfillment of the requirements for the degree of Master of Science in Civil Engineering, June, 1987.

5. Canadian Prestressed Concrete Institute (CPCI), "Metric Design Manual", Ottawa, Ontario, 1987.

6. American Concrete Institute (ACI), "Building Code Requirements for Reinforced Concrete (ACI 318M-83)", Detroit, Michigan, 1984.

7. Prestressed Concrete Institute (PCI), "PCI Design Handbook", Chicago, Illinois, 1978.

8. Harris, H.G., and Iyengar, S., "Full-Scale Tests on Horizontal Joints of Large Panel Precast Concrete Buildings", PCI Journal, Vol.25, No.2, March-April, 1980, pp.72-92.

9. Harris, H.G., and Abboud, B.E., "Cyclic Shear Behavior of Horizontal Joints in Precast Concrete Large Panel Buildings", Proceedings of a Workshop on Design of Prefabricated Concrete Buildings for Earthquake Loads, Applied Technology Council, April 27-29, 1981, pp.403-438.

10. Harris, H.G., Abboud, B.E., and Wang, G.J.J., "Performance of Wet Horizontal Joints and Simple Shear Walls in Precast Concrete Large Panel Buildings Under Earthquake Loading", Proceedings of the 7th European Conference on Earthquake Engineering, Athens, Greece, 1982, pp.123-133.

11. PCI Committee on Precast Bearing Wall Buildings, "Considerations for the Design of Precast Concrete Bearing Wall Buildings to Withstand Abnormal Loads", PCI Journal, Vol.21, No.2, March-April 1976, pp.18-51.

12. Hanson, N.W., and Johal, L.S., "Design for Vertical Load on Horizontal Connections in Large Panel Structures", PCI Journal, Vol.27, No.1, January-February 1982, pp.63-79.

13. Canadian Standards Association (CSA), "Design of Concrete Structures for Buildings (CAN3-A23.3-M84)", Rexdale, Ontario, 1984.

14. Johal, L.S., et al., Design and Construction of Large Panel Structures, Office of Policy Development and Research, Department of Housing and Urban Development, Washington, D.C., January, 1979.

15. Canadian Standards Association (CSA), "Concrete Materials and Methods of Concrete Construction (CAN3-A23.1-M77)", Rexdale, Ontario, 1977.

16. Soroka, I., Portland Cement Paste and Concrete, Chemical Publishing Co., Inc., New York, New York, 1979.

17. Serrette, R.L., "Multiple Shear Key Connections For Load-bearing Shear Wall Panels", a thesis presented to the University of Manitoba in partial fulfillment of the requirements for the degree of Master of Science in Civil Engineering, August, 1988.

Table 2.1 Coefficients of Friction

Type of Surface	Friction Coefficient		
	ACI	PCI	CPCI
Cracked monolithic concrete	1.4	1.4	1.25
Intentionally roughened	1.0	1.0	0.9
Not intentionally roughened	0.6	0.4	0.5
Bearing pad to concrete	-	-	0.4

λ = 1.0 for normal density concrete
λ = 0.75 for structural low density concrete

Table 3.1 Test Specimens

Connection Configuration		Normal Load Level (MPa)	Specimen Mark
With Hollow-core Slab	Drypack only	4	1HD4
		8	2HD8
		8	3HD8
	Post-tensioned	4	4HP4
		8	5HP8
		8	6HP8
Drypack Only	Post-tensioned	4	7PD4
		8	8PD8
		8	9PD8

Table 4.1 Concrete Strength of Panels

Specimen	Compressive Strength at Time of Testing (MPa)
1HD4	40.9
2HD8	41.3
3HD8	39.7
4HP4	34.1
5HP8	38.8
6HP8	37.6
7PD4	38.1
8PD8	46.2
9PD8	37.8

Table 4.2 Concrete Fill Strength

Specimen	Compressive Strength at Time of Testing	
	Prism Strength (MPa)	Equivalent Cylinder Strength (MPa)
1HD4	61.3	55.7
2HD8	49.6	45.1
3HD8	61.7	56.1
4HP4	57.5	52.3
5HP8	45.2	41.1
6HP8	58.6	53.3

Table 4.3 Drypack Strength

Specimen	Compressive Strength at Time of Testing (MPa)	
	Cube Strength	Equivalent Cylinder Strength
1HD4	18.7	13.7
2HD8	18.3	13.4
3HD8	20.2	14.7
4HP4	21.4	15.6
5HP8	19.6	14.3
6HP8	17.4	12.7
7PD4	13.4	9.7
8PD8	13.5	9.7
9PD8	15.8	11.5

Table 4.4 Post-tensioning Duct Grout Strength

Specimen	Compressive Strength at Time of Testing (MPa)
4HP8	15.8
5HP8	18.1
6HP8	13.5
7PD4	11.4
8PD8	15.2
9PD8	13.8

Table 4.5 Summary of Experimental Shear Capacities

Joint Type	Normal Load (MPa)	Specimen	Maximum Load (kN)	Ultimate Load (kN)
HD	4	1HD4	550	535
	8	2HD8	905	750
	8	3HD8	885	675
HP	4	4HP4	704	660
	8	5HP8	957	680
	8	6HP8	947	880
PD	4	7PD4	690	680
	8	8PD8	1160	1130
	8	9PD8	1157	1125

Table 4.6 Specimen 1HD4 Load vs Slip Values

Applied Shear Load (kN)	Relative Slip Between Panels (mm)
0	0.00
100	0.00
200	0.00
300	0.05
400	0.10
450	0.15
500	0.29
525	0.45
546	0.66
548	1.22
550	1.86
534	2.92
534	3.50
537	4.57
533	5.60
536	6.69
533	8.53
526	10.52

Table 4.7 Specimen 2HD8 Load vs Slip Values

Applied Shear Load (kN)	Relative Slip Between Panels (mm)
0	0.0
100	0.0
200	0.0
300	0.0
400	0.0
500	0.1
600	0.1
700	0.2
800	0.4
850	0.5
889	0.8
893	0.9
902	1.2
844	5.2
844	5.9
844	6.4
761	9.2
751	10.4
734	11.3
726	11.7
719	12.0

Table 4.8 Specimen 3HD8 Load vs Slip Values

Applied Shear Load (kN)	Relative Slip Between Panels (mm)
0	0.0
200	0.0
300	0.0
600	0.0
700	0.1
800	0.1
850	0.2
874	0.2
877	0.2
885	0.3
722	2.1
708	2.7
695	2.7
689	3.1
688	3.2
680	3.4
676	3.5
675	3.6
652	4.0
650	5.1
665	6.9
707	9.9
725	12.9

Table 4.9 Specimen 4HP4 Load vs Slip Values

Applied Shear Load (kN)	Relative Slip Between Panels (mm)
0	0.0
100	0.0
200	0.0
300	0.0
400	0.0
500	0.1
600	0.1
650	0.2
677	0.3
694	0.5
703	0.6
703	0.8
704	0.8
665	1.5
645	2.2
650	2.7
655	3.9
670	5.4
670	7.1
655	10.2
645	12.2

Table 4.10 Specimen 5HP8 Load vs Slip Values

Applied Shear Load (kN)	Relative Slip Between Panels (mm)
0	0.0
100	0.0
200	0.0
300	0.0
400	0.1
500	0.1
600	0.1
700	0.1
800	0.2
900	0.3
940	0.5
950	0.7
957	0.8
914	1.2
895	1.5
895	2.0
850	2.7
841	3.7
680	5.2

Table 4.11 Specimen 6HP8 Load vs Slip Values

Applied Shear Load (kN)	Relative Slip Between Panels (mm)
0	0.0
100	0.0
200	0.0
300	0.0
400	0.0
500	0.1
600	0.1
700	0.2
800	0.3
900	0.5
932	0.8
935	1.2
940	1.5
947	1.9
946	2.2
945	2.5
900	4.5
880	5.3
855	6.2

Table 4.12 Specimen 7PD4 Load vs Slip Values

Applied Shear Load (kN)	Relative Slip Between Panels (mm)
0	0.0
100	0.0
200	0.0
300	0.0
400	0.0
500	0.0
600	0.1
650	0.2
670	0.3
675	0.5
685	0.6
690	0.8
690	1.0
690	1.2
690	1.4
690	1.6
690	1.8
690	1.9
690	2.1
690	2.3
677	2.8
677	3.4
677	3.7
684	4.5
680	5.5
708	8.7
719	14.0

Table 4.13 Specimen 8PD8 Load vs Slip Values

Applied Shear Load (kN)	Relative Slip Between Panels (mm)
0	0.0
100	0.0
200	0.0
300	0.0
400	0.0
500	0.0
550	0.0
600	0.0
650	0.1
700	0.1
750	0.1
800	0.1
850	0.1
900	0.1
950	0.2
1000	0.2
1050	0.3
1080	0.3
1100	0.4
1130	0.6
1150	0.8
1160	0.9
1150	1.3
1145	2.6
1140	4.4
1130	6.0
1126	7.0
1125	8.0
1111	9.7
1100	12.1
1060	16.4

Table 4.14 Specimen 9PD8 Load vs Slip Values

Applied Shear Load (kN)	Relative Slip Between Panels (mm)
0	0.0
100	0.0
200	0.0
300	0.0
400	0.1
500	0.1
600	0.1
700	0.1
800	0.2
900	0.2
950	0.2
1000	0.3
1050	0.4
1100	0.9
1145	1.1
1156	1.3
1152	1.5
1157	1.7
1157	1.9
1125	2.8
1125	4.0
1125	4.8
1115	5.9
1110	8.1
1100	11.0
1085	13.3
1075	14.7

Table 5.1 Maximum Shear Capacity: Model Predictions vs Experimental Results

Specimen	Hollow-Core Capacity (kN)	Shear Friction (kN)	Maximum Shear Capacity (kN)	Test Results (kN)	RATIO: Model / Results
1HD4	725	504	504	550	0.92
2HD8	881	1008	881	905	0.97
3HD8	881	1008	881	885	1.00
4HP4	774	655	655	704	0.93
5HP8	921	1160	921	957	0.96
6HP8	921	1160	921	947	0.97
7PD4	-	655	655	690	0.95
8PD8	-	1160	1160	1160	1.00
9PD8	-	1160	1160	1157	1.00

Table 5.2 Ultimate and Partially Cracked Shear Capacity: Model Predictions vs Experimental Results

Specimen	Partially Cracked Prediction (kN)	Ultimate Capacity Prediction (kN)	Ultimate Test Results (kN)	RATIO: Ult. Model / Ult. Results
1HD4	-	433	535	0.81
2HD8	639	549	750	0.73
3HD8	851	549	675	0.81
4HP4	-	471	660	0.71
5HP8	692	579	680	0.85
6HP8	670	579	880	0.66
7PD4	-	655	680	0.96
8PD8	-	1160	1130	1.03
9PD8	-	1160	1125	1.03

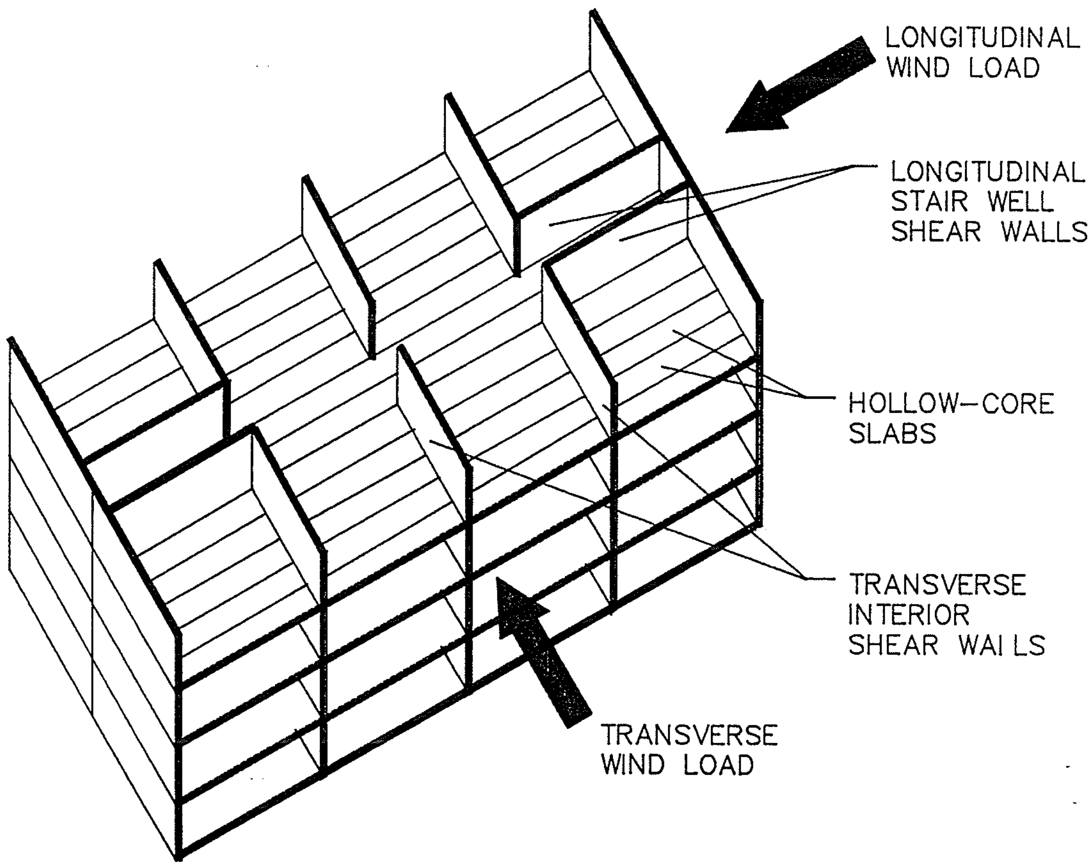

Figure 1.1 Load-Bearing Shear Wall Panel System

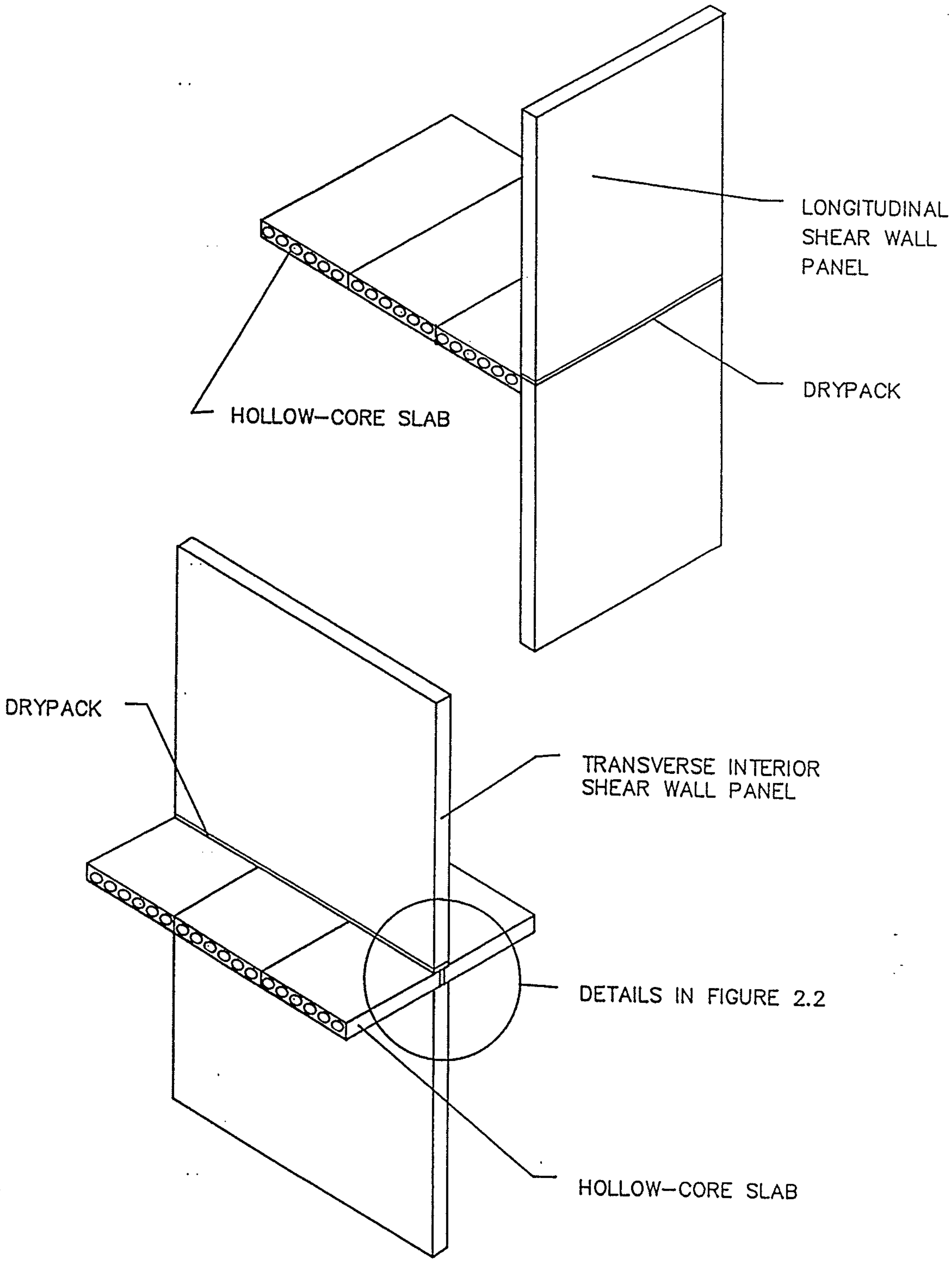

Figure 1.2 Horizontal Connections for Longitudinal and Transverse Shear Walls

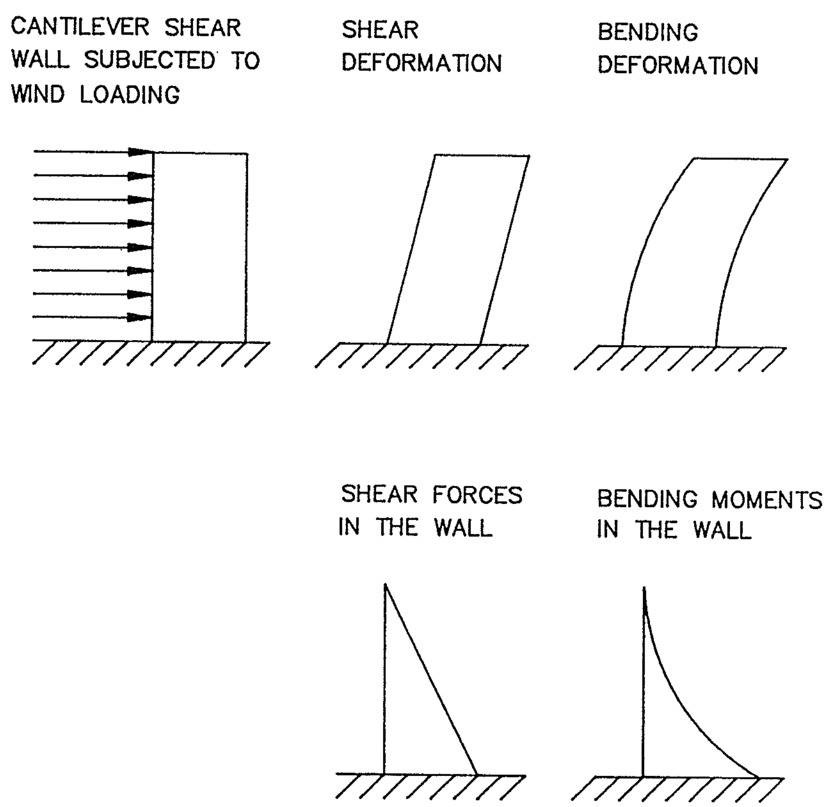

Figure 2.1 Cantilever Shear Walls Subjected to Lateral Load

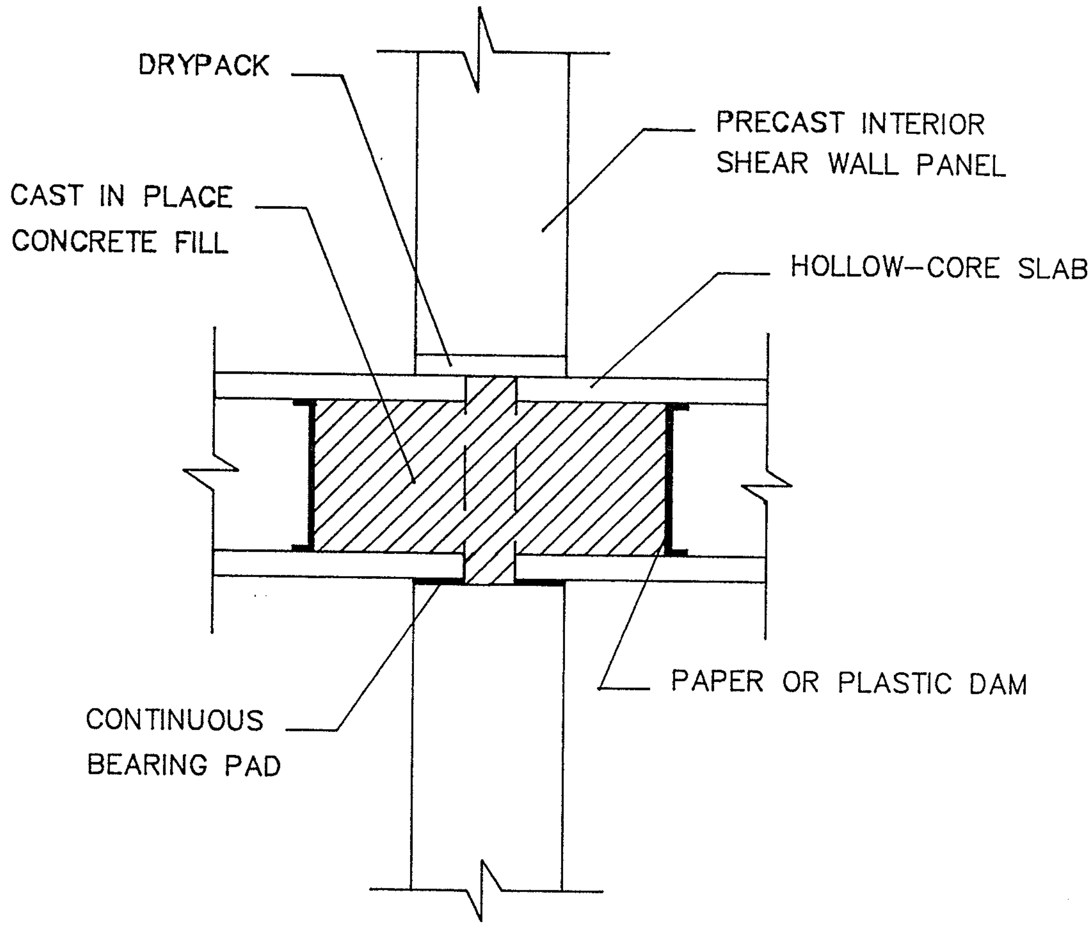

Figure 2.2 a) Typical North American Horizontal Joint With Hollow-Core Slab

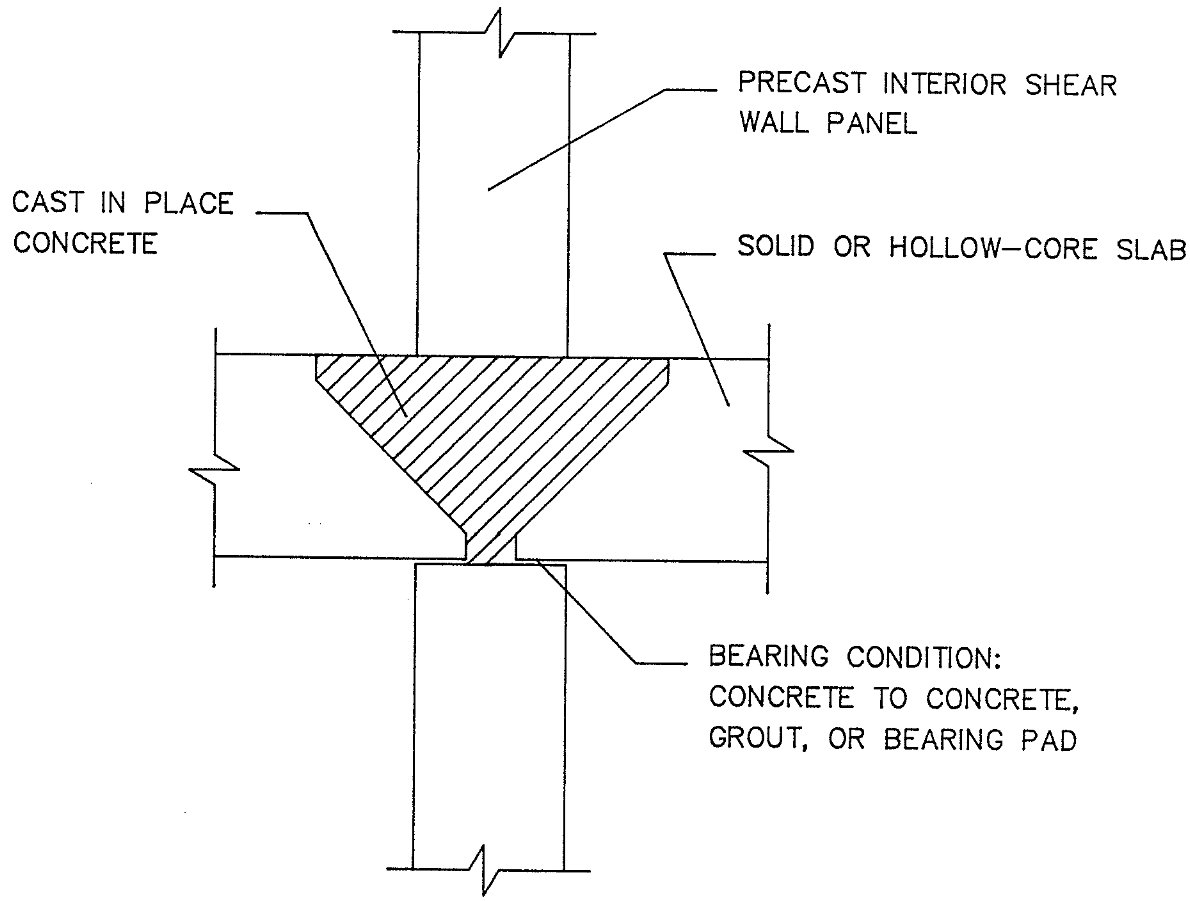

Figure 2.2 b) Typical European Horizontal Joint With Hollow-Core Slab

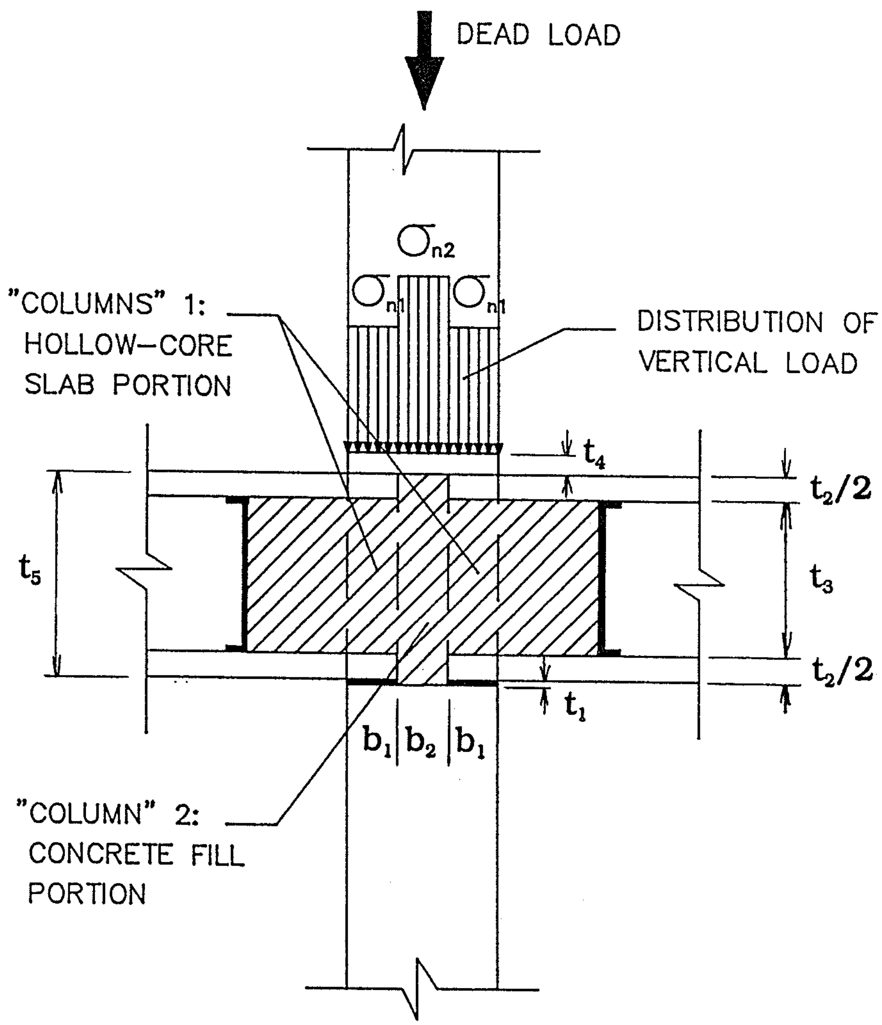

Figure 2.3 Distribution of Vertical Load at Horizontal Connection

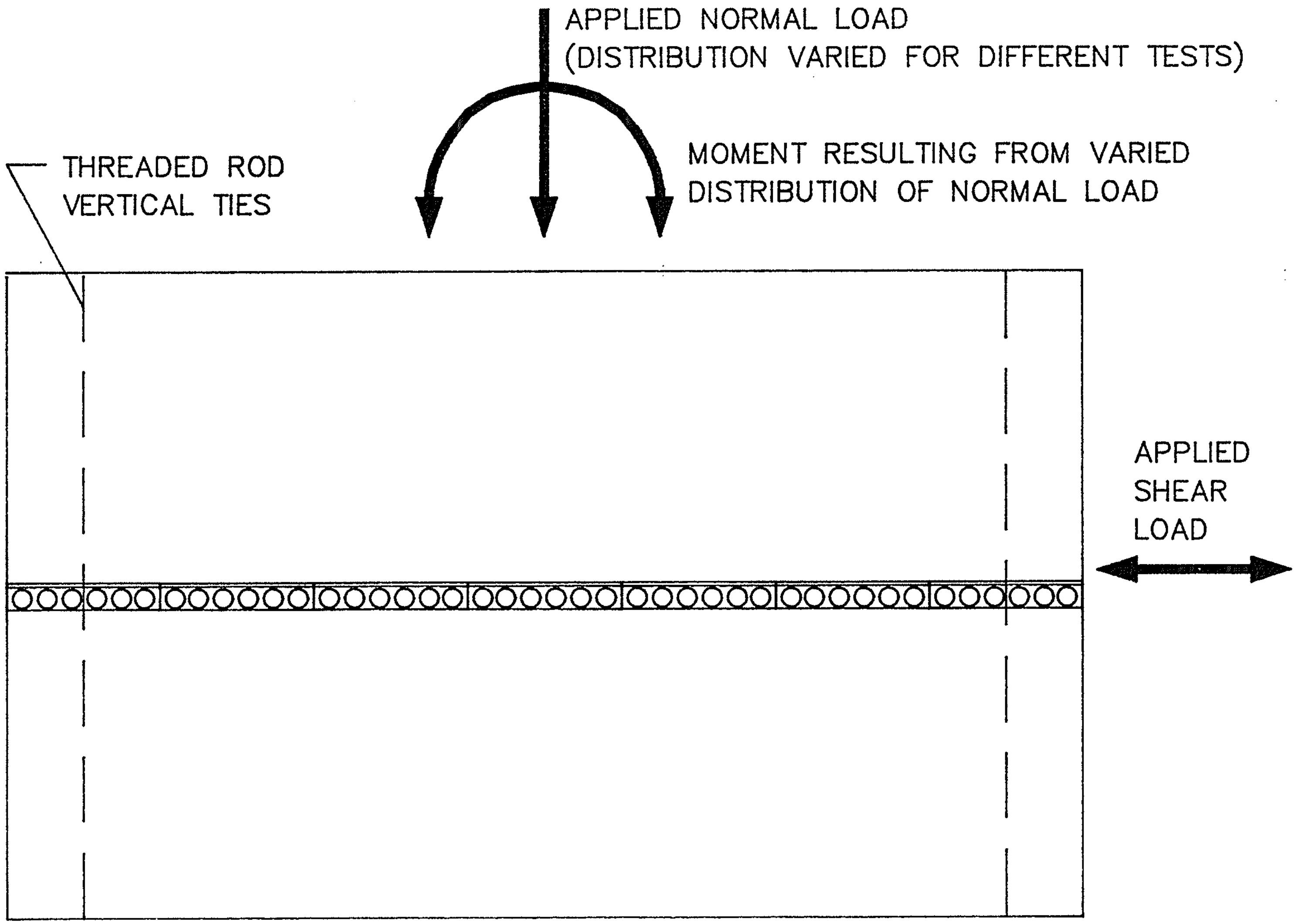

3/32 SCALE MODEL SPECIMEN

Figure 2.4 Test Specimen Used by Harris et. al.

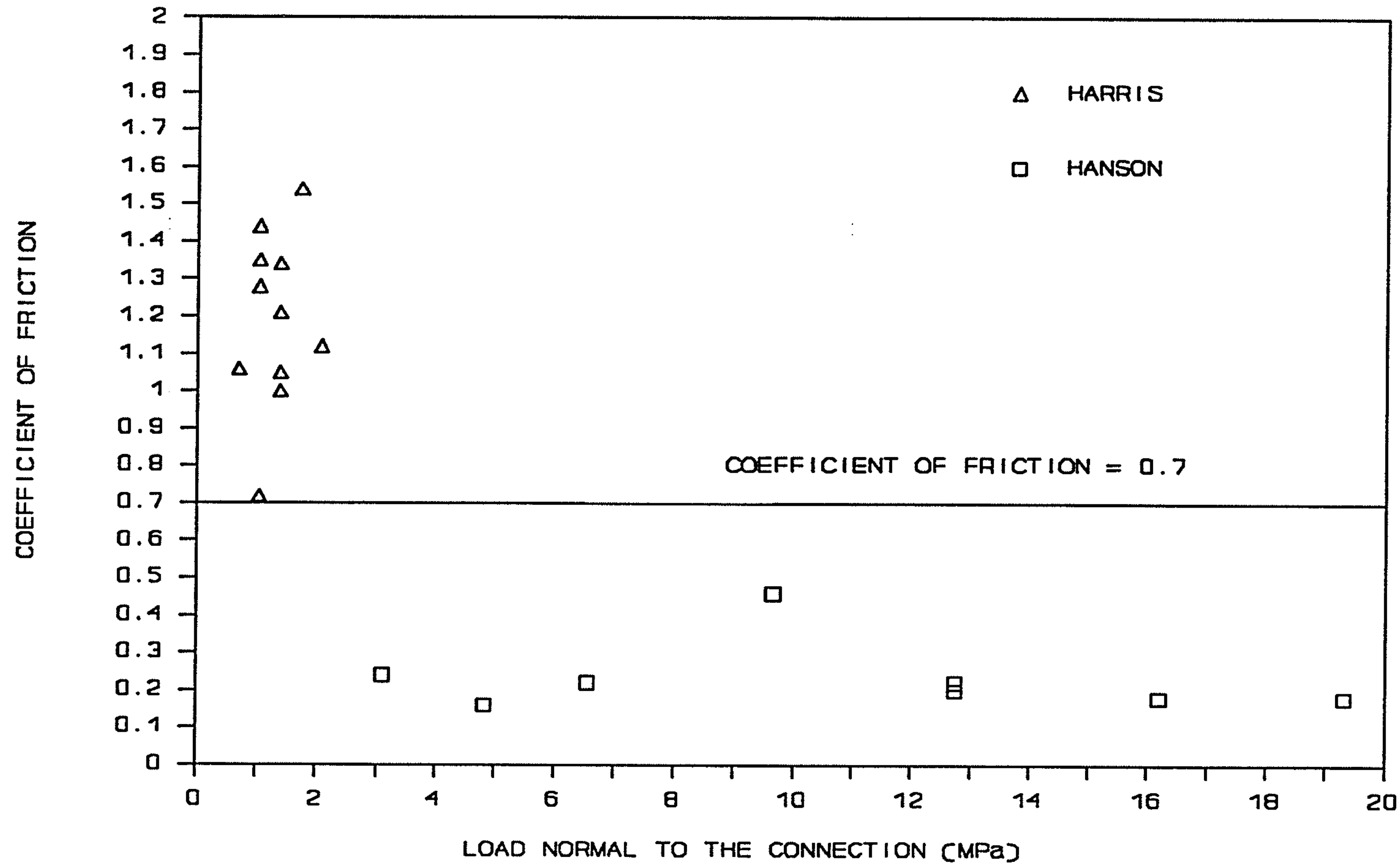

Figure 2.5 Comparison of Shear Friction Coefficients

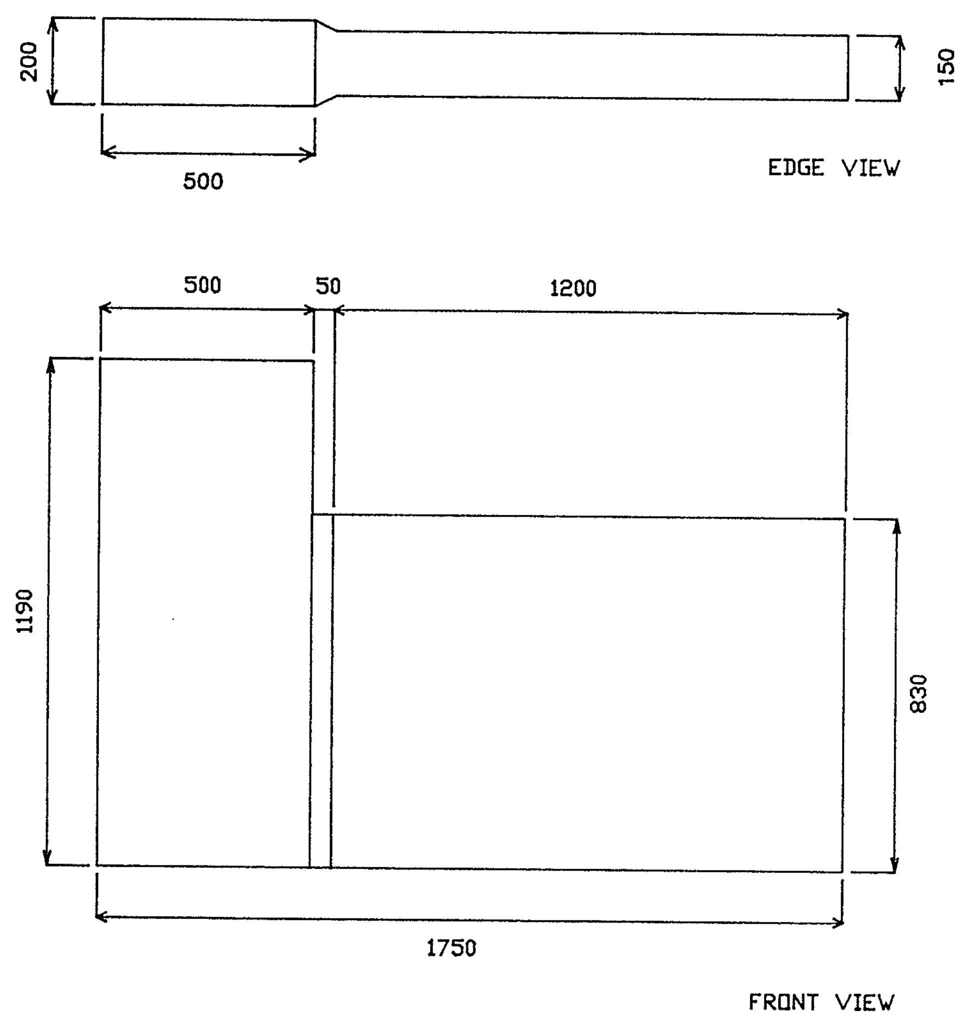

Figure 3.1 Panel Dimensions

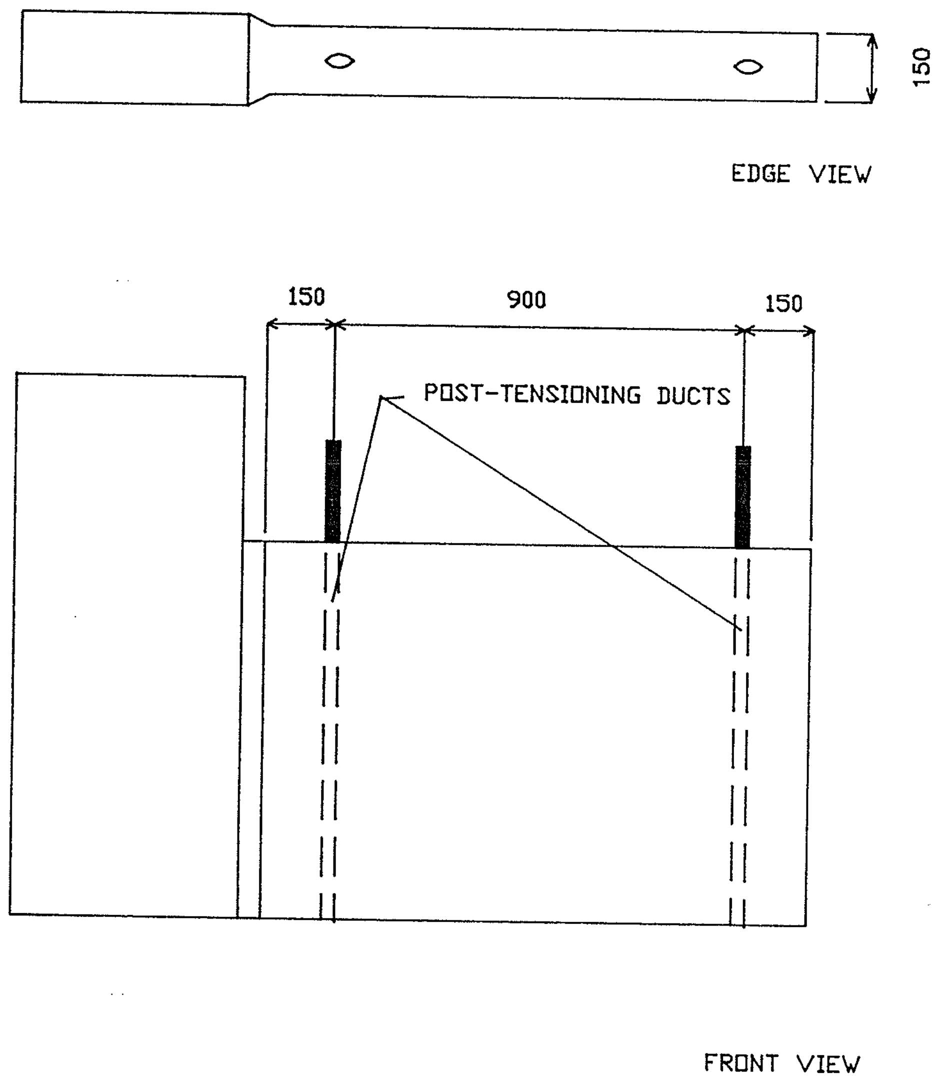

Figure 3.2 Post-tensioning Duct Location

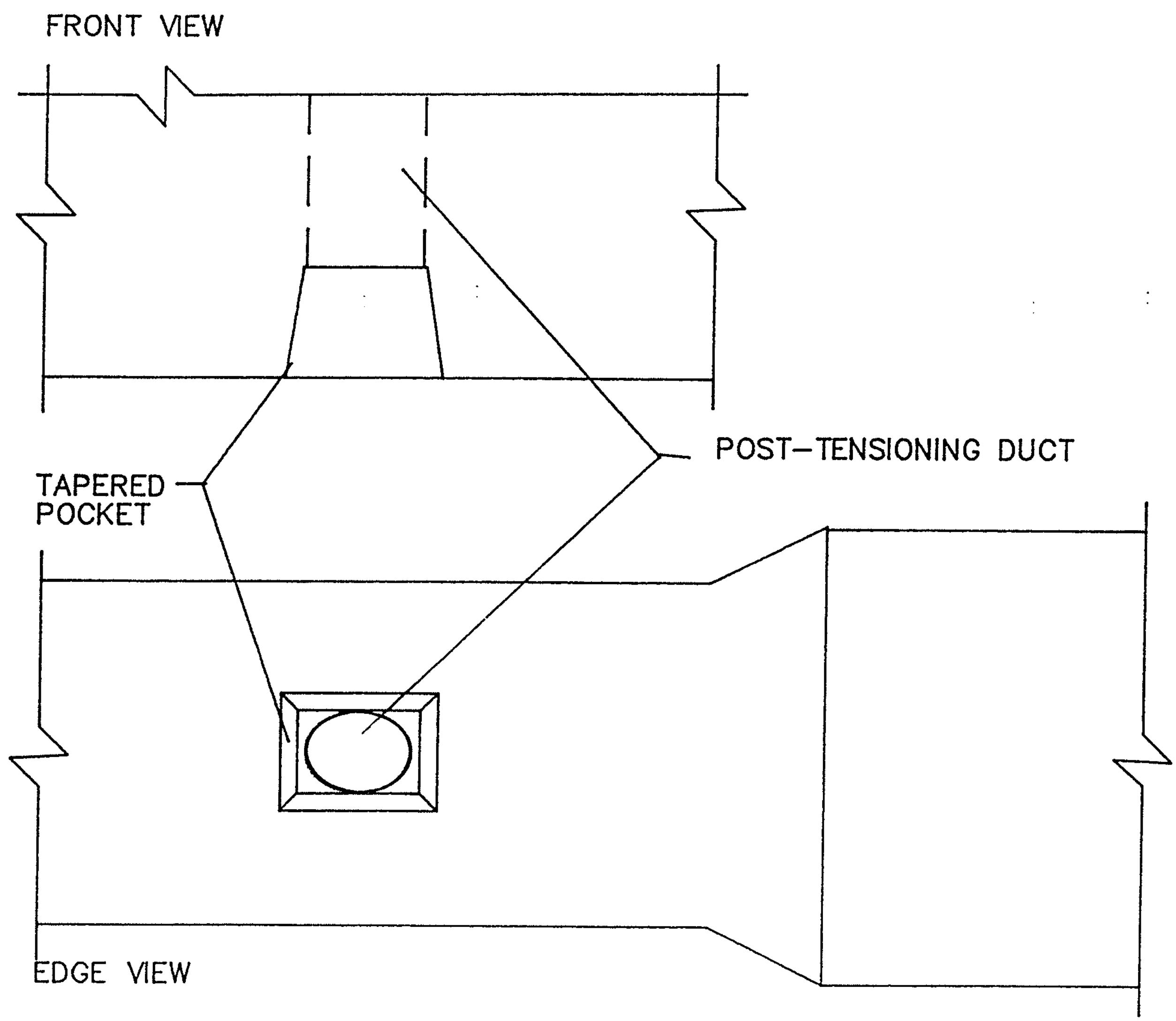

Figure 3.3 . Pockets for Coupling of Post-tensioning Ducts

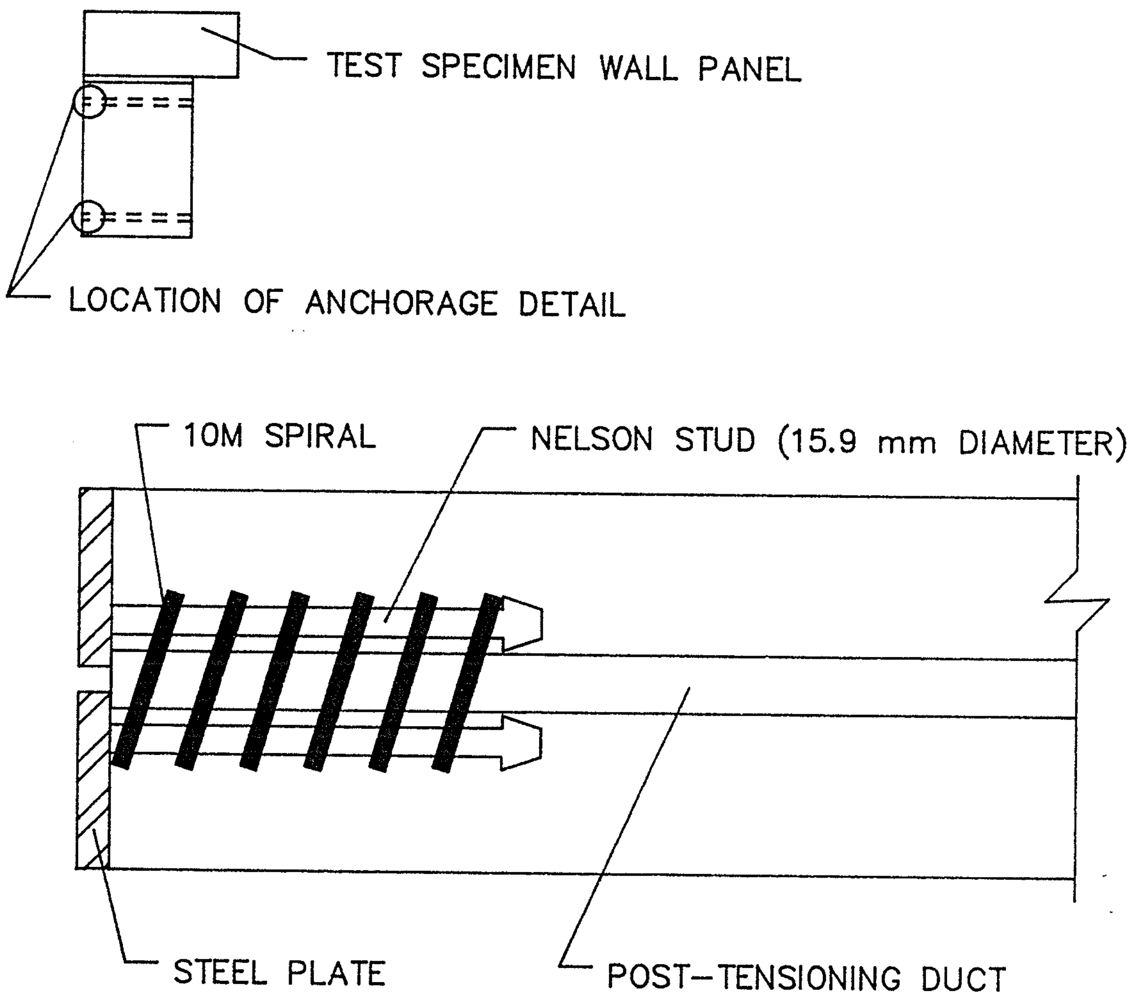

Figure 3.4 Post-tensioning Anchorage Detail

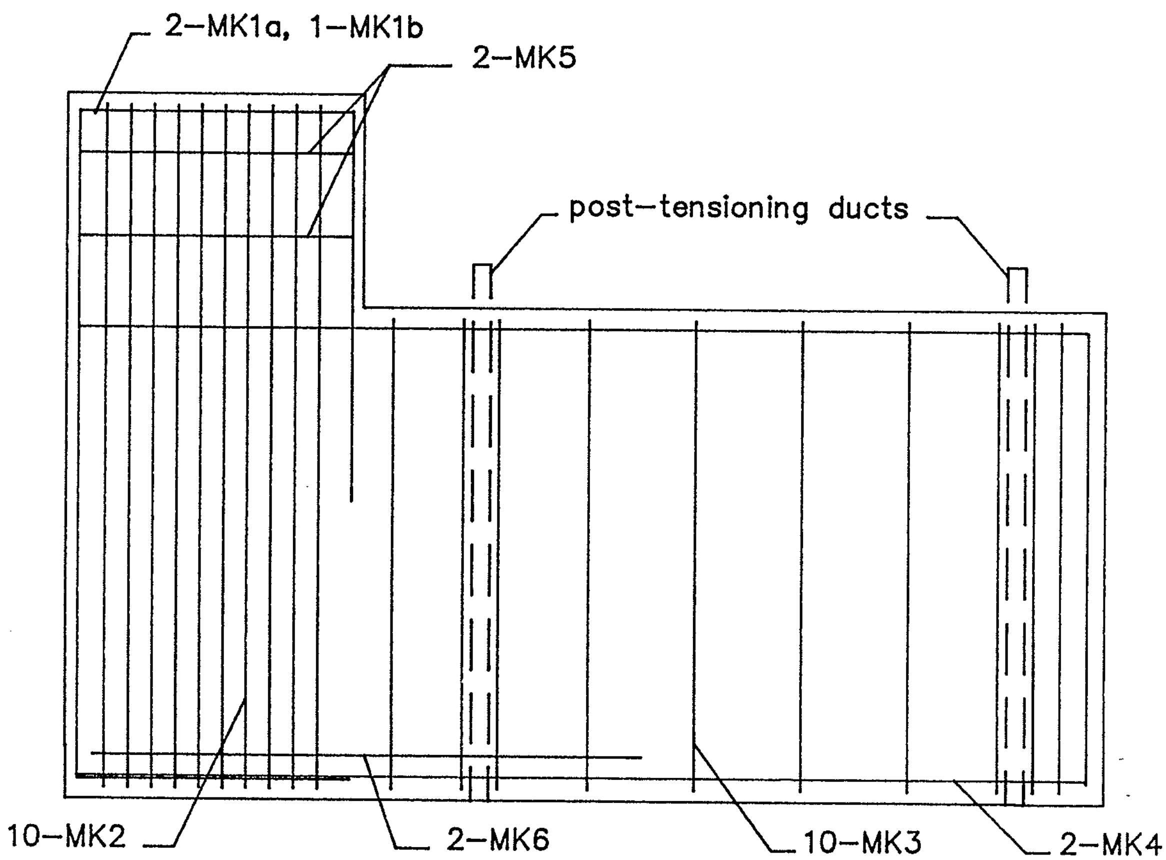

Figure 3.5 Specimen Reinforcement

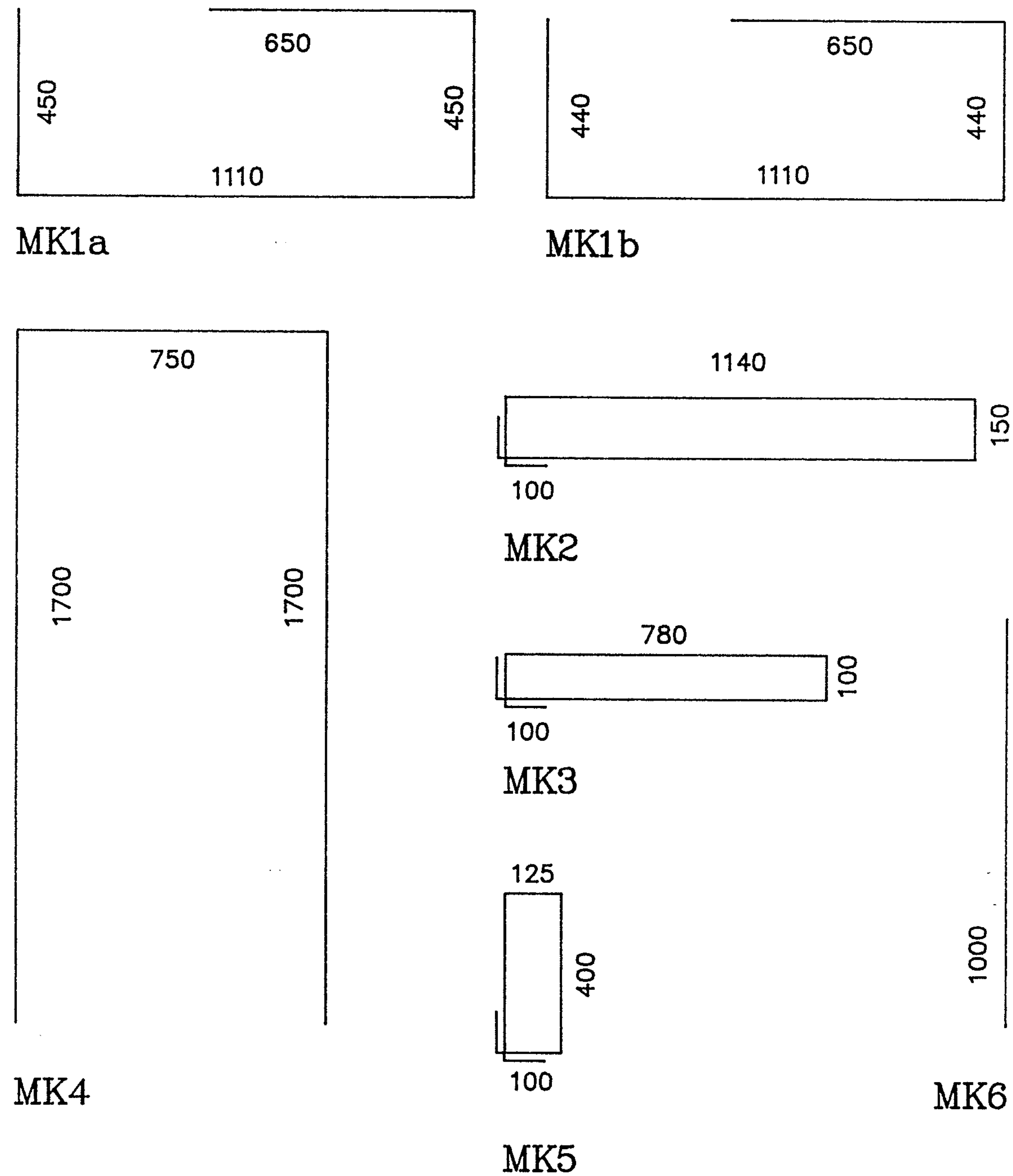

Figure 3.6 Reinforcement Details

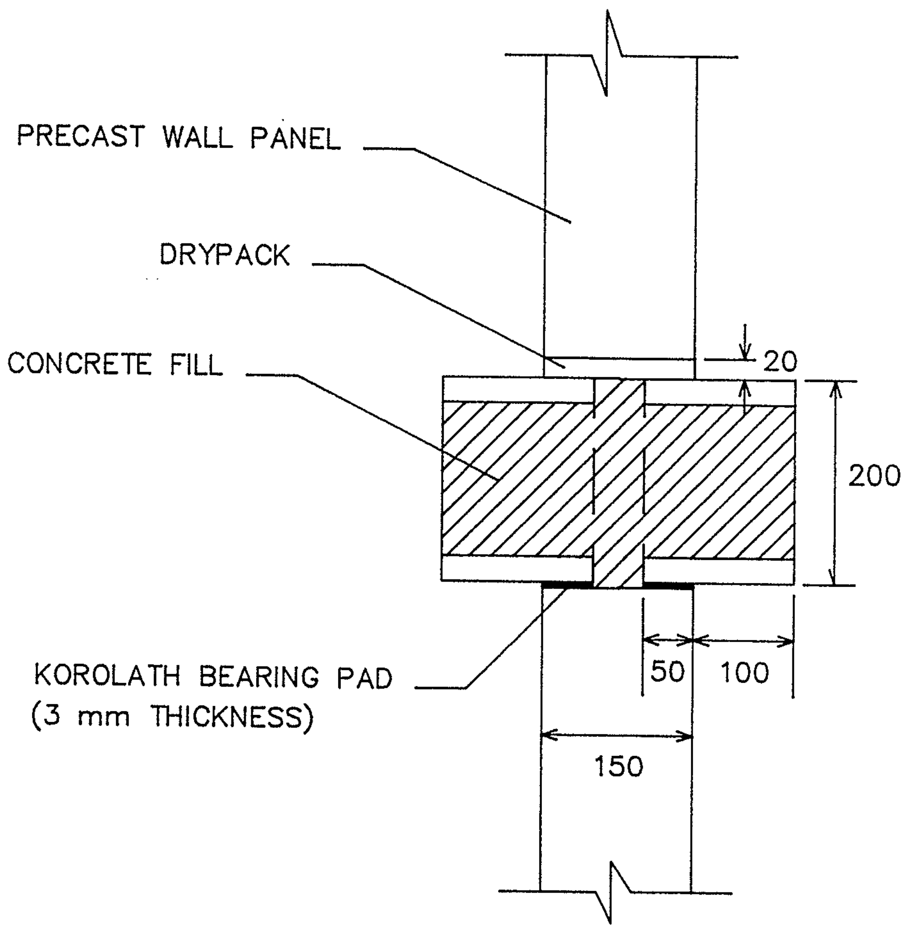

Figure 3.7 a) Connection Configuration: HD Series

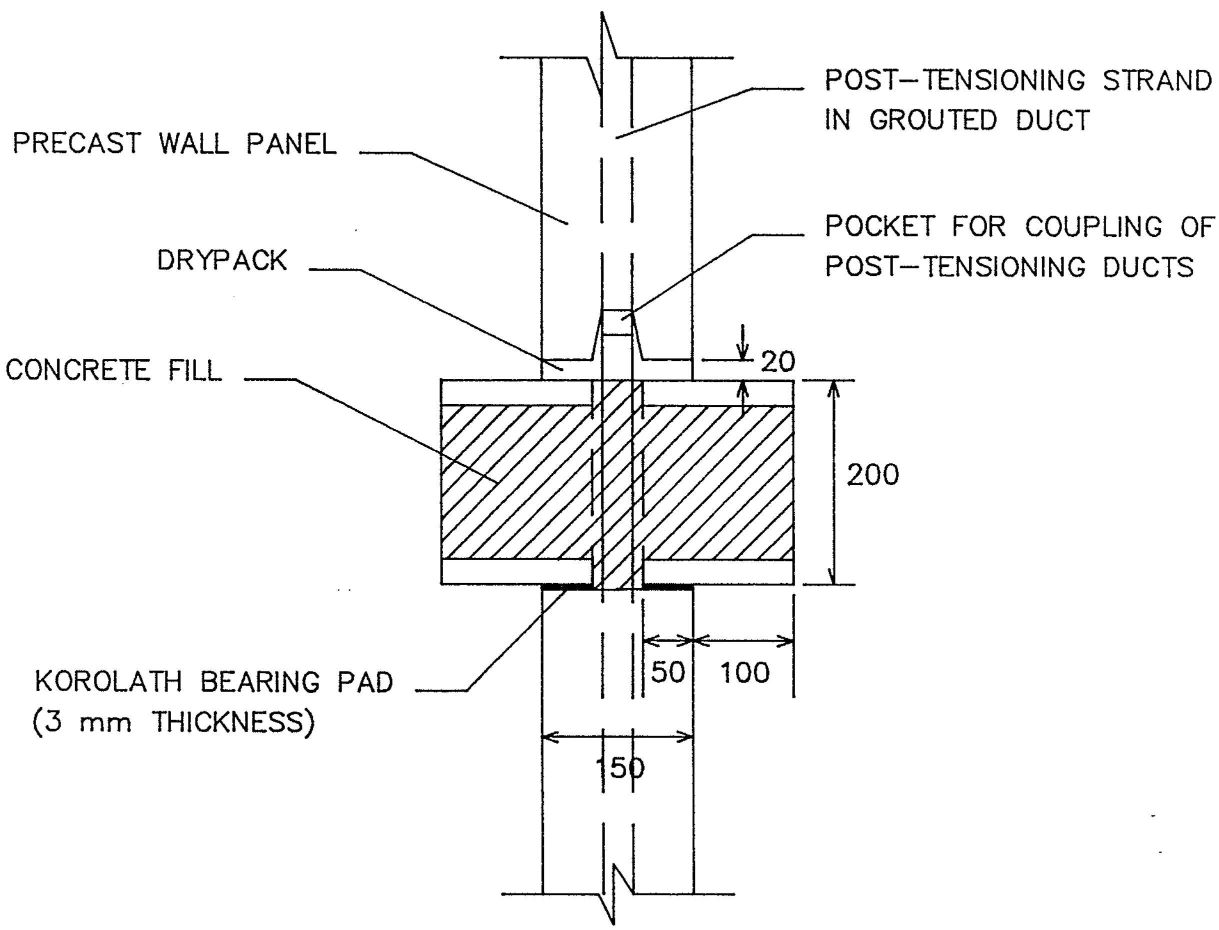

Figure 3.7 b) Connection Configuration: HP Series

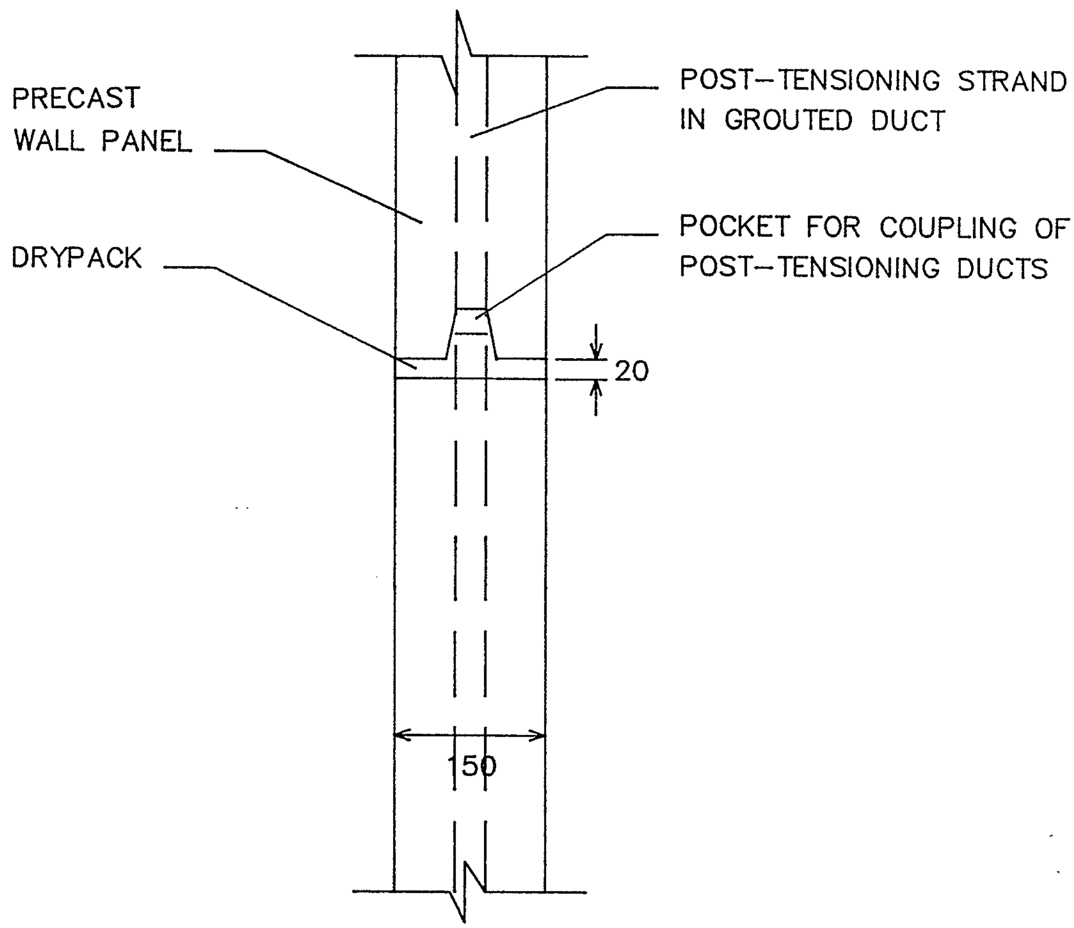

Figure 3.7 c) Connection Configuration: PD Series

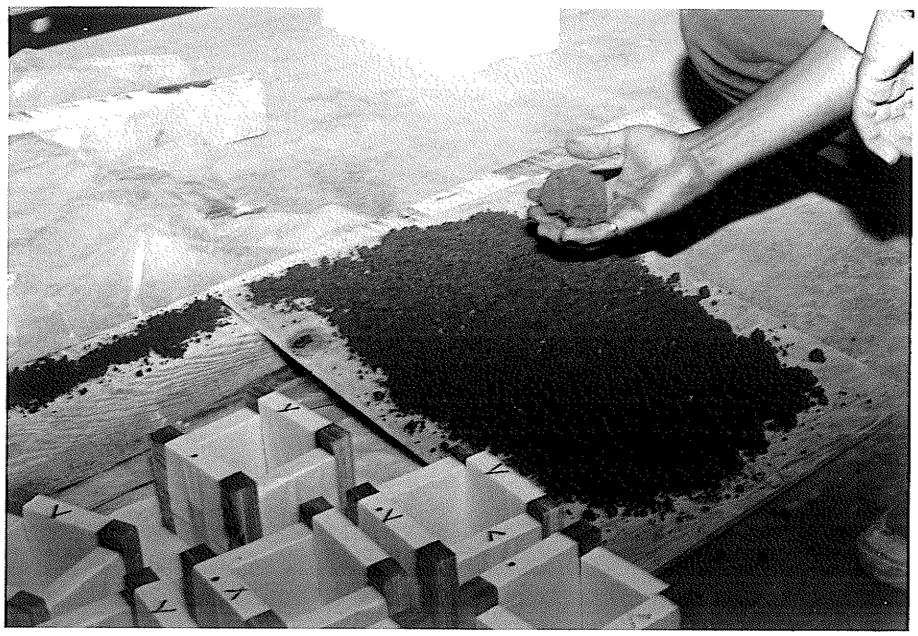

Figure 3.8 Drypack Consistency

Figure 3.9 Expansive Characteristic of Post-tensioning Duct Grout

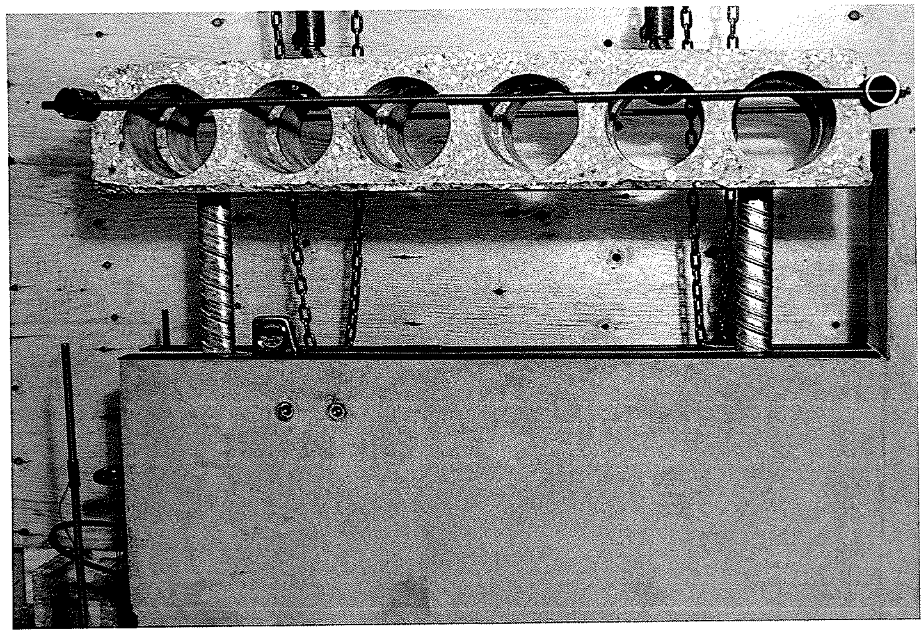

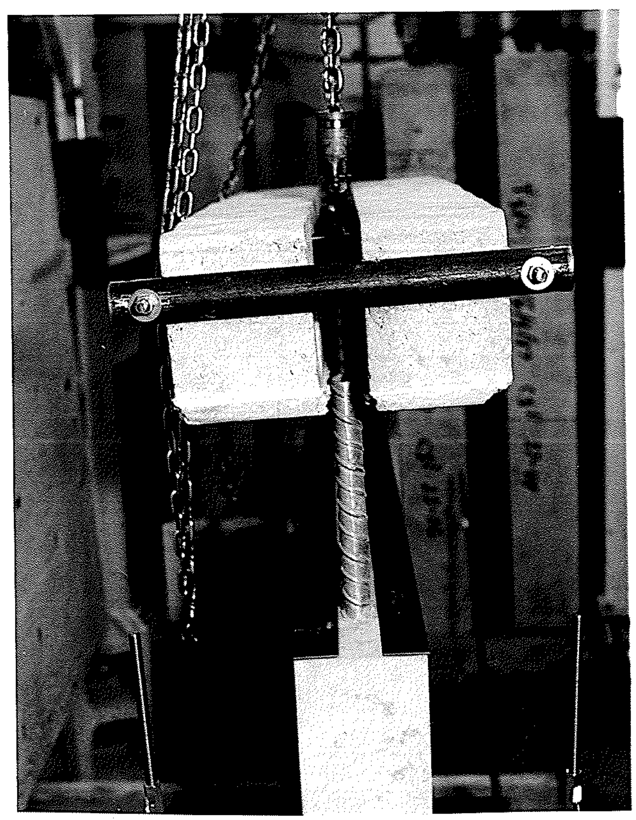

Figure 3.10 Specimen Assembly: Positioning of Hollow-core Slab on Bottom Wall Panel

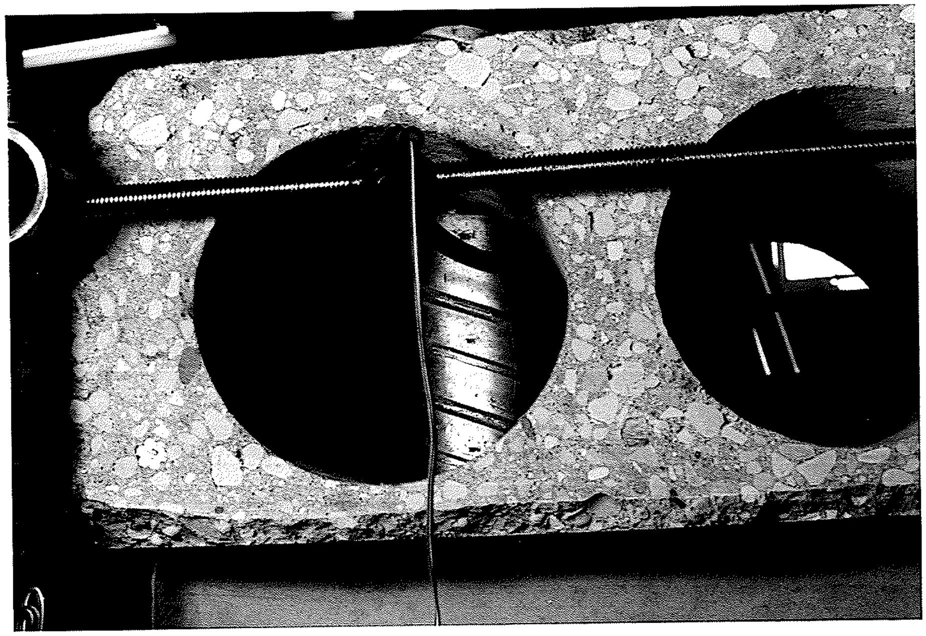

Figure 3.11 Hollow-core Slab Loading Apparatus

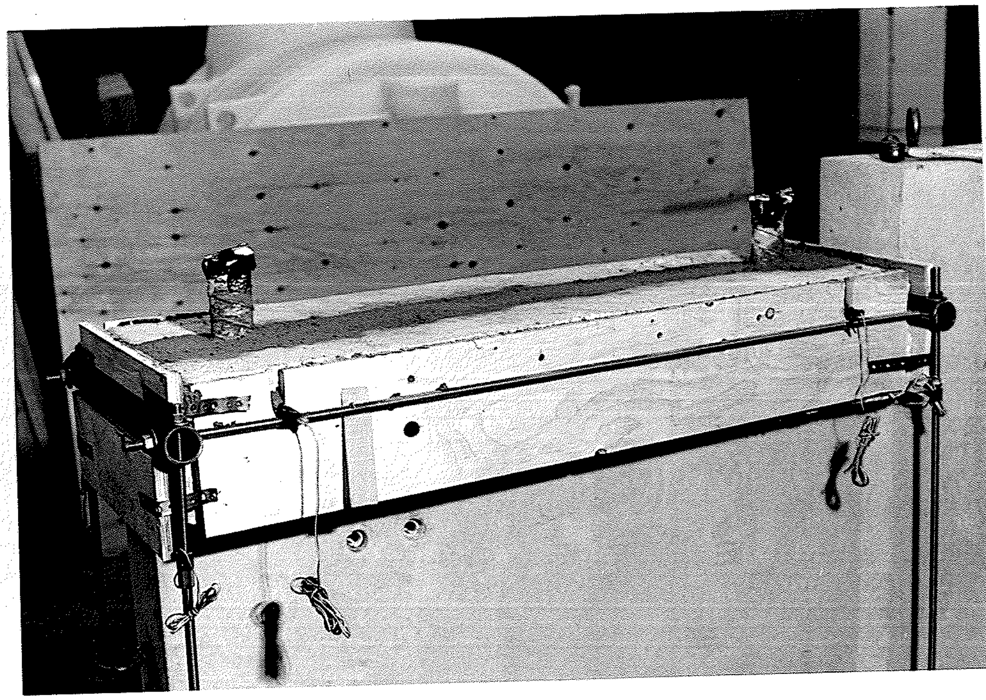

Figure 3.12 Concrete Fill Cast in Hollow-core Slab

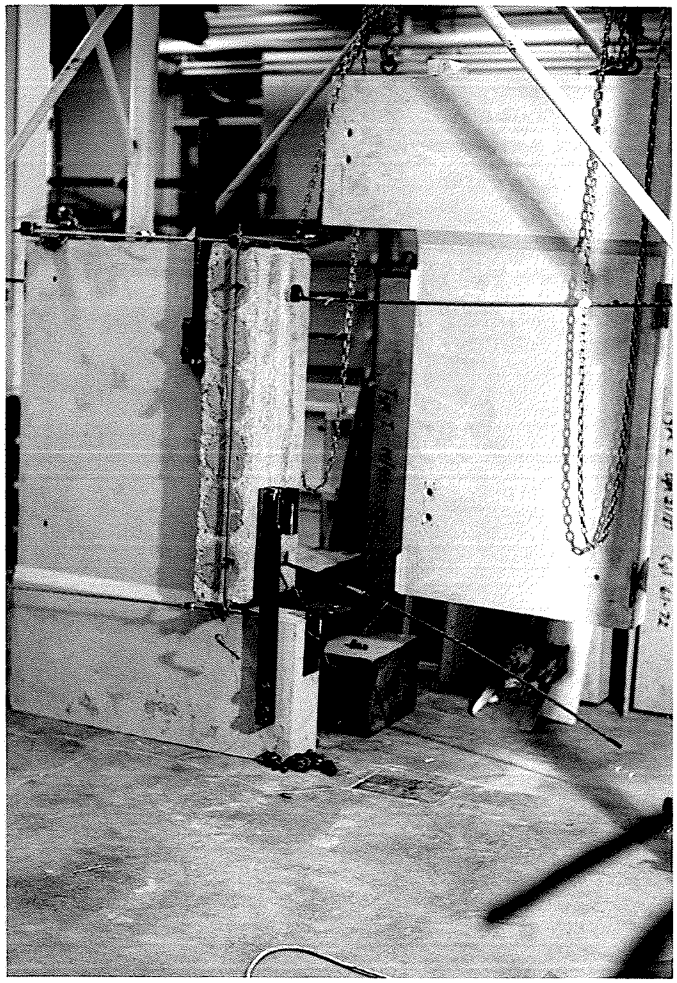

Figure 3.13 Specimen Assembly: Postitioning of Top Wall Panel

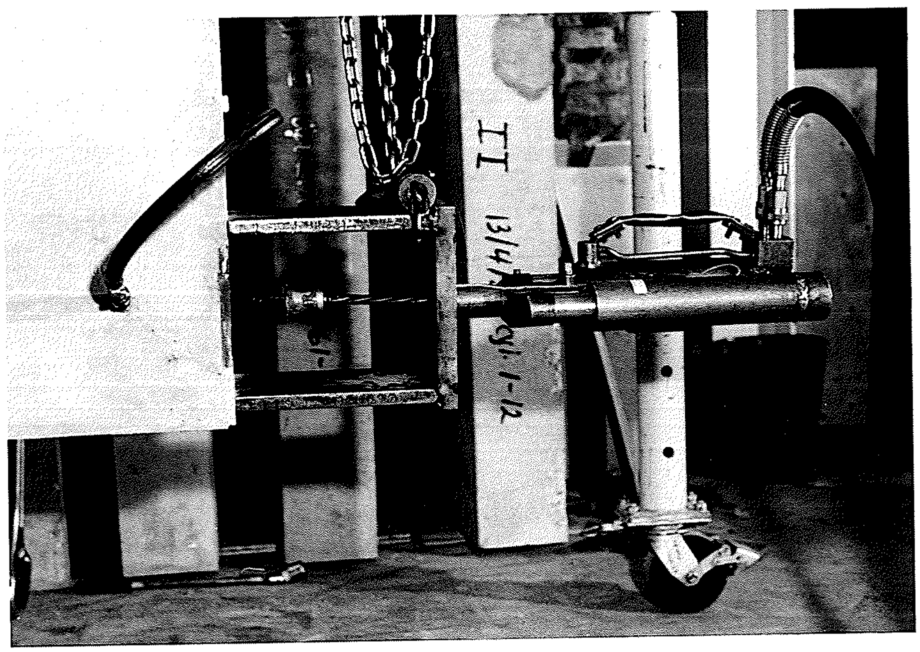

Figure 3.14 Post-tensioning with Hydraulic Jack

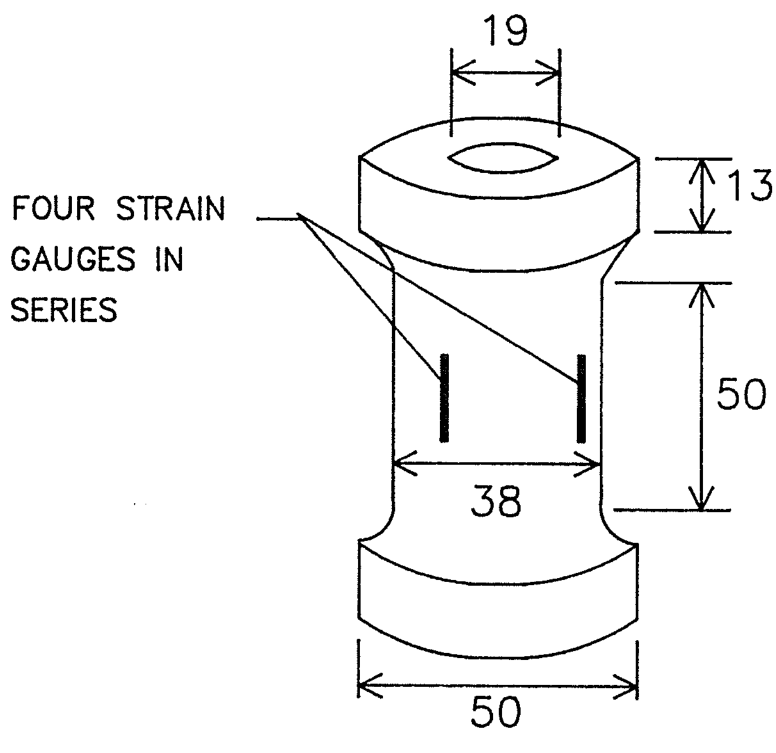

Figure 3.15 a) Calibrated Post-tensioning Load Cell Details

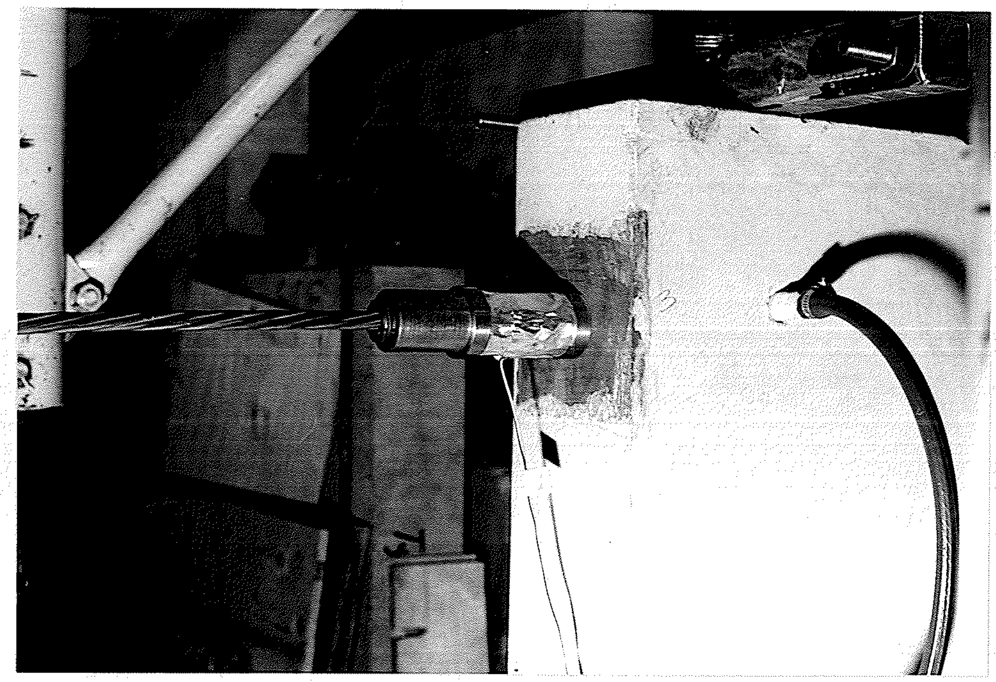

Figure 3.15 b) Location of Post-tensioning Load Cell on Specimen

Figure 3.16 Typical Measurement Station with Dial Gauges

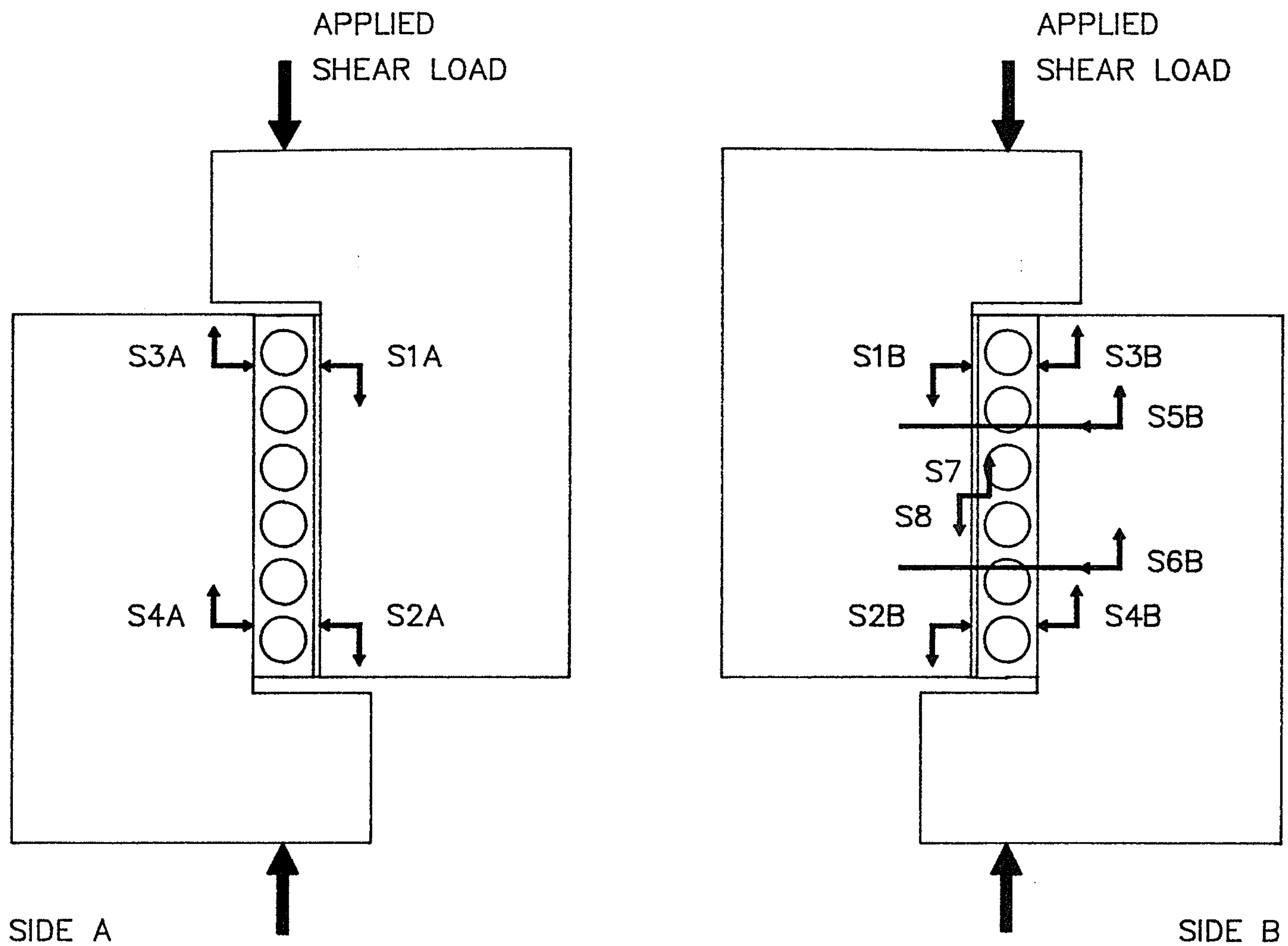

Figure 3.17 Location of Measurement Stations on Specimens With Hollow-core Slab

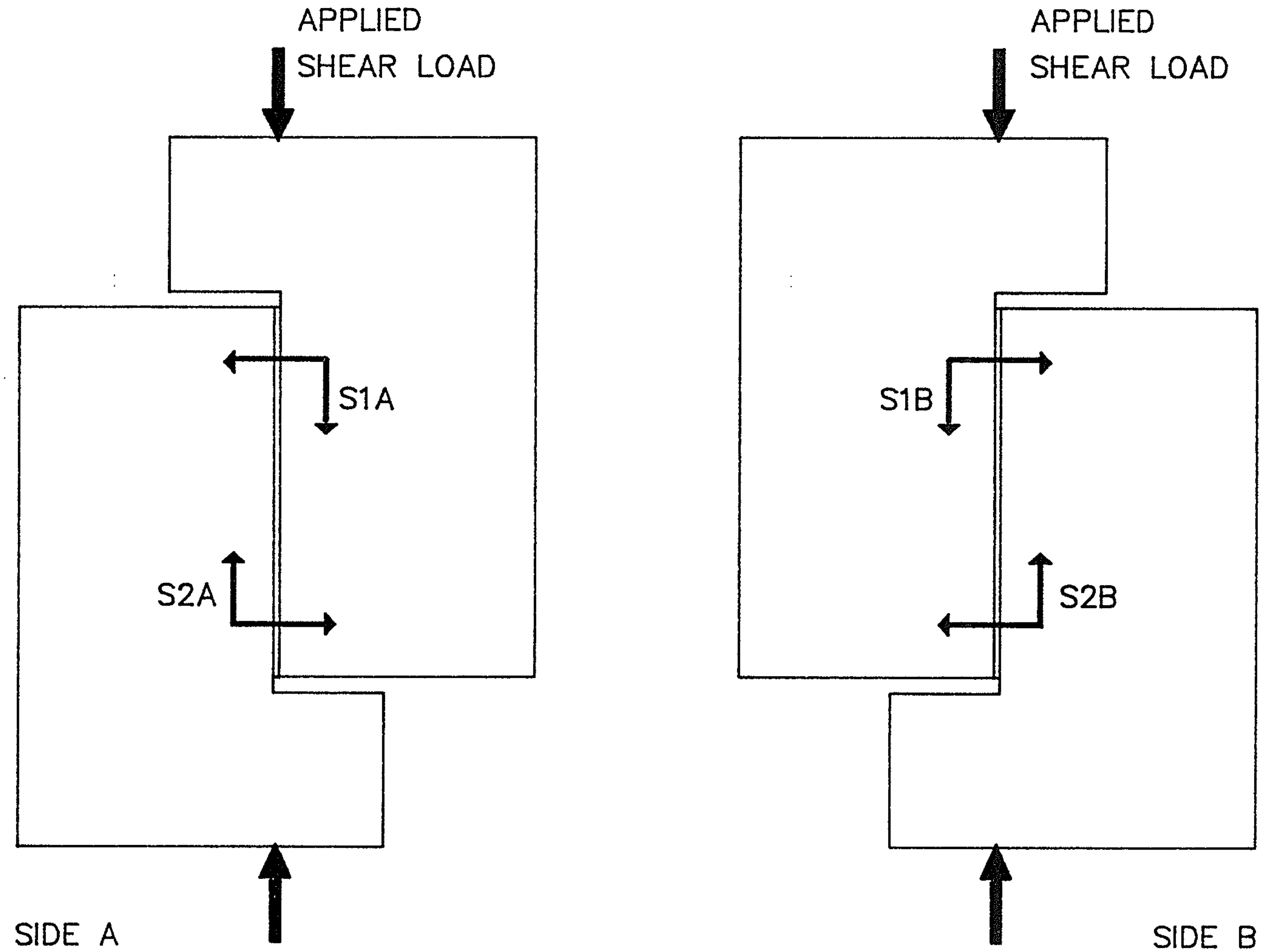

Figure 3.18 Location of Measurement Stations on Specimens Without Hollow-core Slab

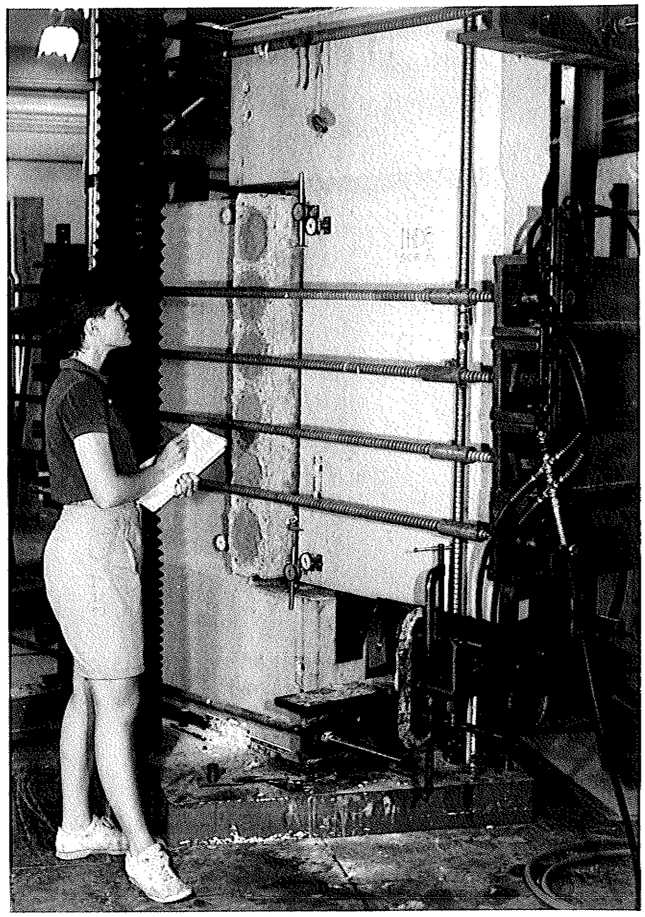

Figure 3.19 Test Set-up: Application of Edge Post-tensioning and Load Normal to the Connection

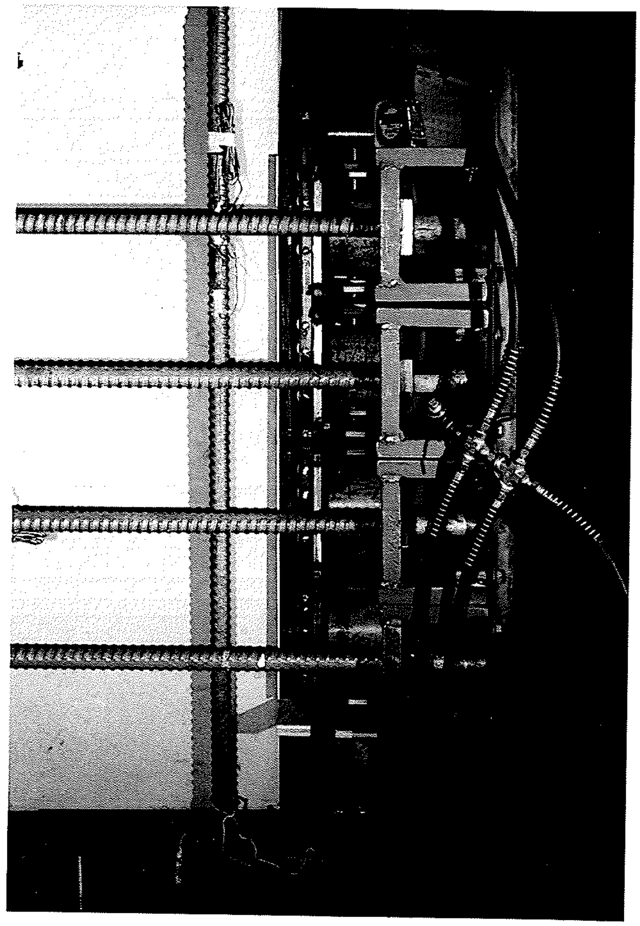

Figure 3.20 Apparatus for Application of Normal Load: End with Hydraulic Jacking System

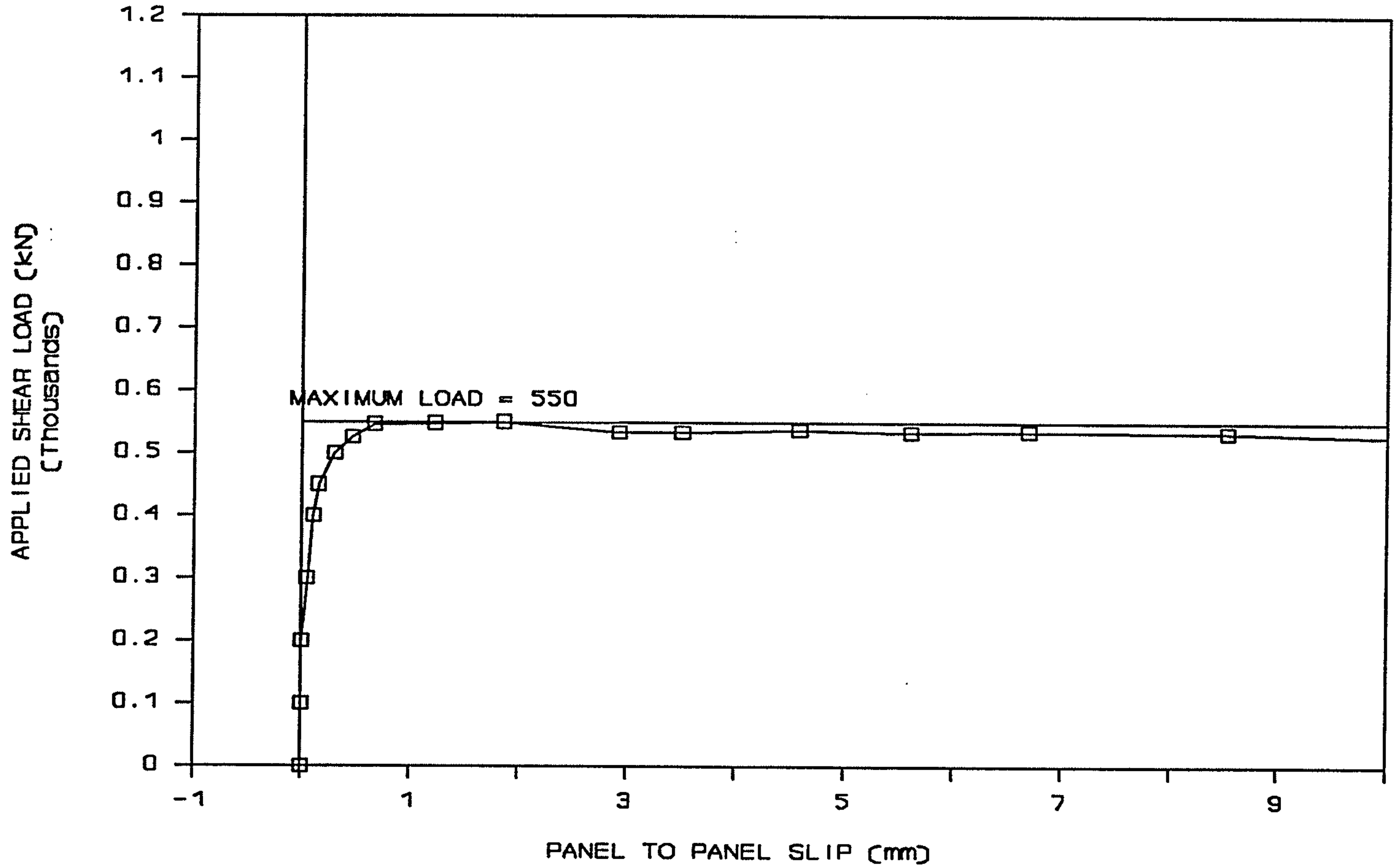

Figure 4.1 Specimen 1HD4 Load vs Slip Relationship

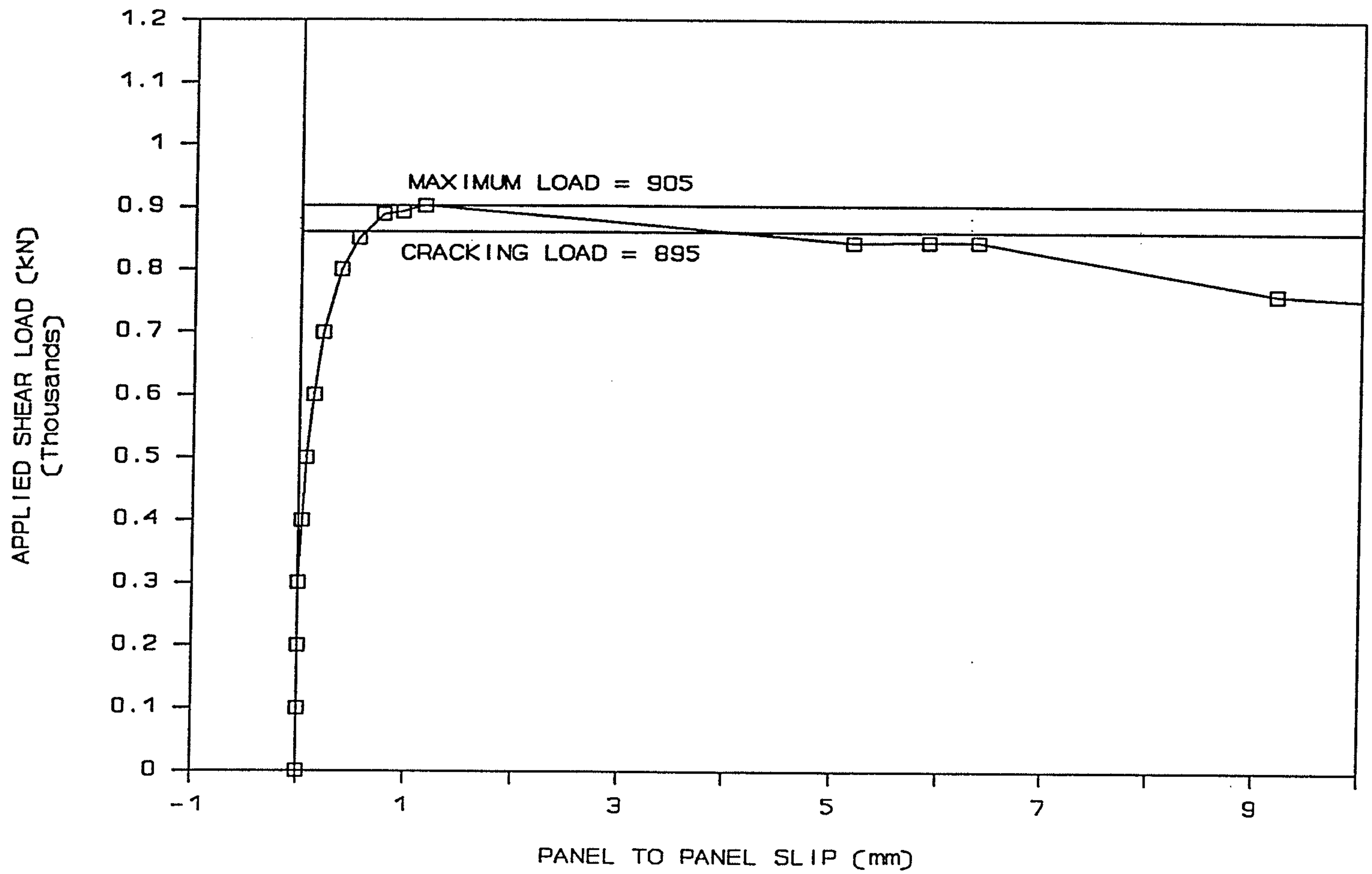

Figure 4.2 Specimen 2HD8 Load vs Slip Relationship

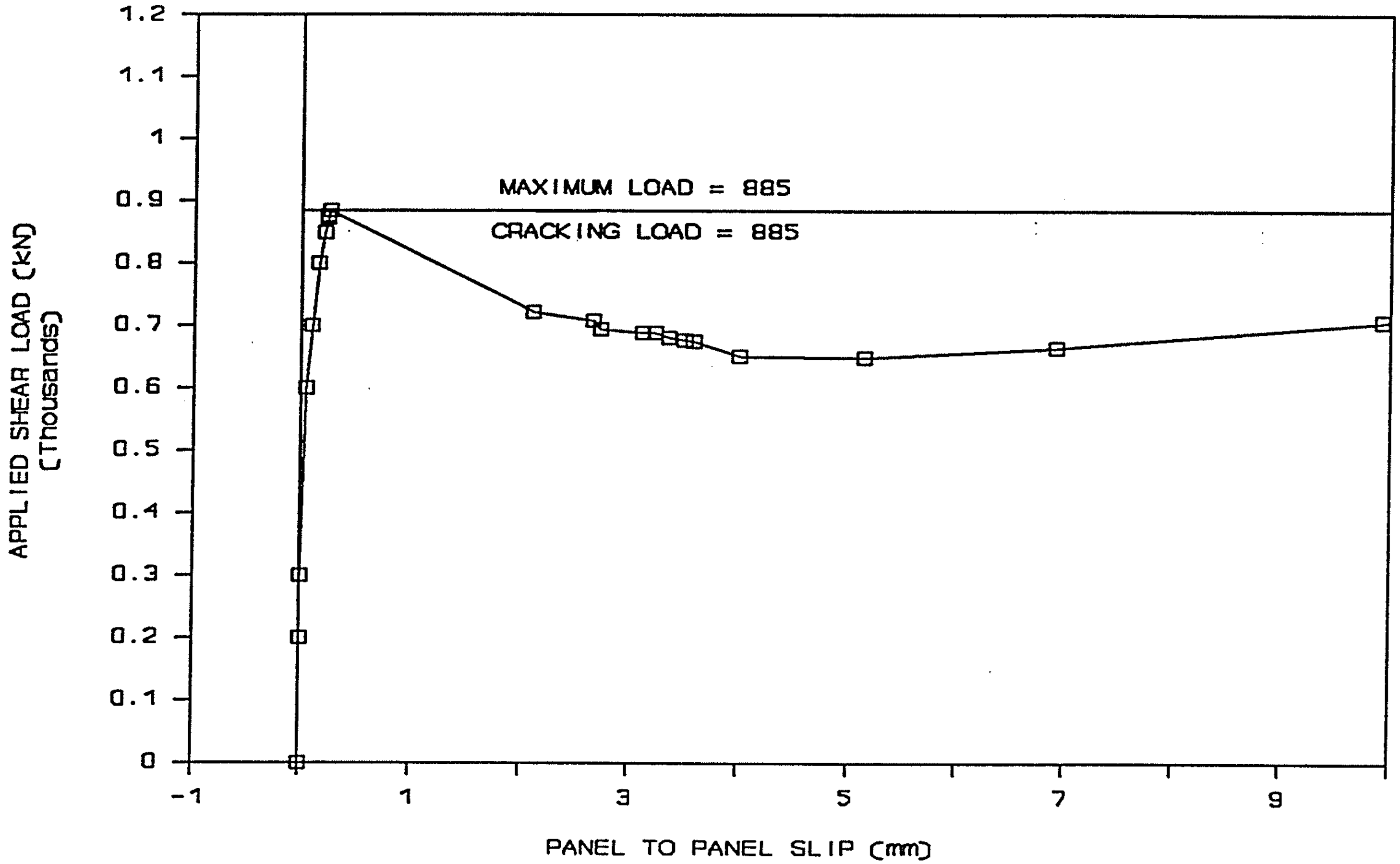

Figure 4.3 Specimen 3HD8 Load vs Slip Relationship

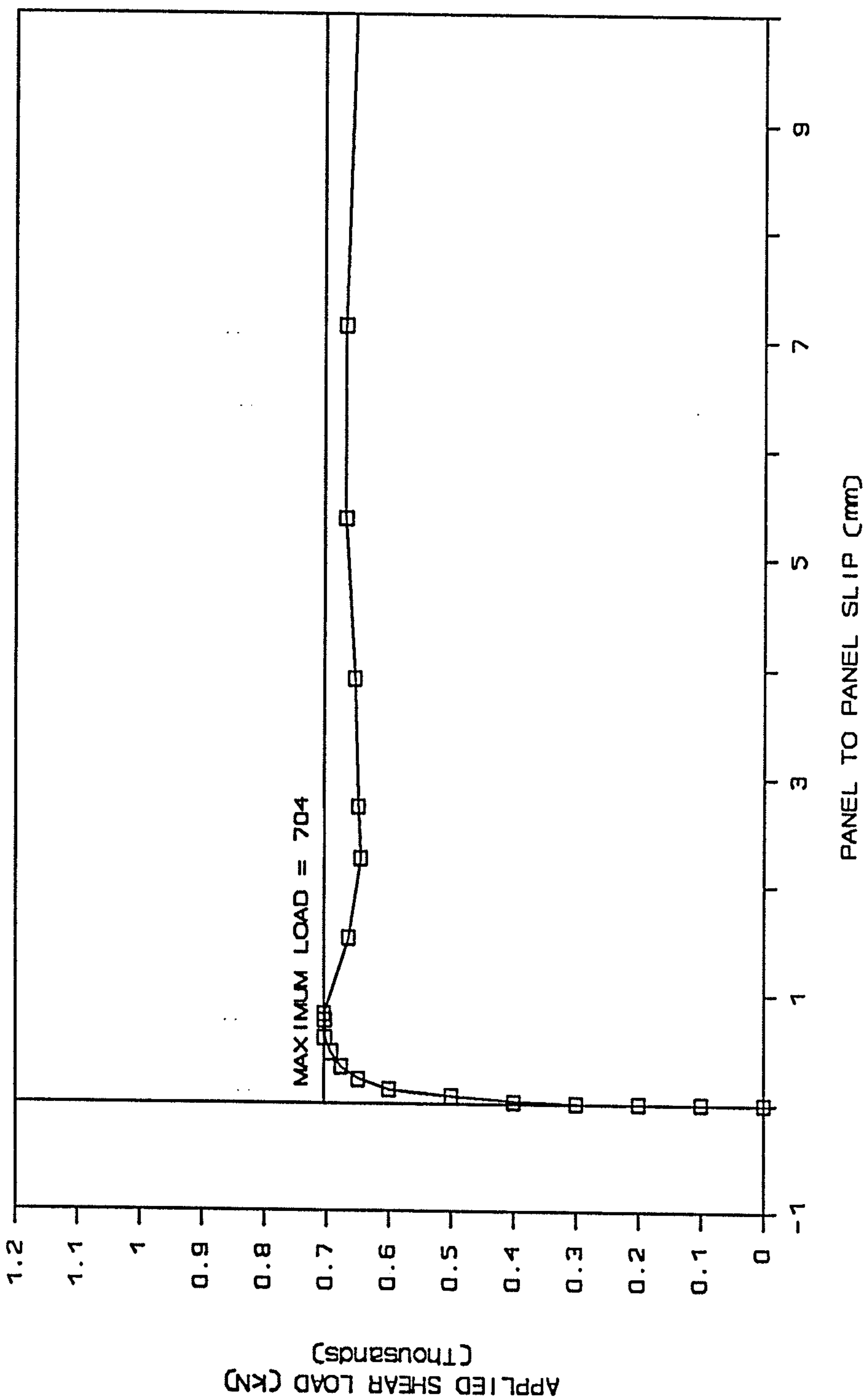

Figure 4.4 Specimen 4HP4 Load vs Slip Relationship

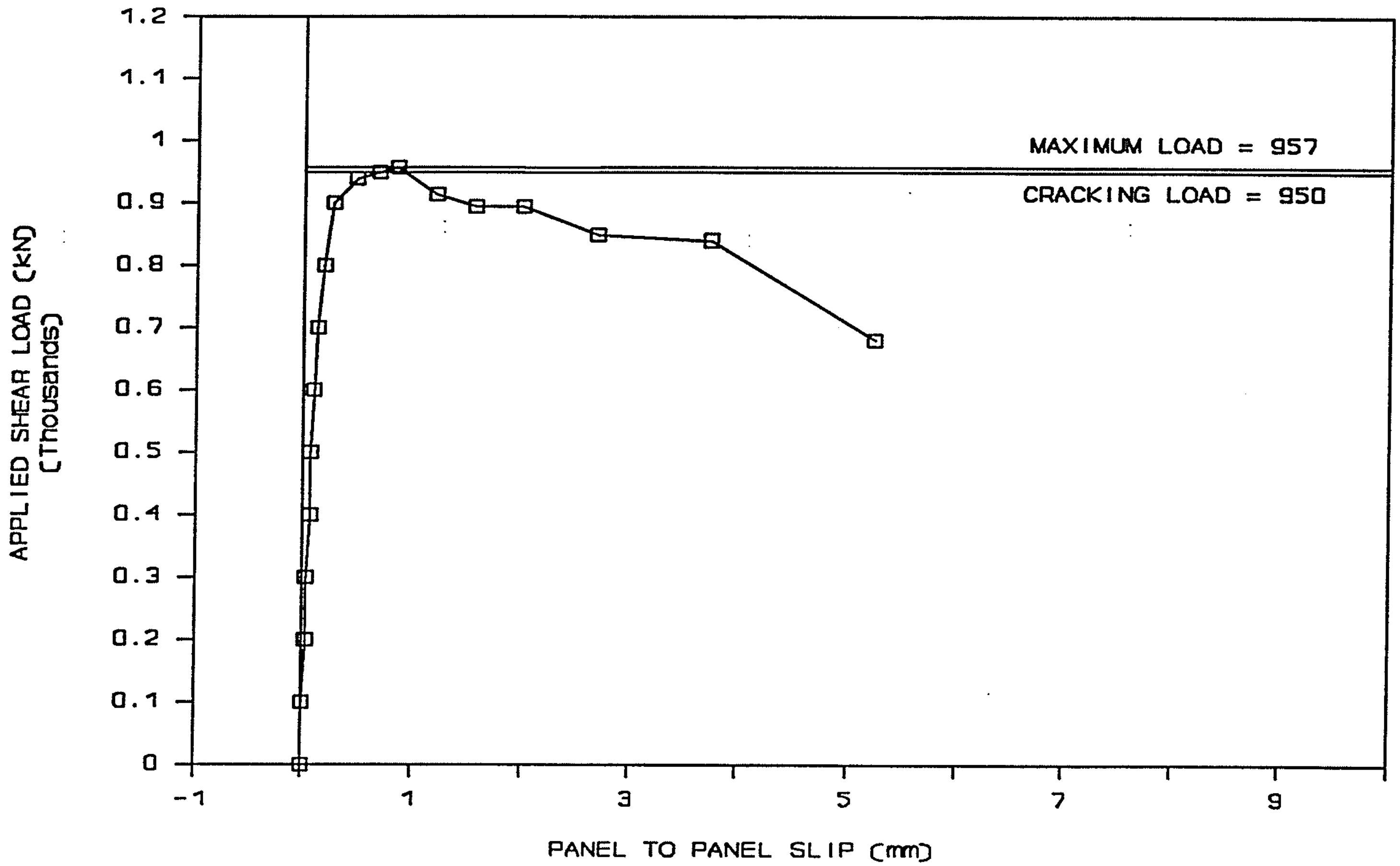

Figure 4.5 Specimen 5HP8 Load vs Slip Relationship

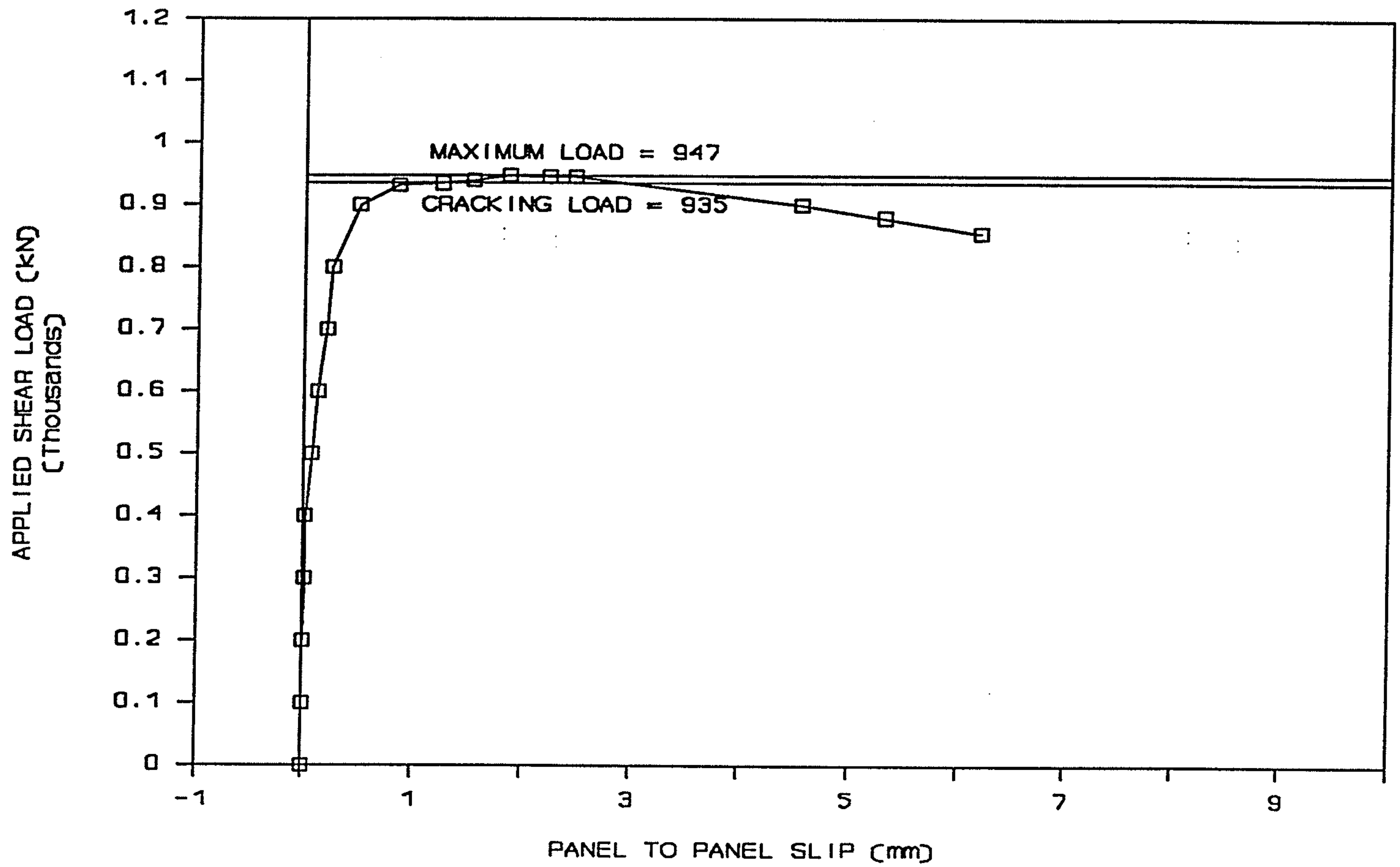

Figure 4.6 Specimen 6HP8 Load vs Slip Relationship

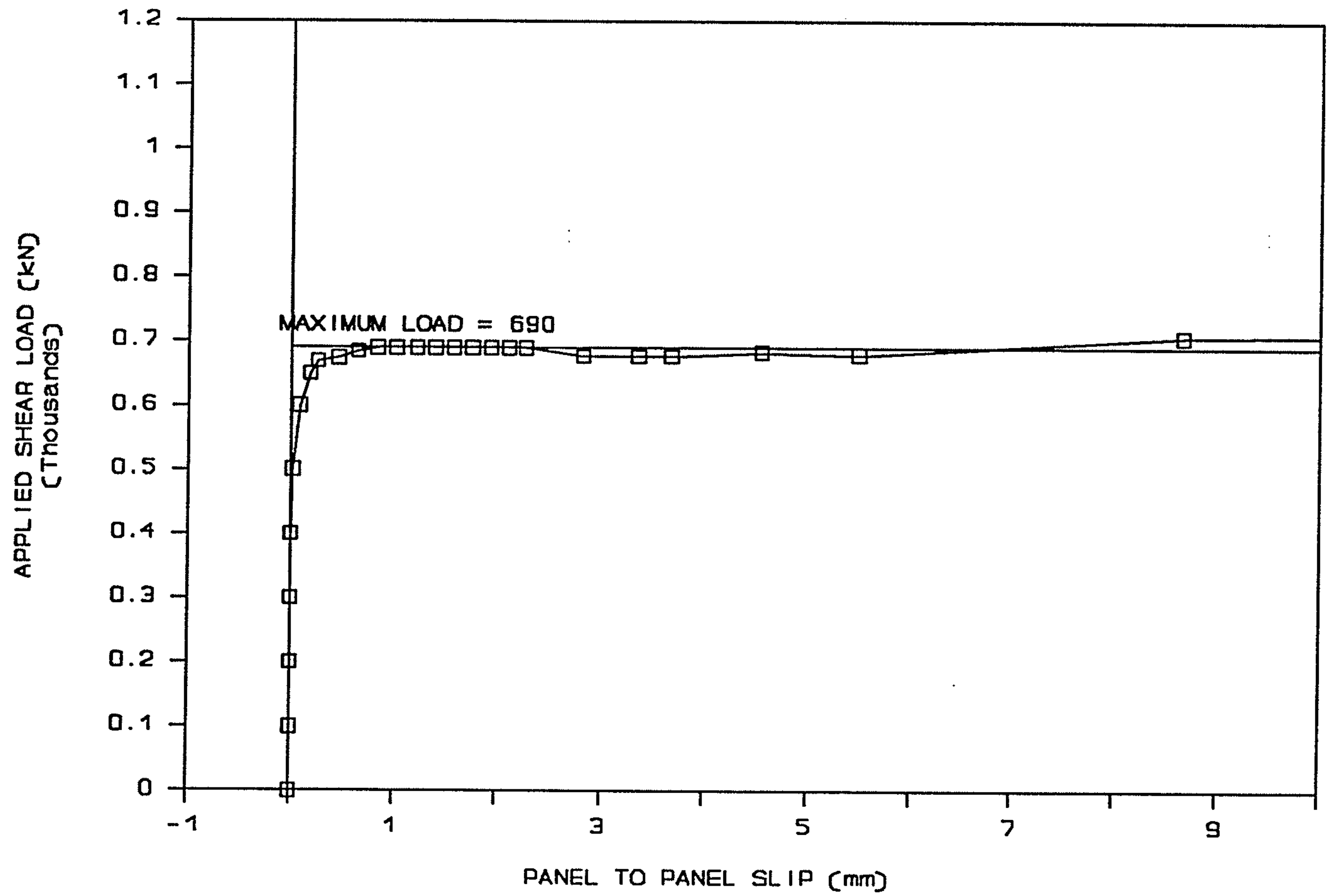

Figure 4.7 Specimen 7PD4 Load vs Slip Relationship

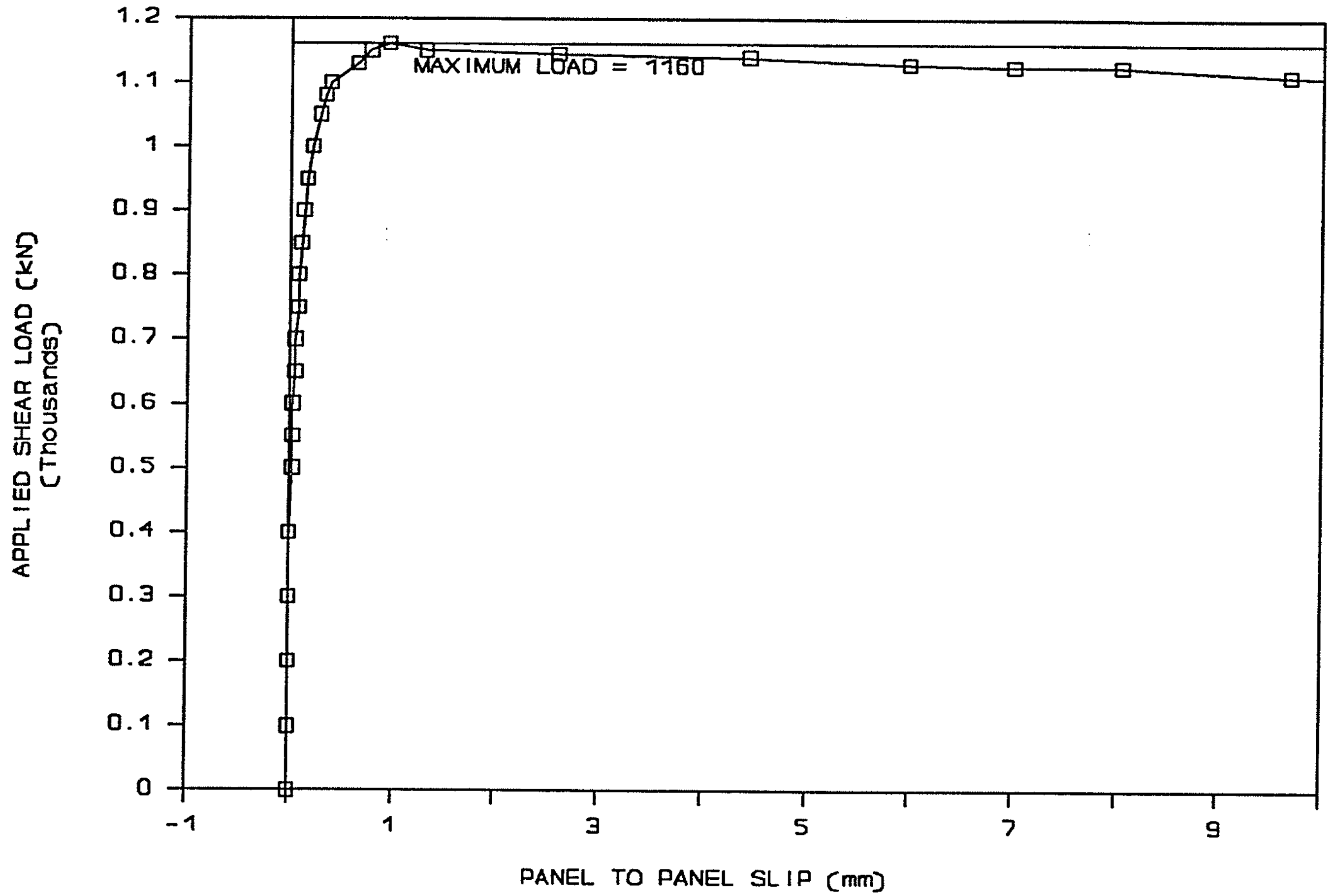

Figure 4.8 Specimen 8PD8 Load vs Slip Relationship

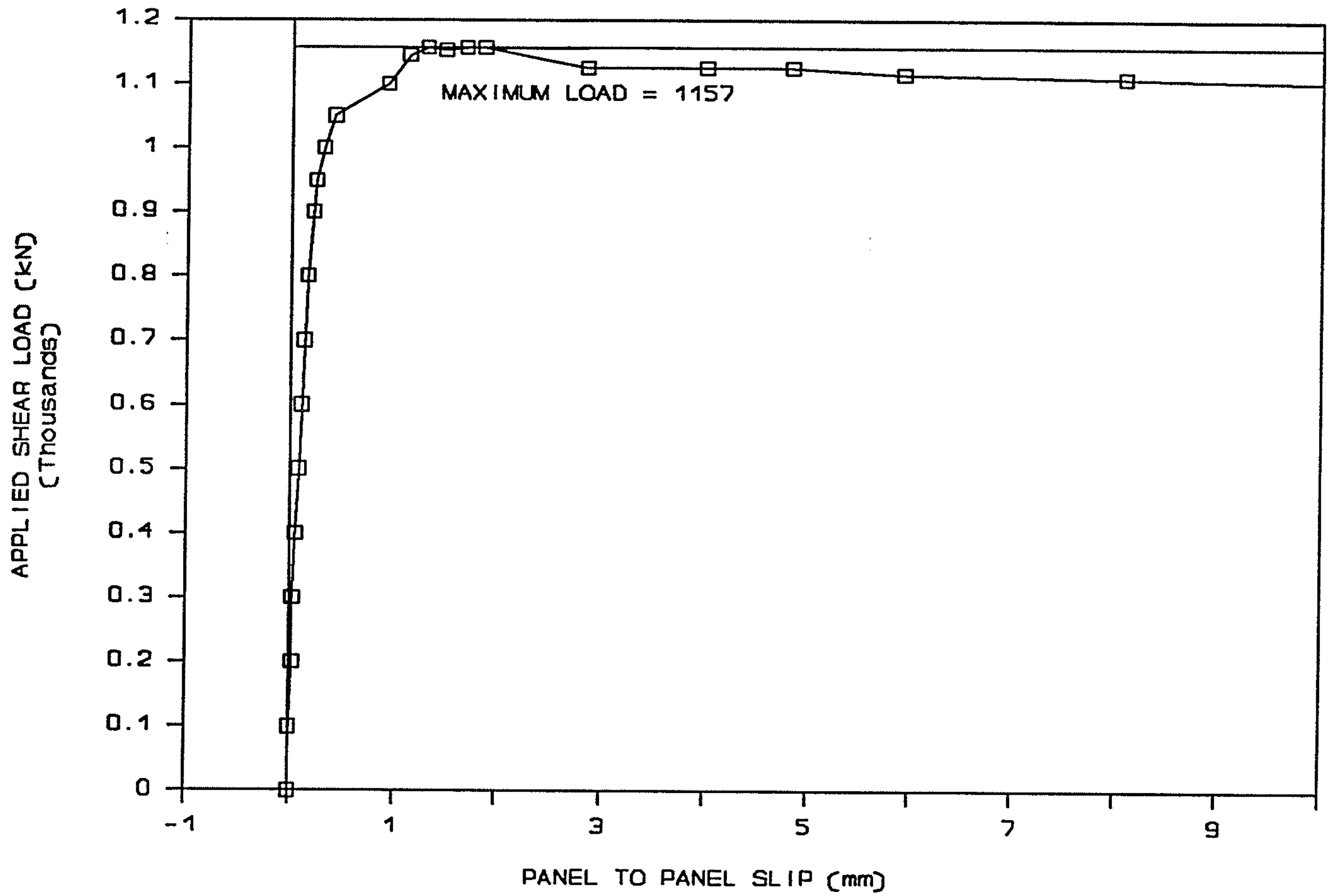

Figure 4.9 Specimen 9PD8 Load vs Slip Relationship

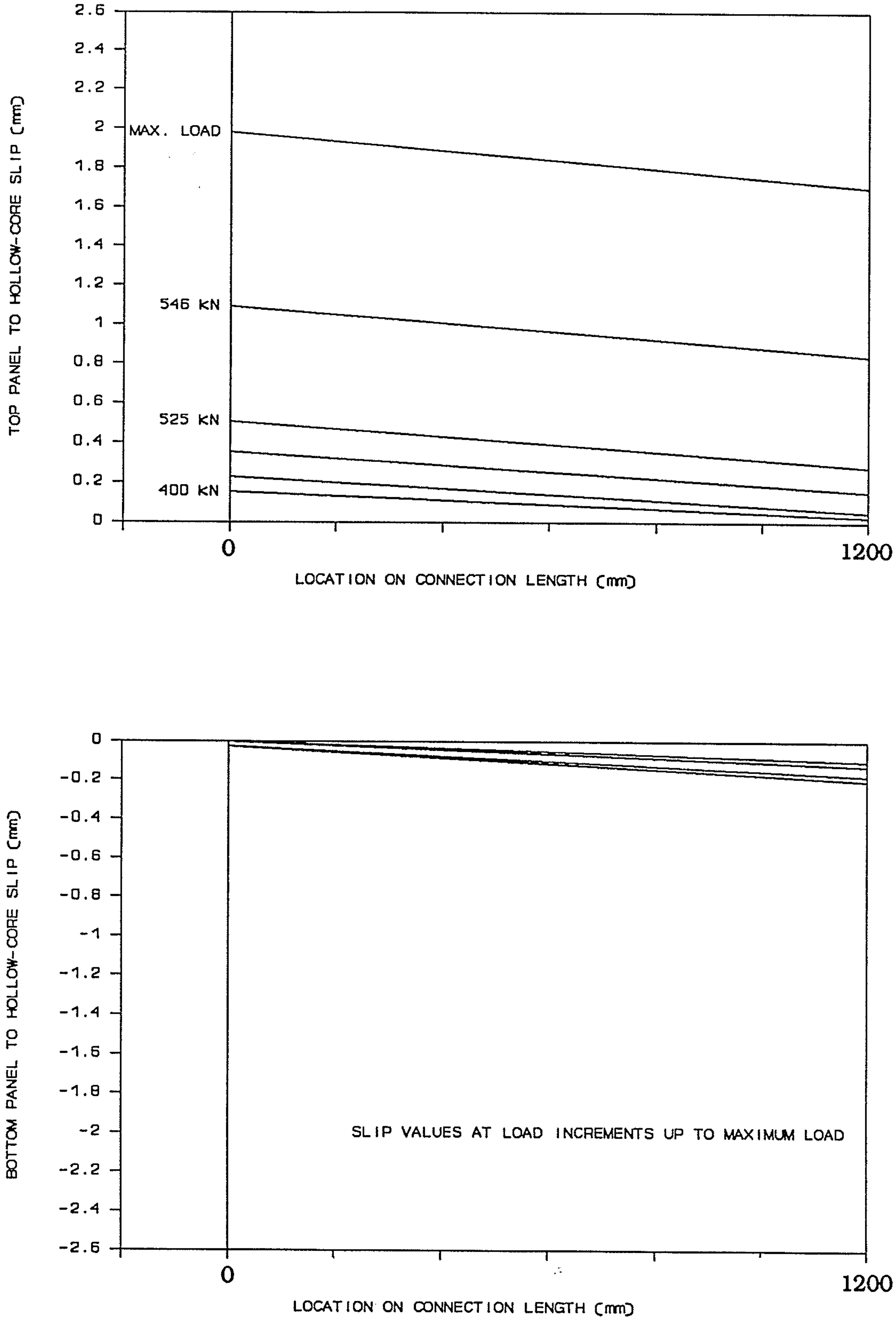

Figure 4.10 Specimen 1HD4 Slip Distribution vs Load

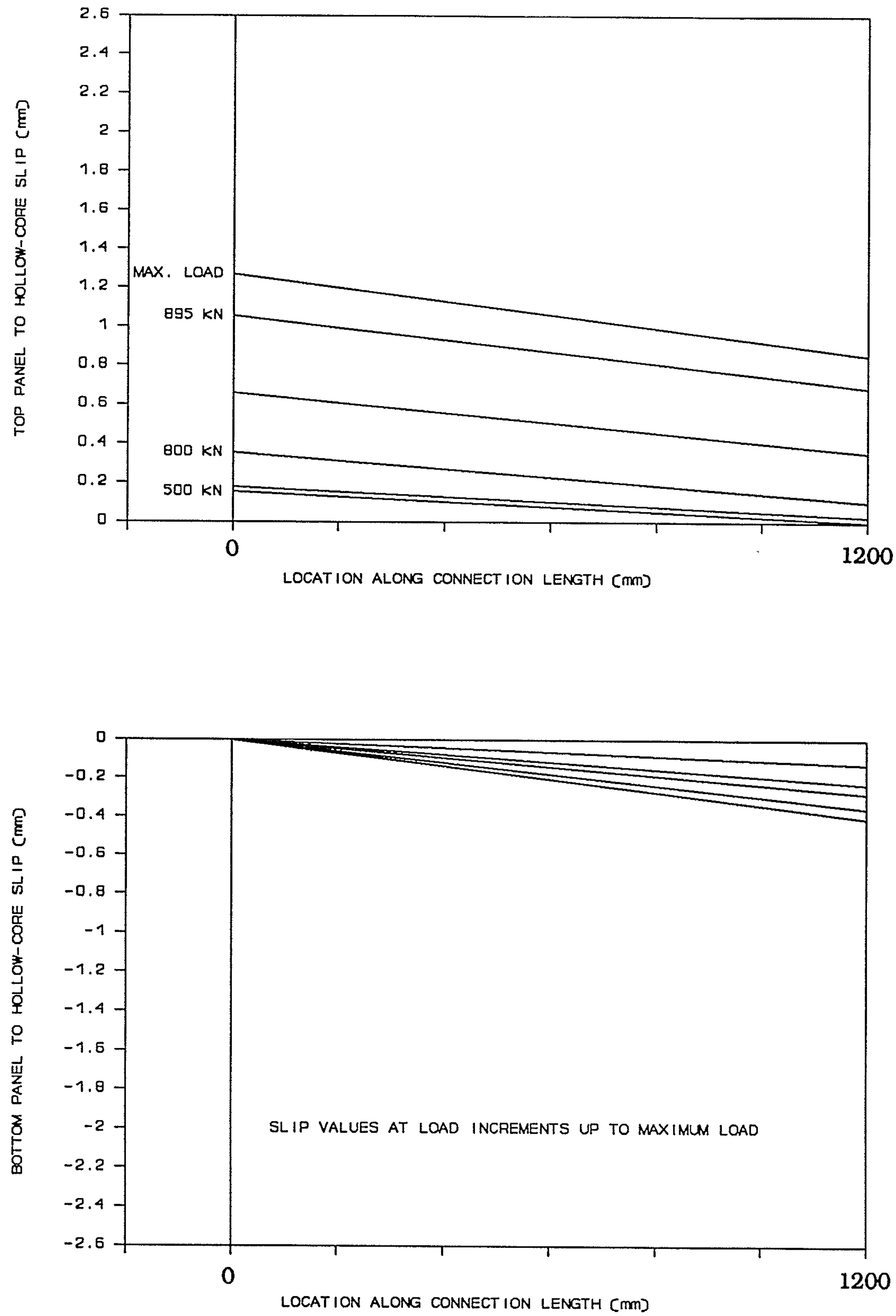

Figure 4.11 Specimen 2HD8 Slip Distribution vs Load

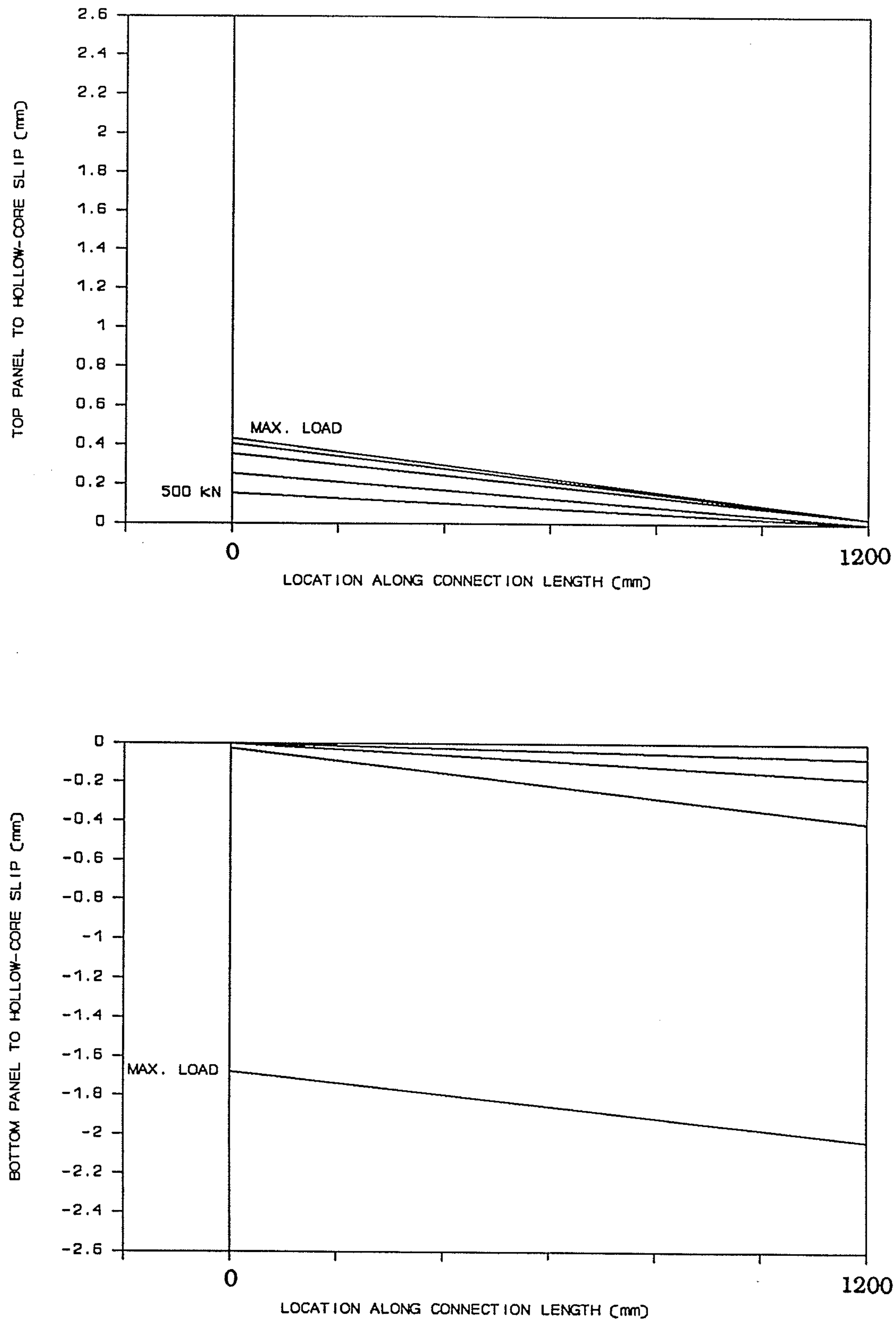

Figure 4.12 Specimen 3HD8 Slip Distribution vs Load

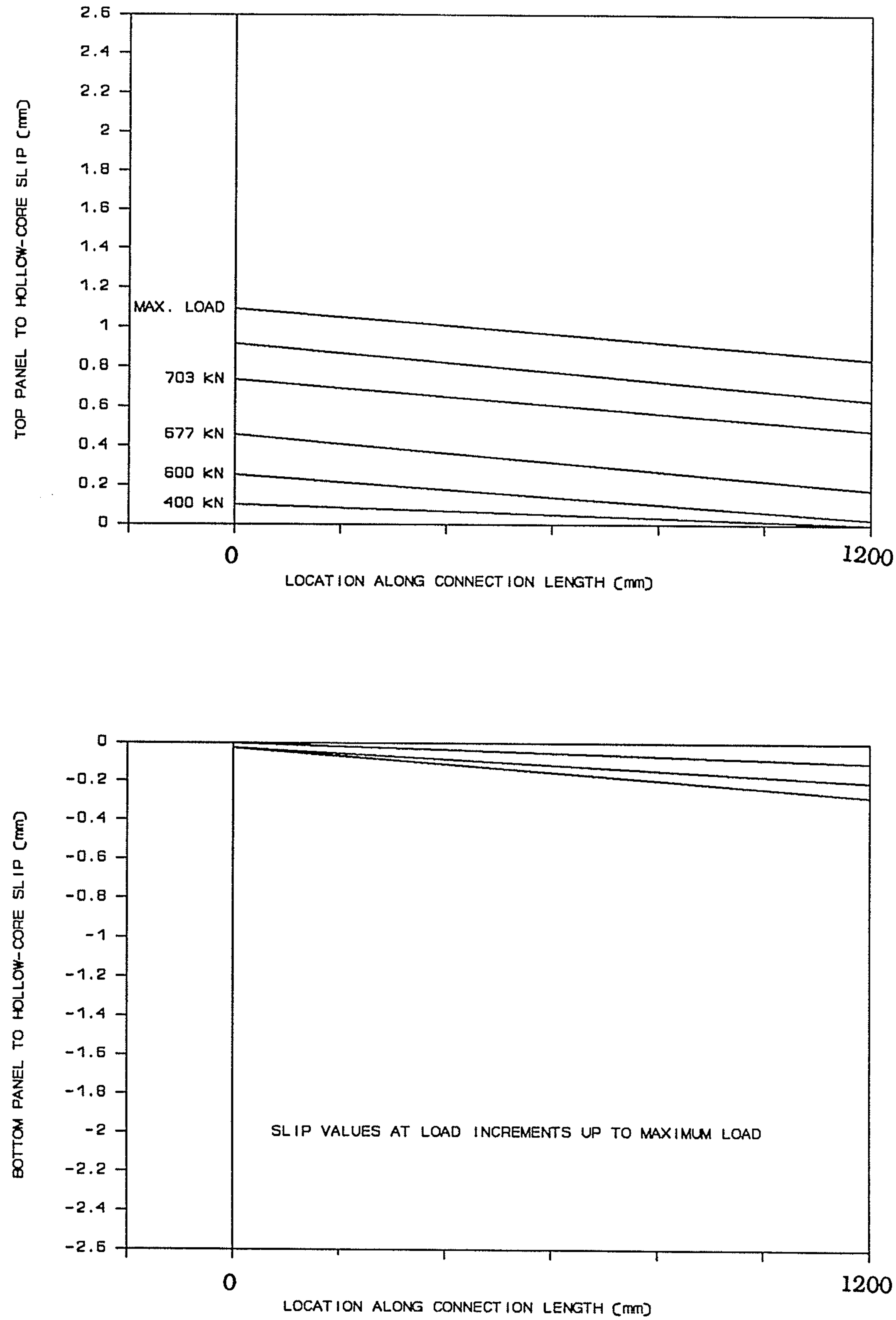

Figure 4.13 Specimen 4HP4 Slip Distribution vs Load

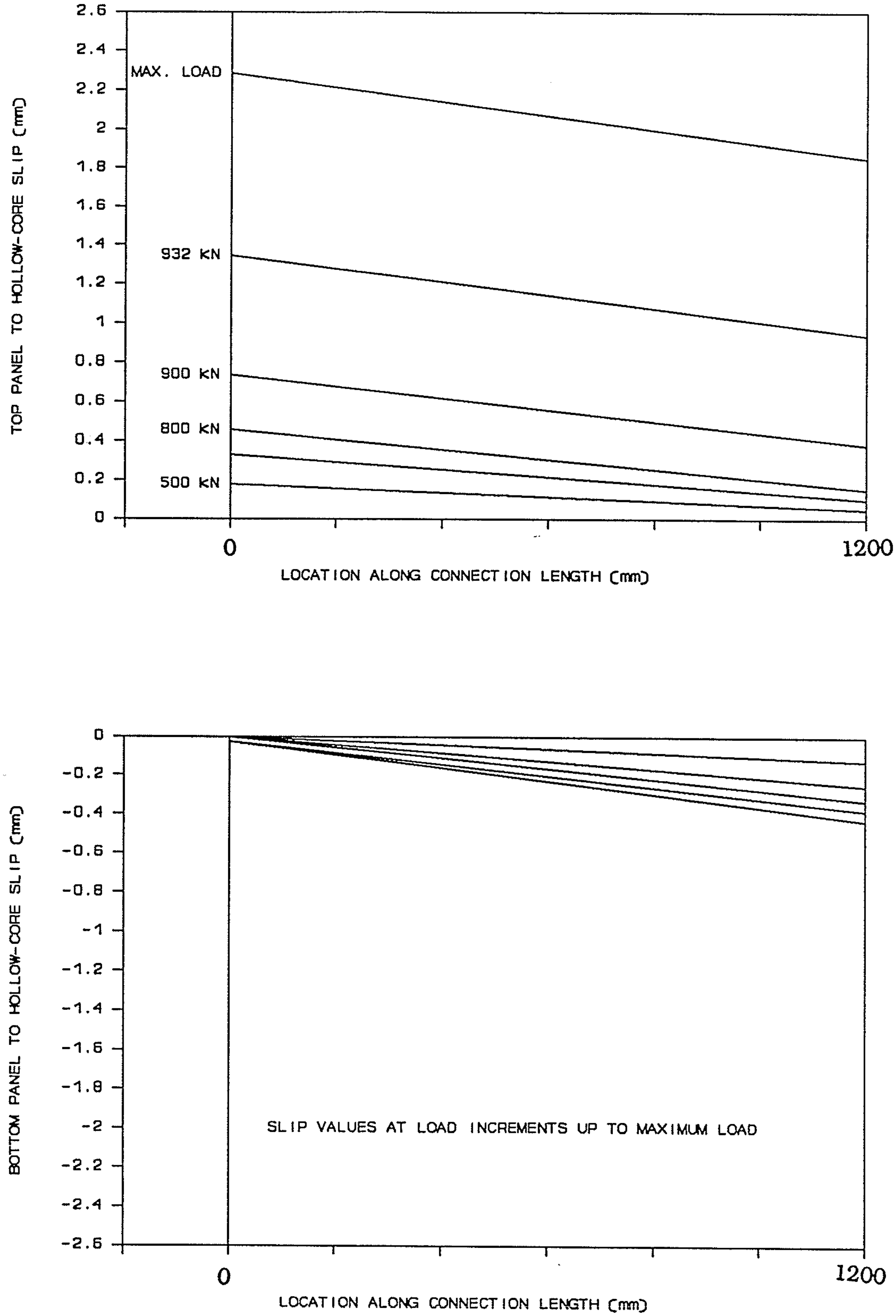

Figure 4.14 Specimen 6HP8 Slip Distribution vs Load

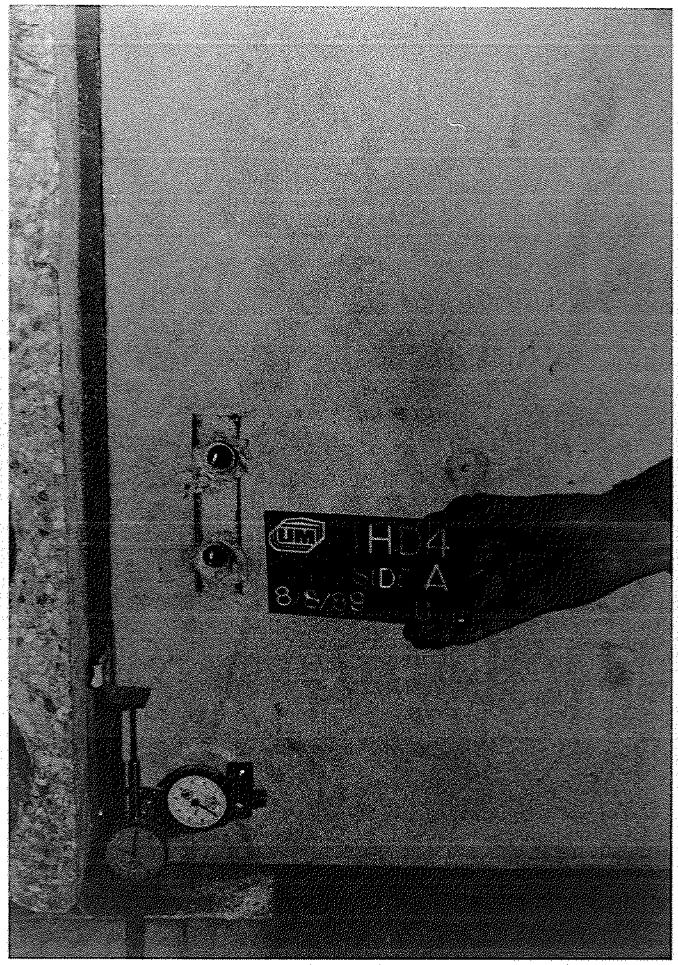

SIDE A

Figure 4.15 Specimen 1HD4 Crack Pattern at Ultimate

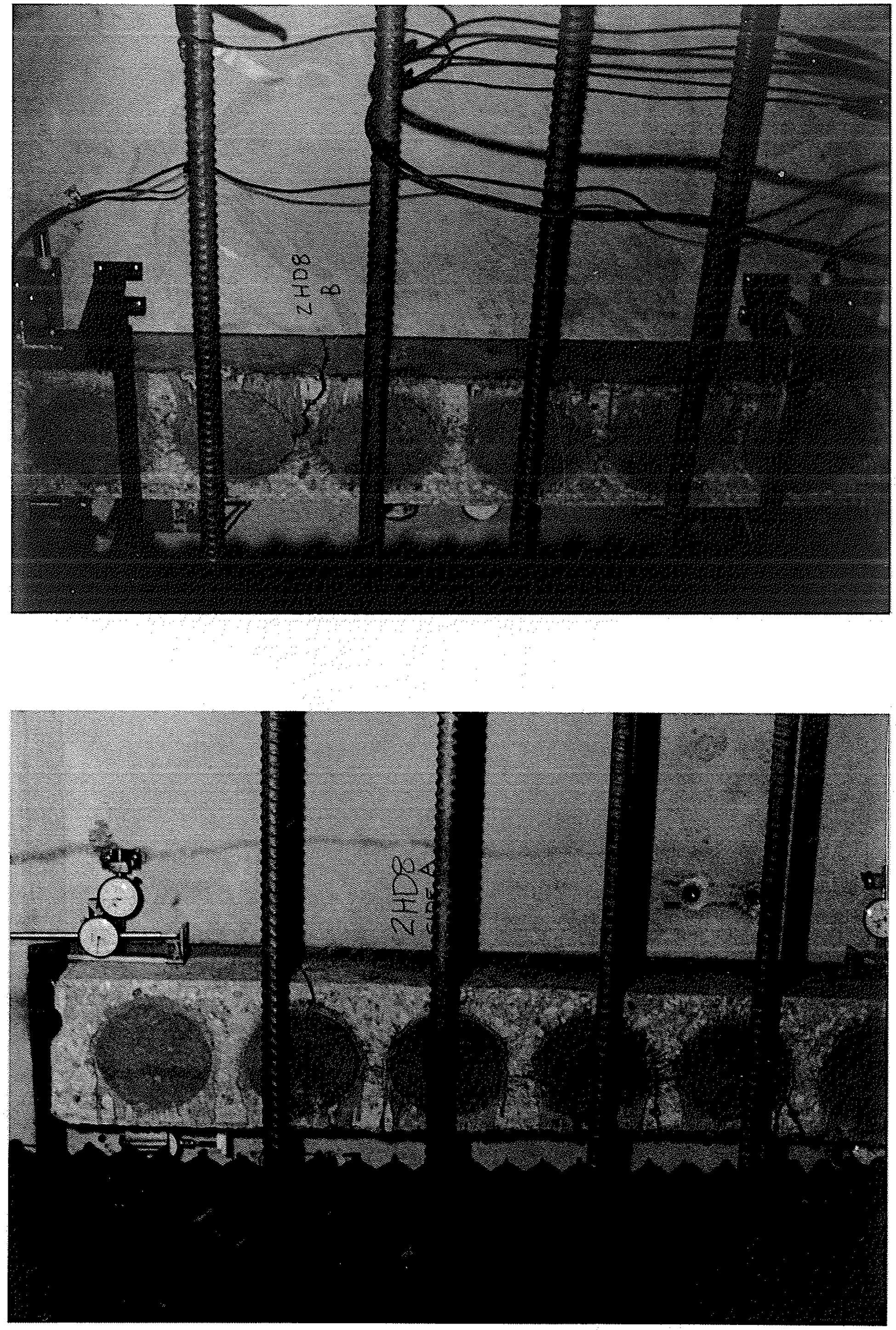

SIDE B

SIDE A

Figure 4.16 Specimen 2HD8 Crack Pattern at Ultimate

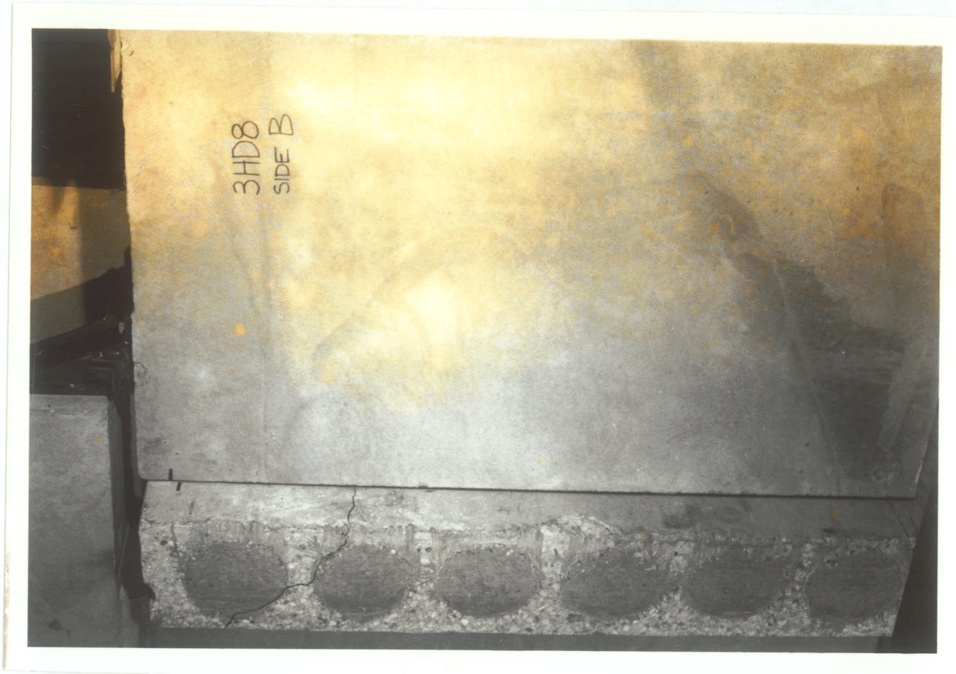

SIDE B

SIDE A

Figure 4.17 Specimen 3HD8 Crack Pattern at Ultimate

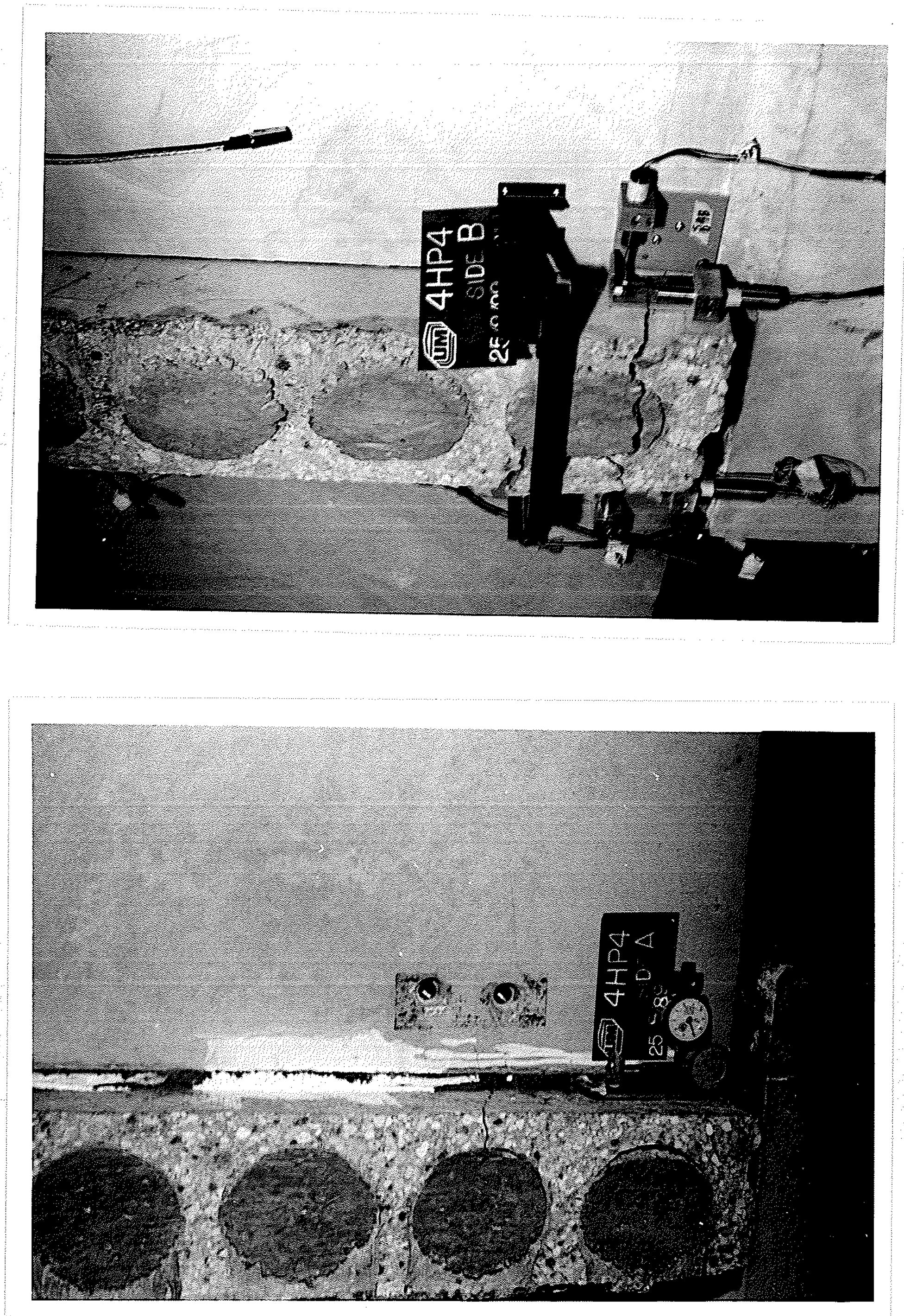

SIDE B

SIDE A

Figure 4.18 Specimen 4HP4 Crack Pattern at Ultimate

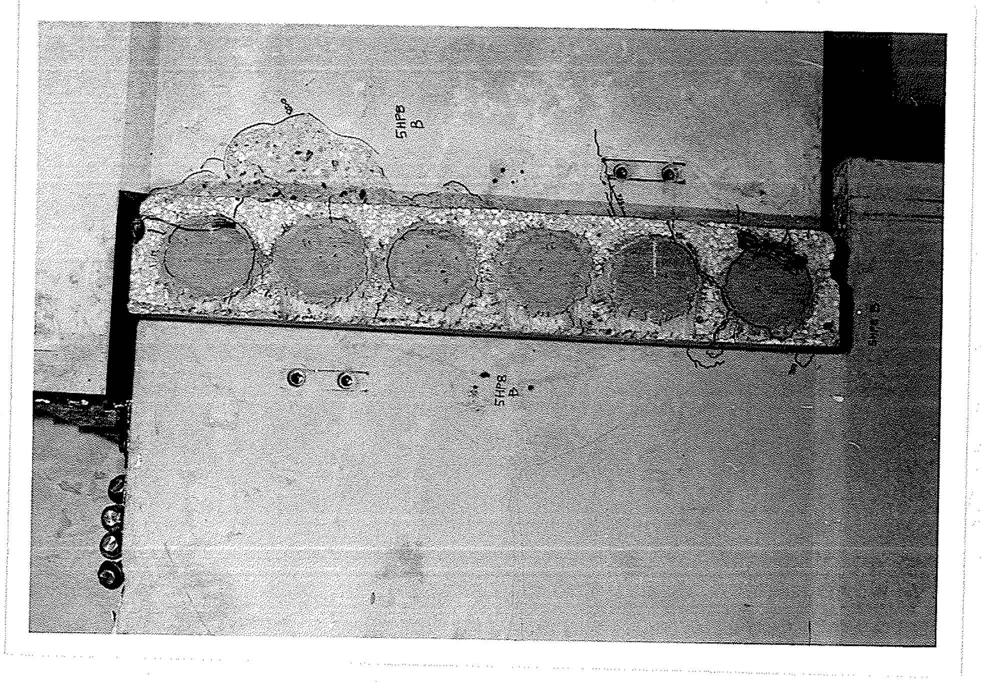

SIDE B

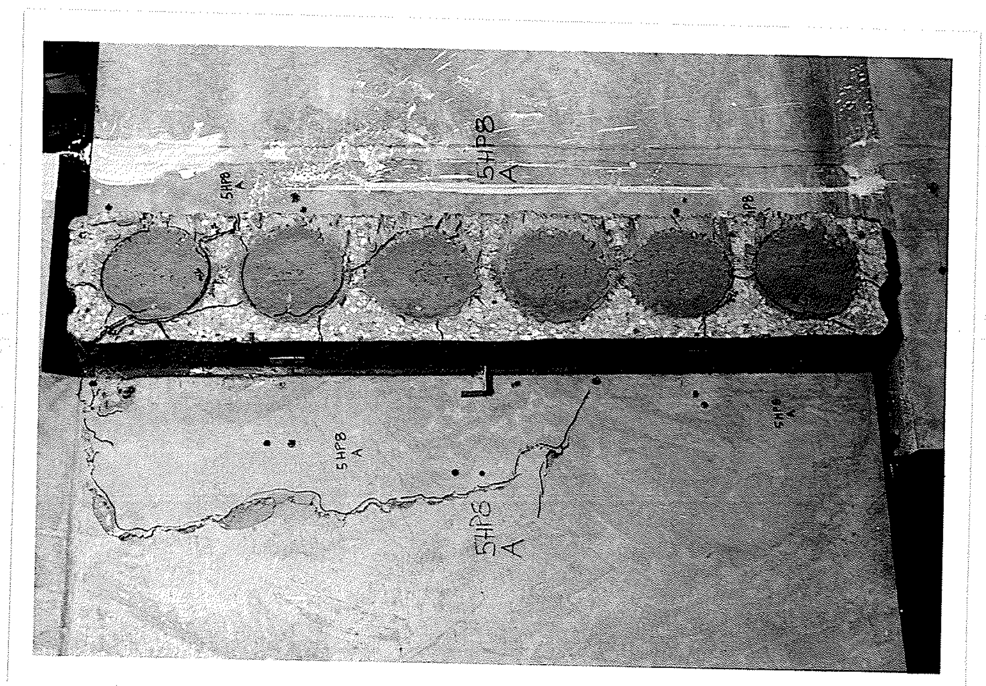

SIDE A

Figure 4.19 Specimen 5HP8 Crack Pattern at Ultimate

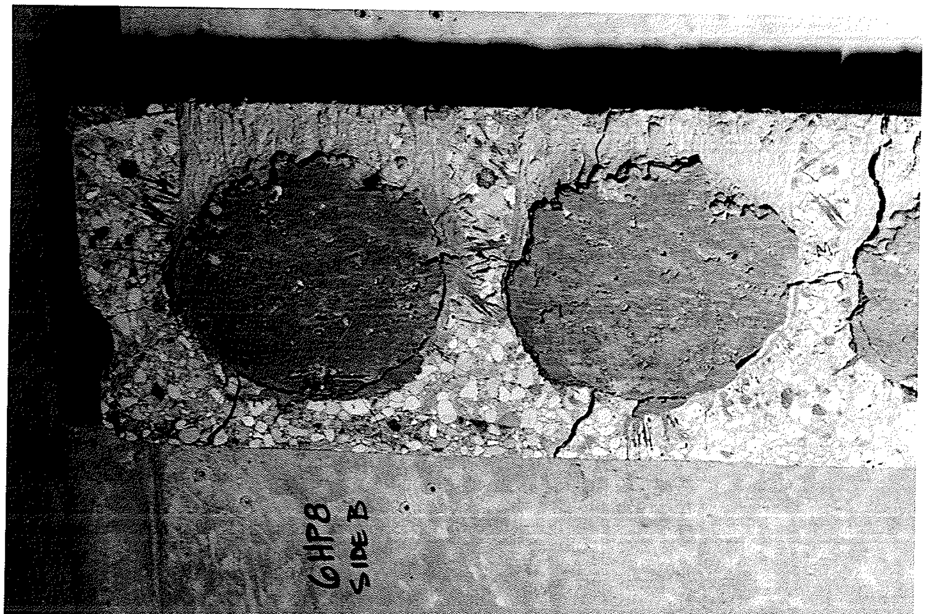

SIDE B

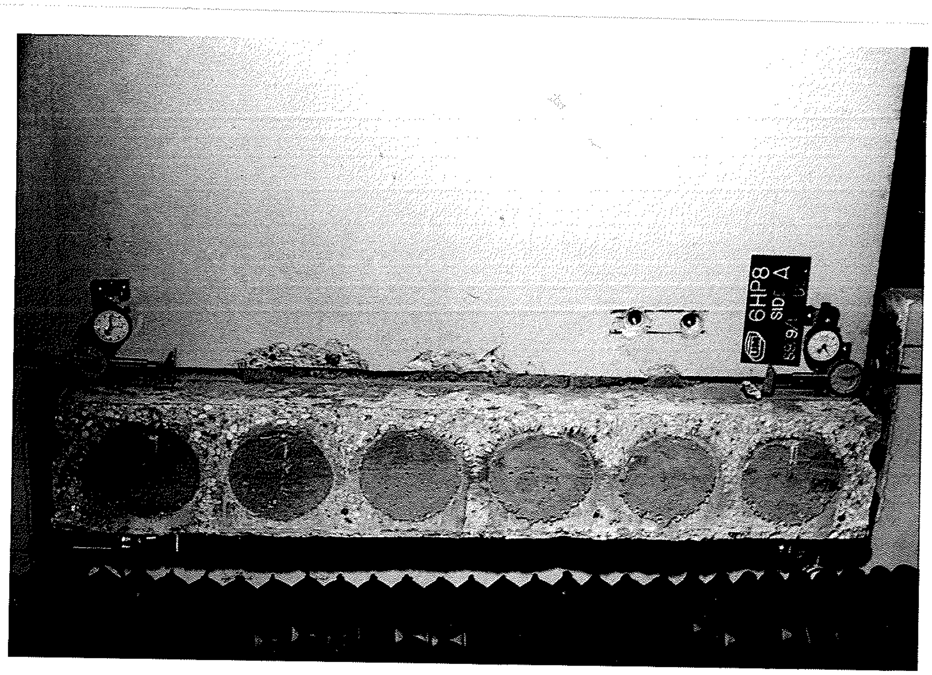

SIDE A

Figure 4.20 Specimen 6HP8 Crack Pattern at Ultimate

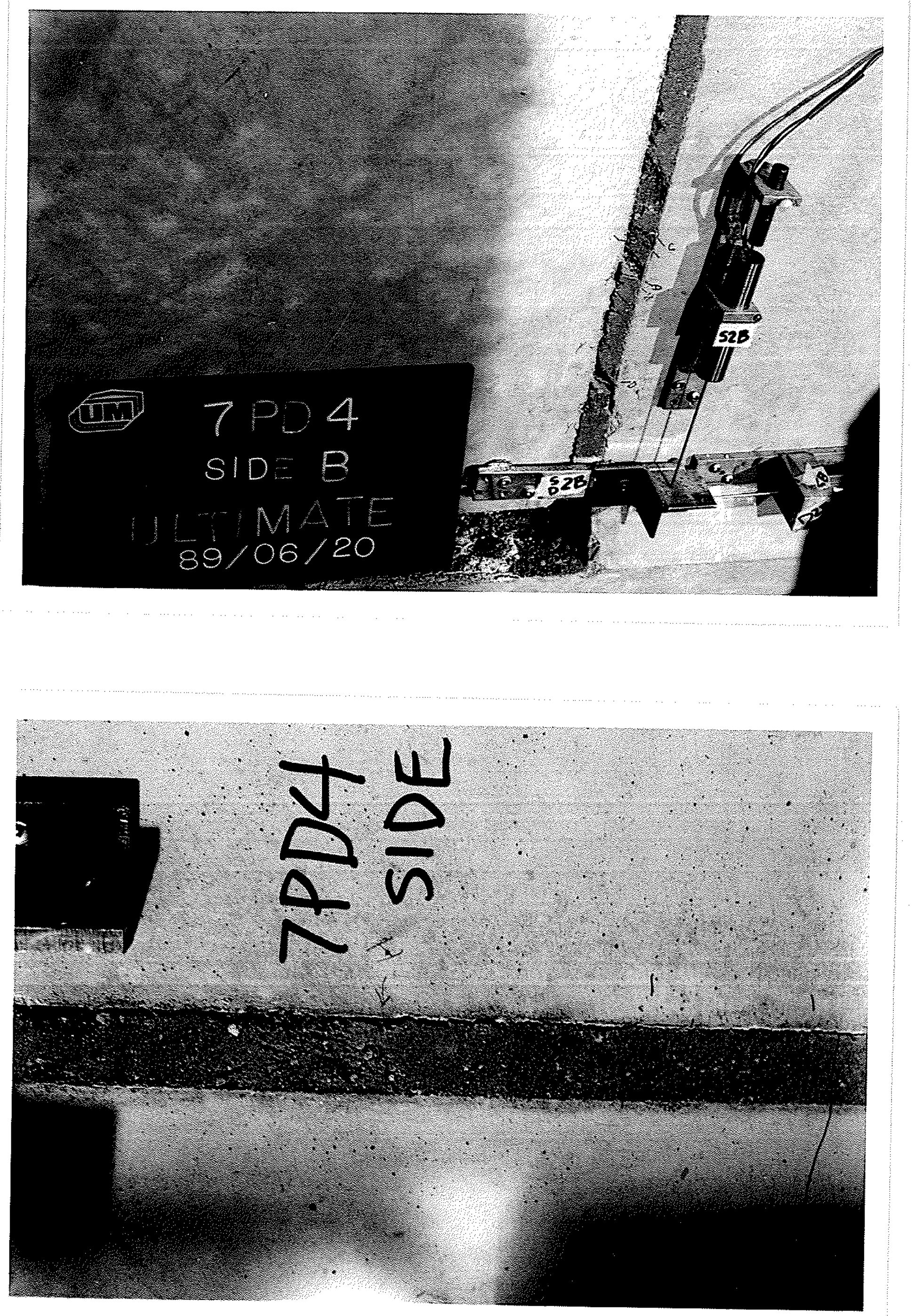

SIDE B

SIDE A

Figure 4.21 Specimen 7PD4 Crack Pattern at Ultimate

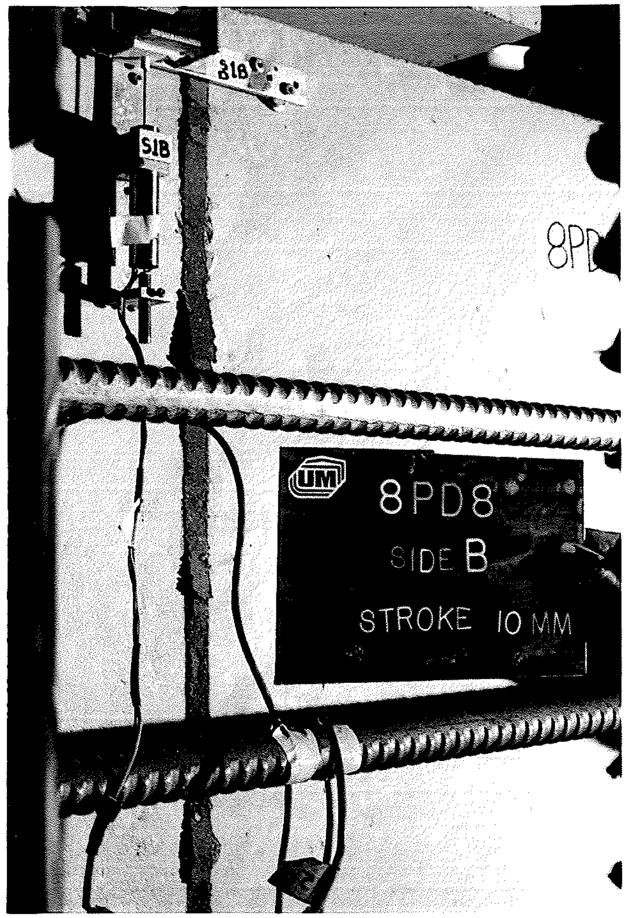

SIDE B

Figure 4.22 Specimen 8PD8 Crack Pattern at Ultimate

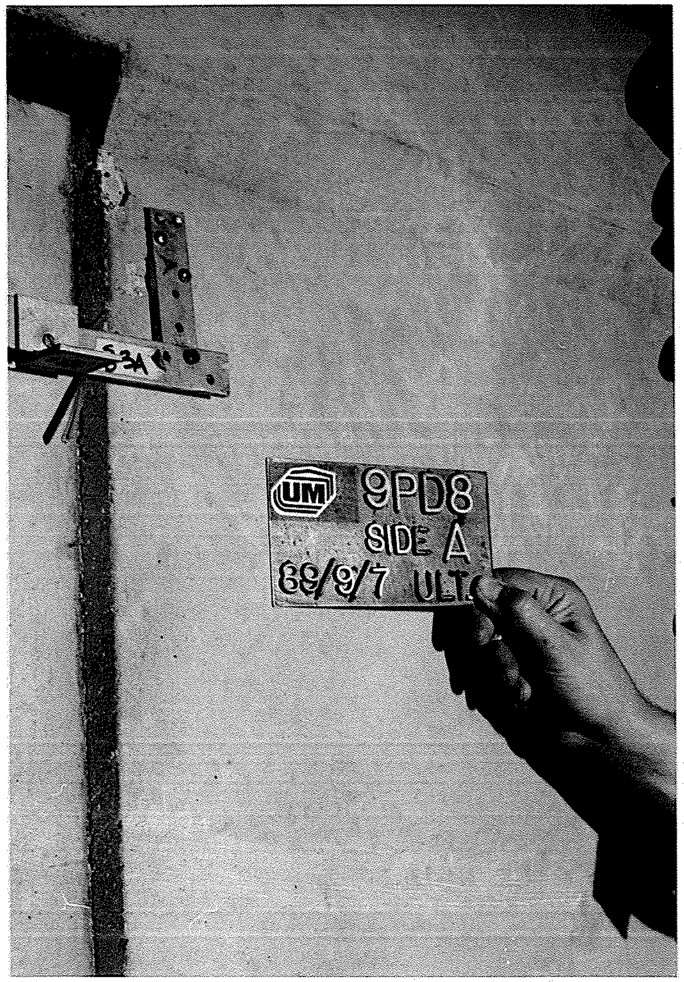

SIDE A

Figure 4.23 Specimen 9PD8 Crack Pattern at Ultimate

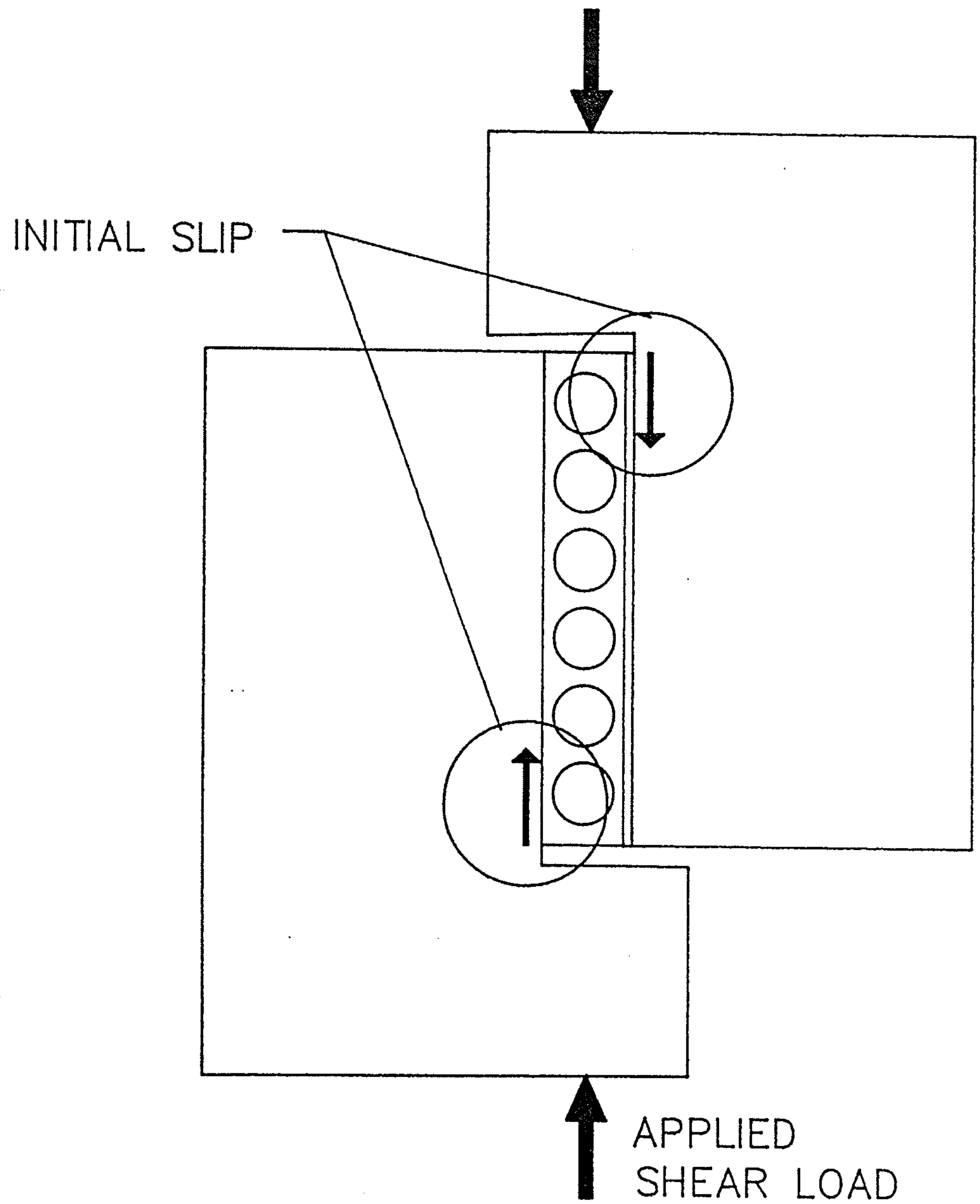

Figure 5.1 Typical Location of Slip for Specimens with Hollow-core Slab

Figure 5.2 Interface Slip Surface of Specimen 1HD4

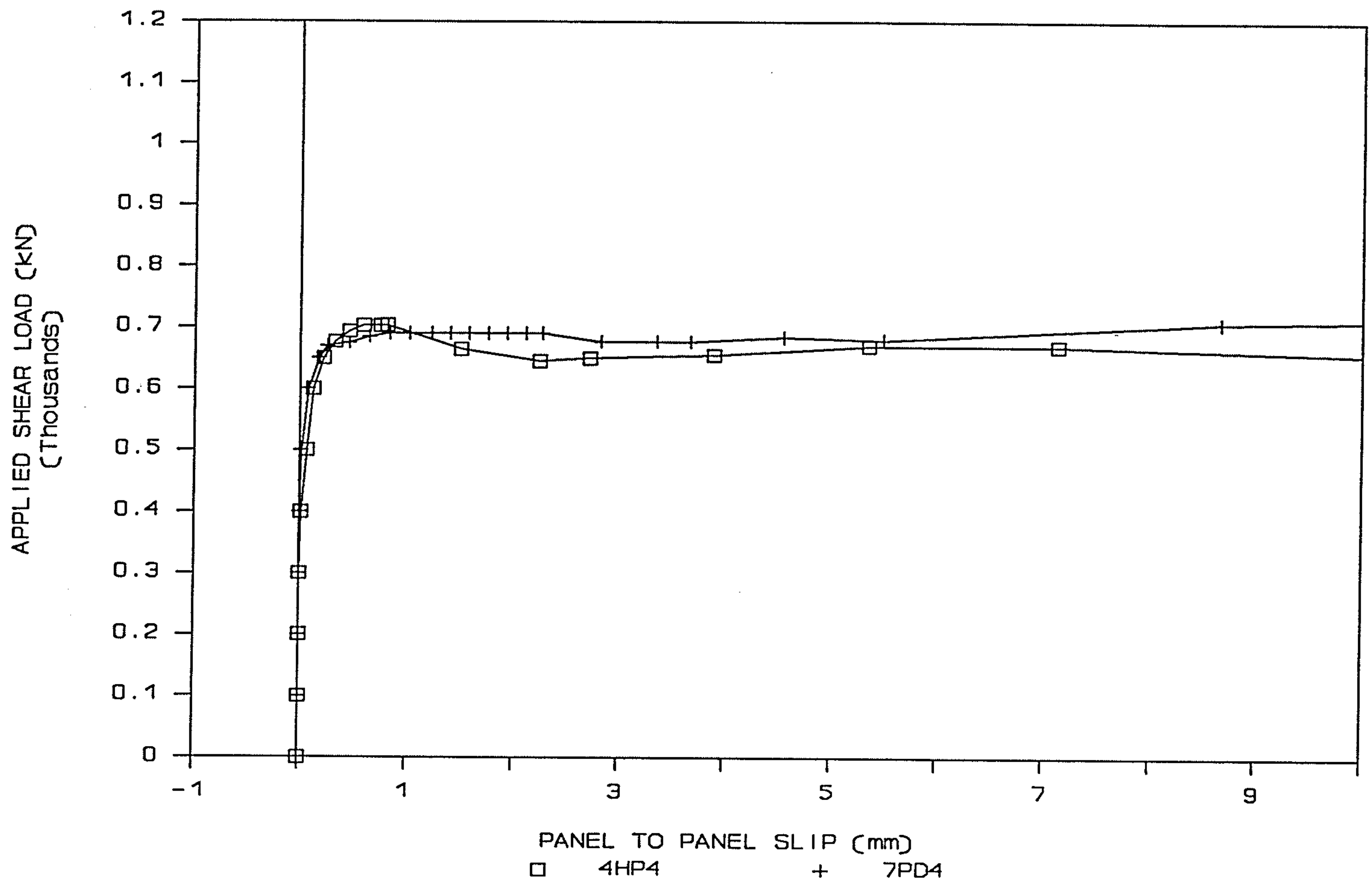

Figure 5.3 Load vs Slip Response for Post-tensioned Specimens at 4MPa Normal Load

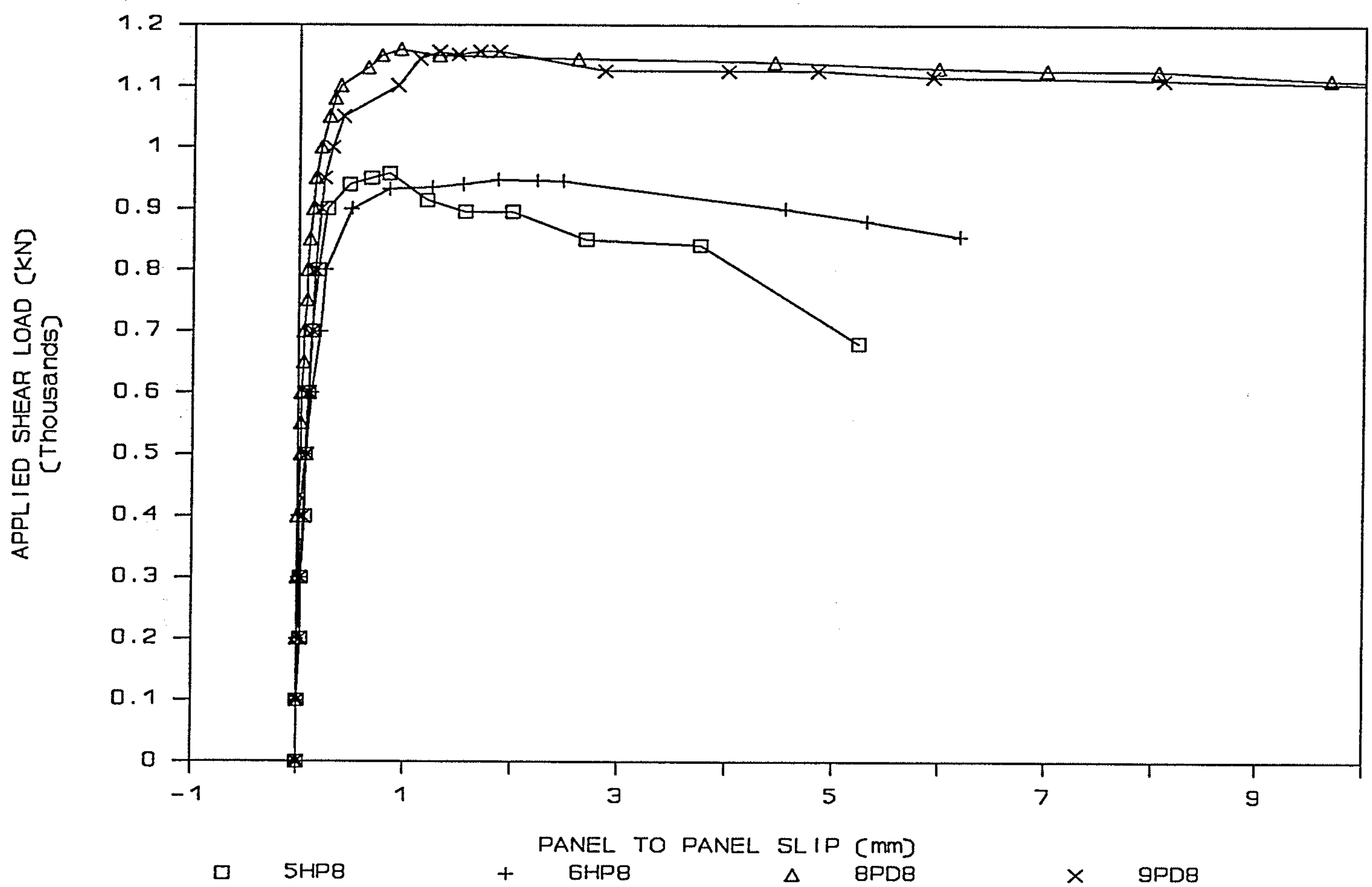

Figure 5.4 a) Load vs Slip Response for Post-tensioned Specimens at 8 MPa Normal Load

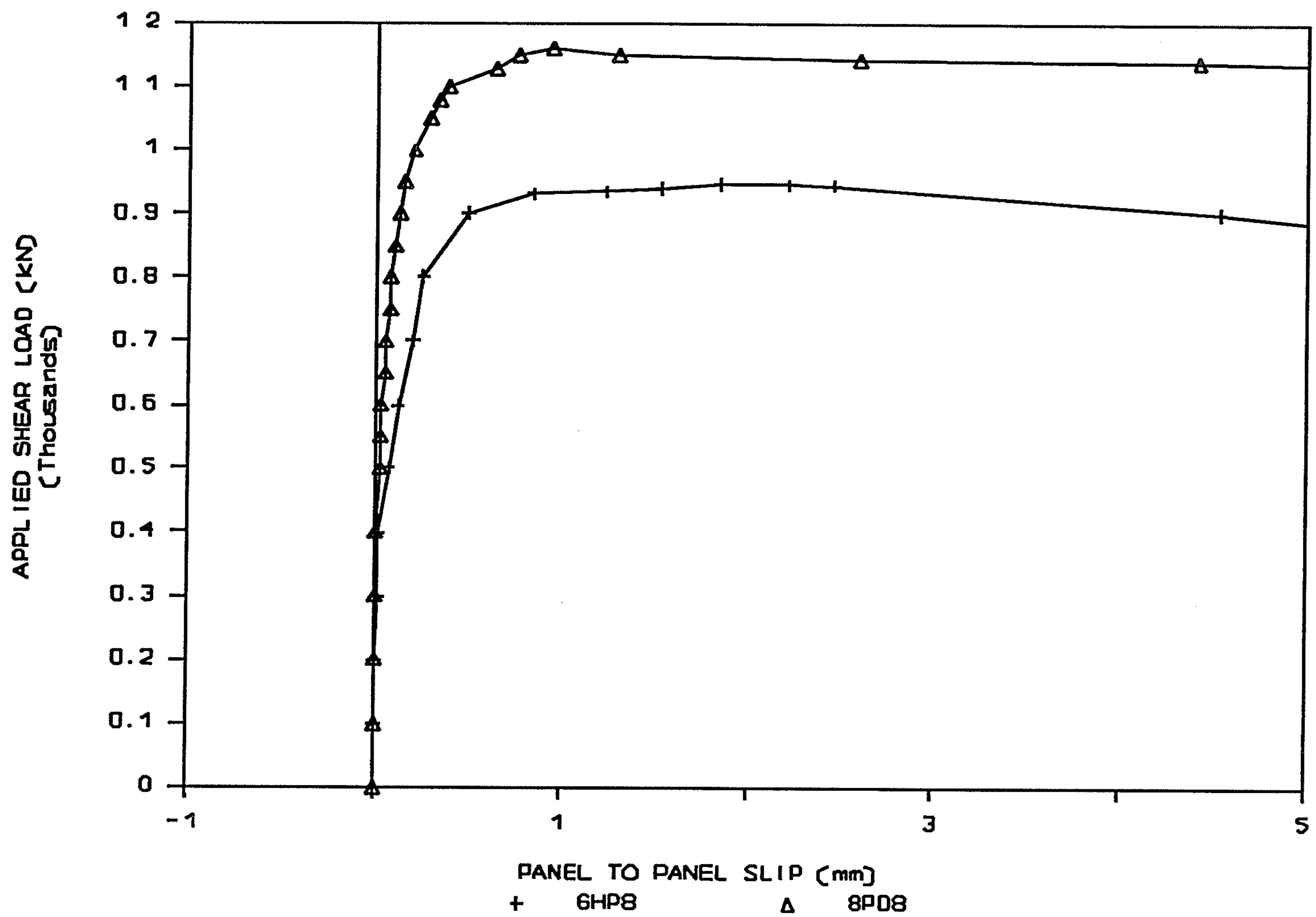

Figure 5.4 b) Magnified Load vs Slip Response for Specimens 6HP8 and 8PD8

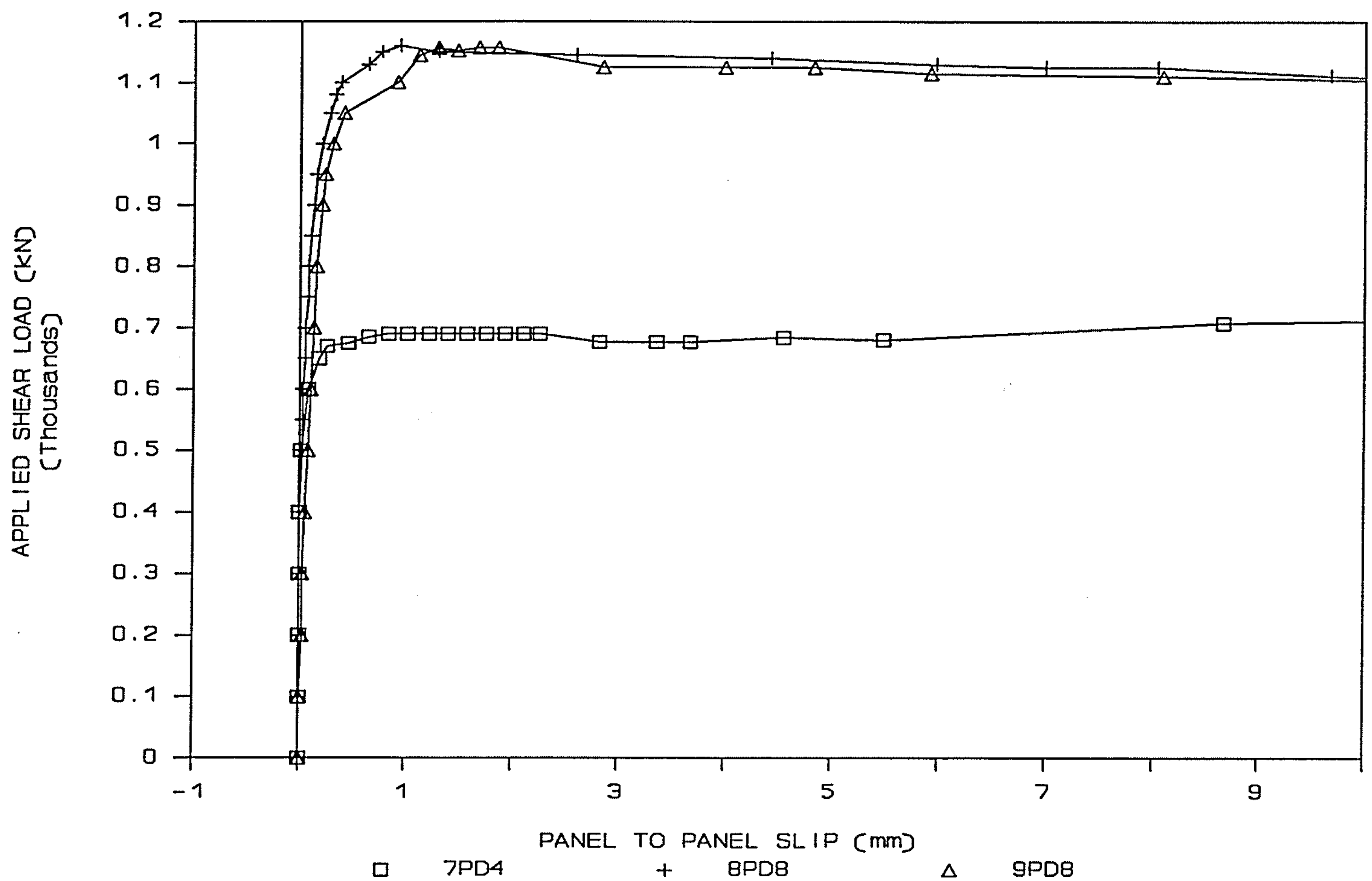

Figure 5.5 Load vs Slip Response for Post-tensioned Specimens with Drypack Only

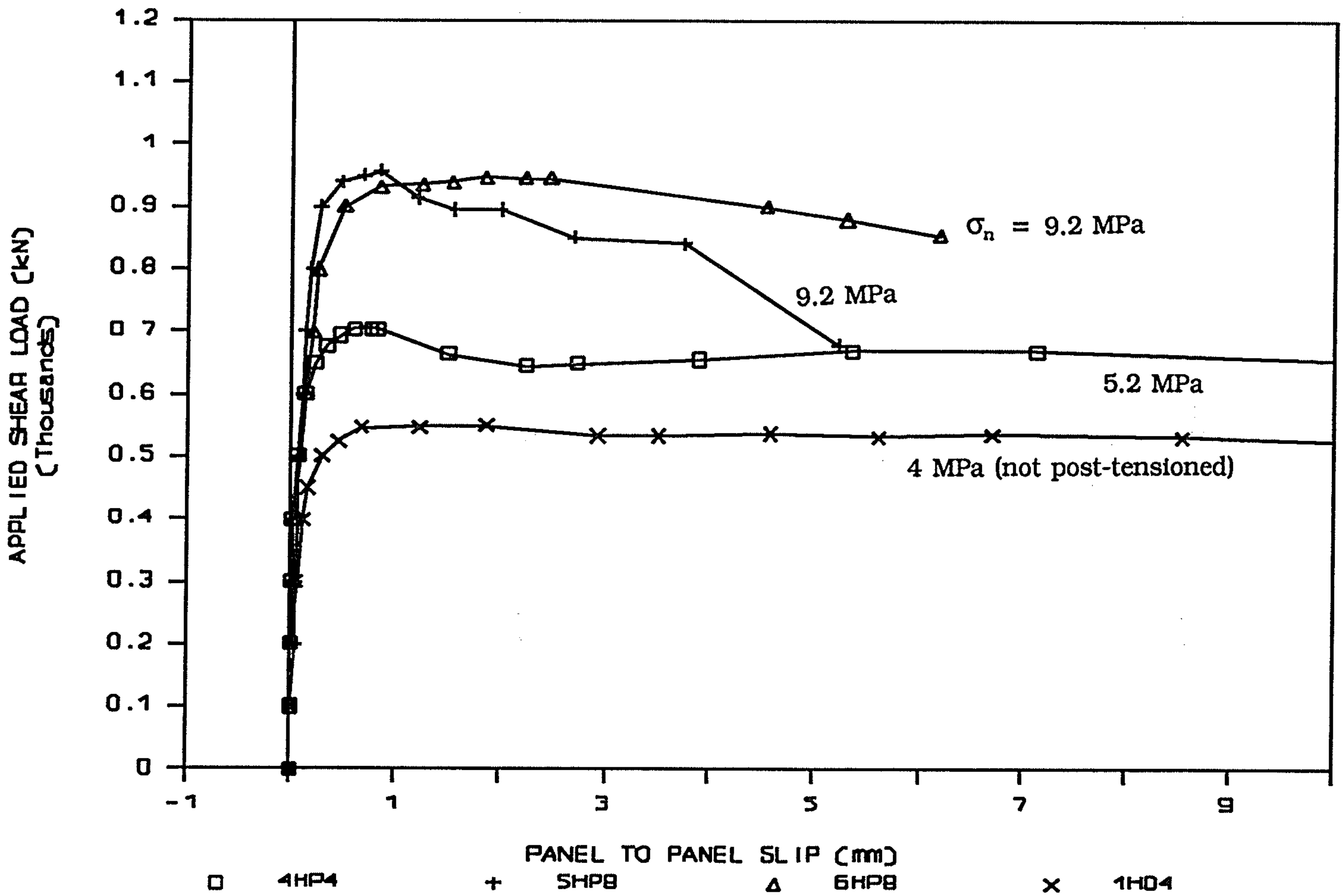

Figure 5.6 Load vs Slip Response for Post-tensioned Specimens with Hollow-core Slab

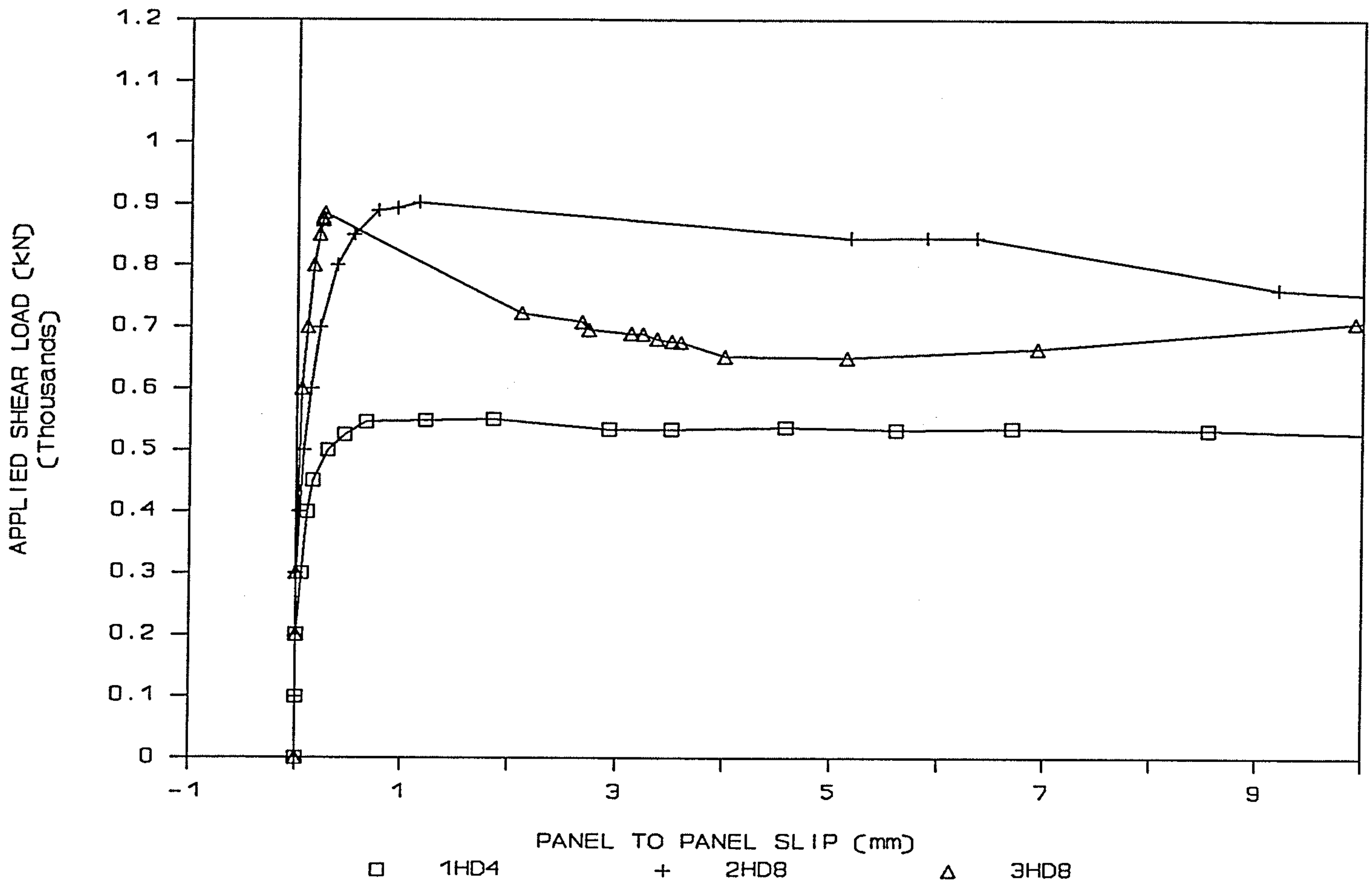

Figure 5.7 Load vs Slip Response for Specimens with Hollow-core Slab and without Post-tensioning

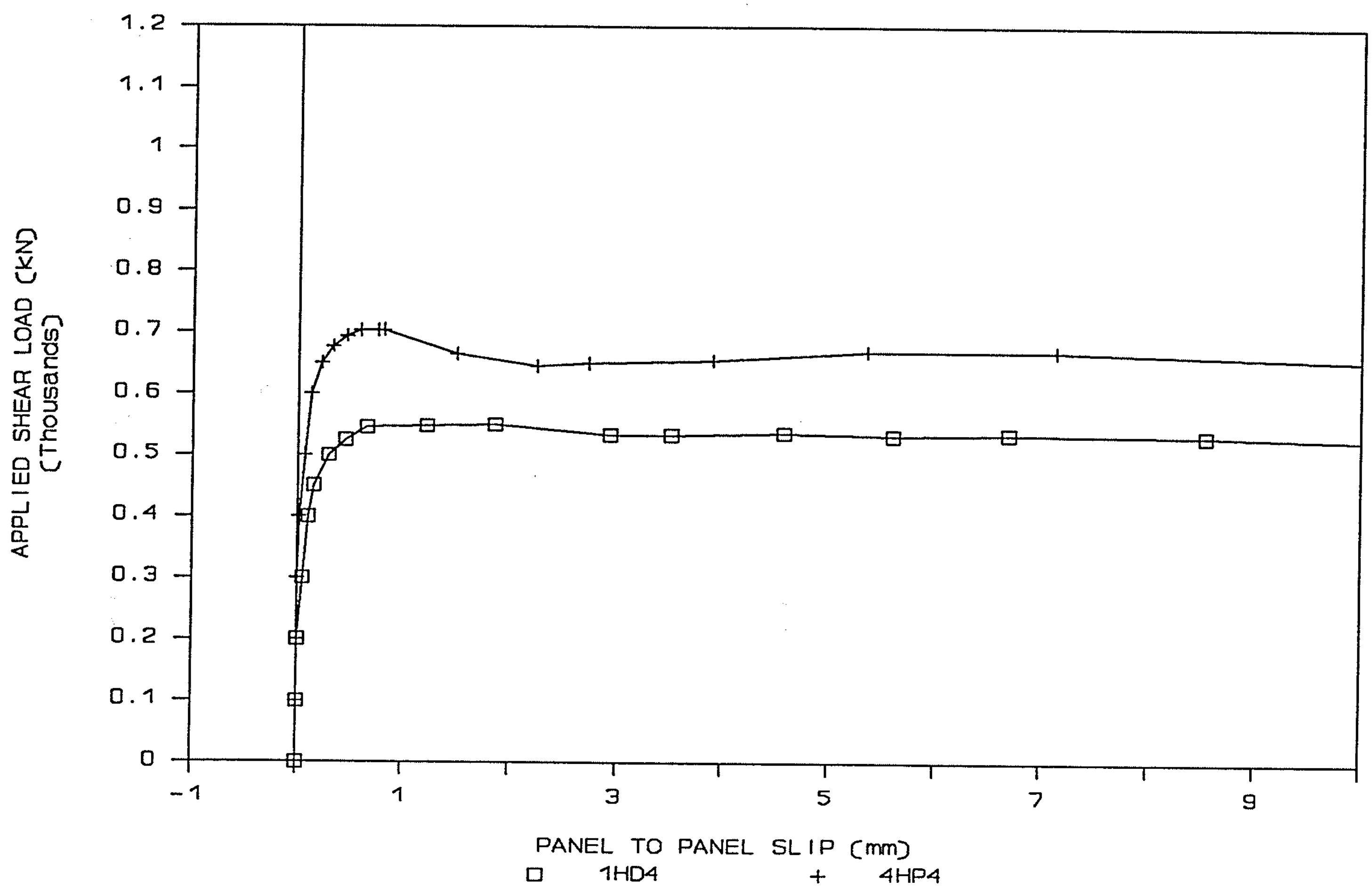

Figure 5.8 Load vs Slip Response for Specimens with Hollow-core at 4 MPa Normal Load

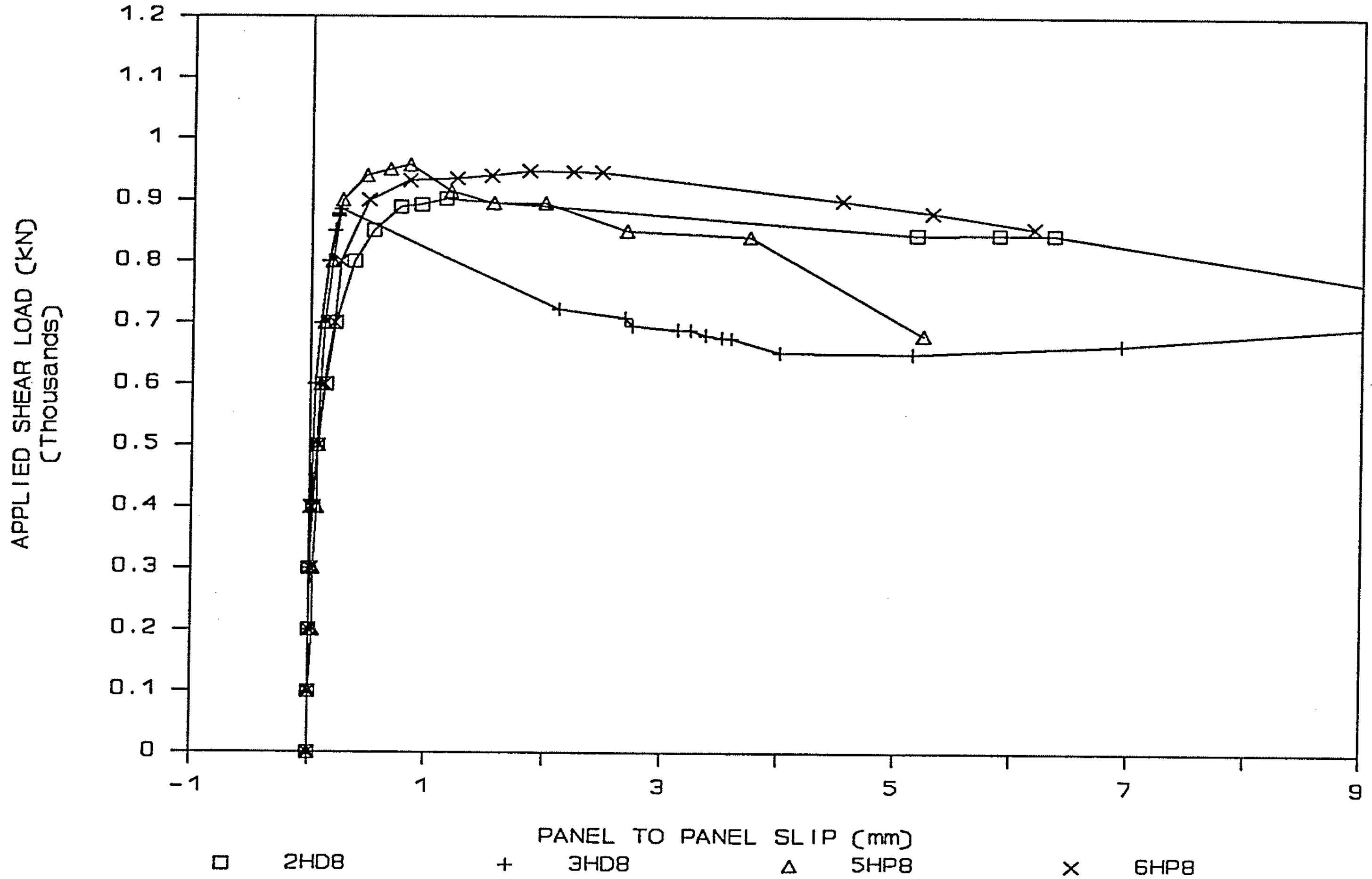

Figure 5.9 Load vs Slip Response for Specimens with Hollow-core at 8 MPa Normal Load

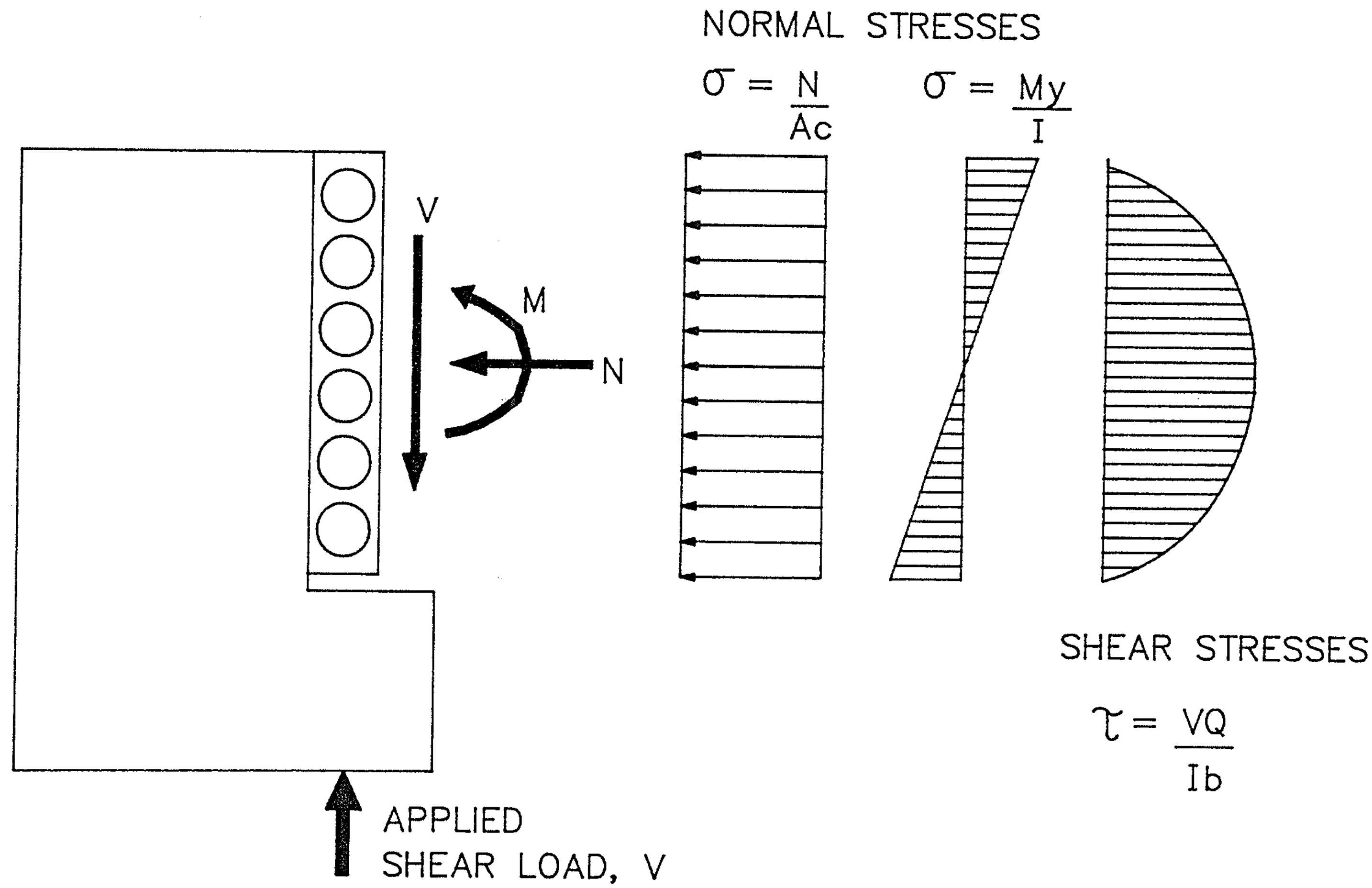

Figure 5.10 Freebody Diagram of Typical Specimen with Hollow-core Slab at Connection

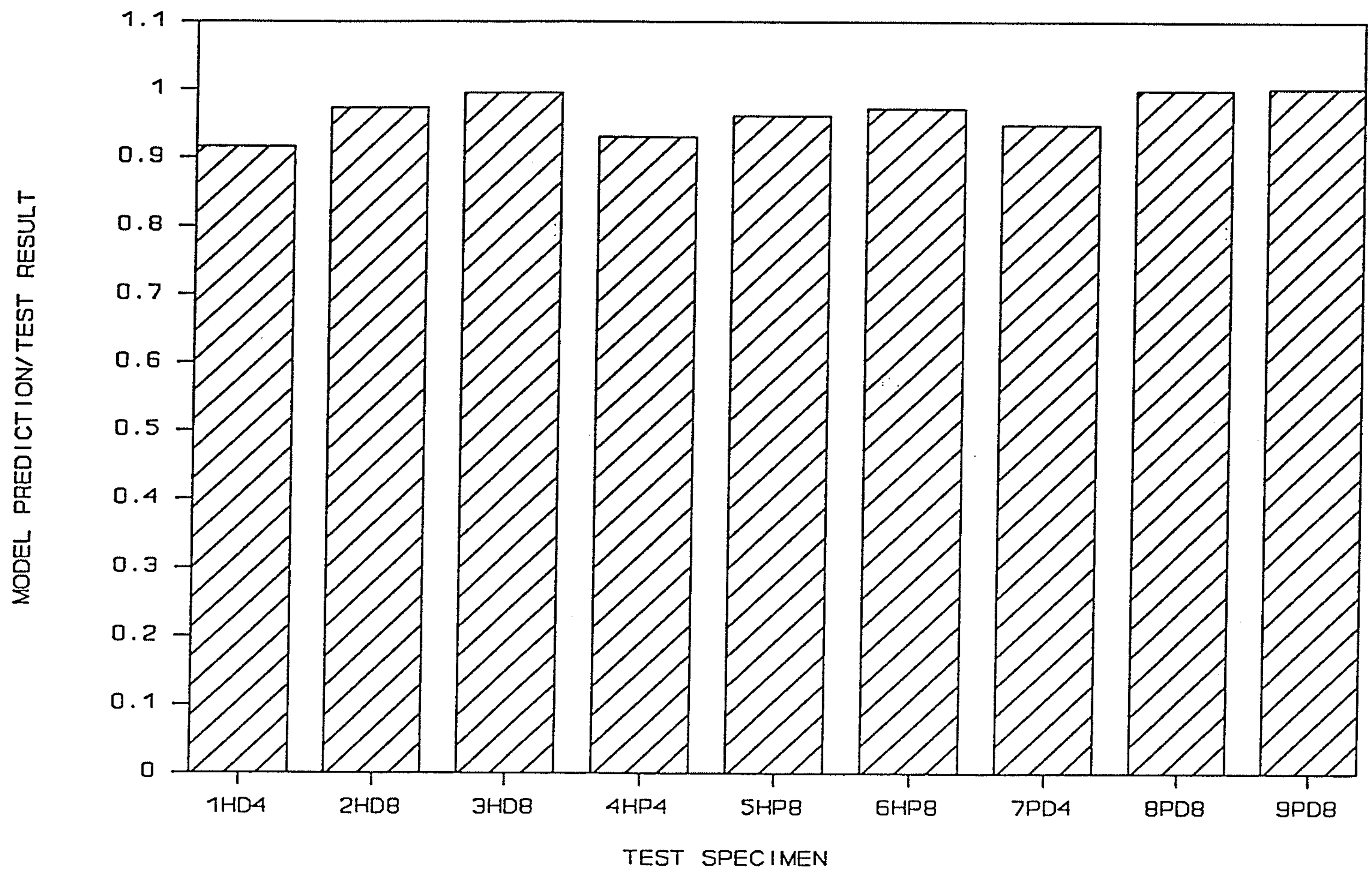

Figure 5.11 Maximum Shear Capacity: Model Predictions vs Experimental Results

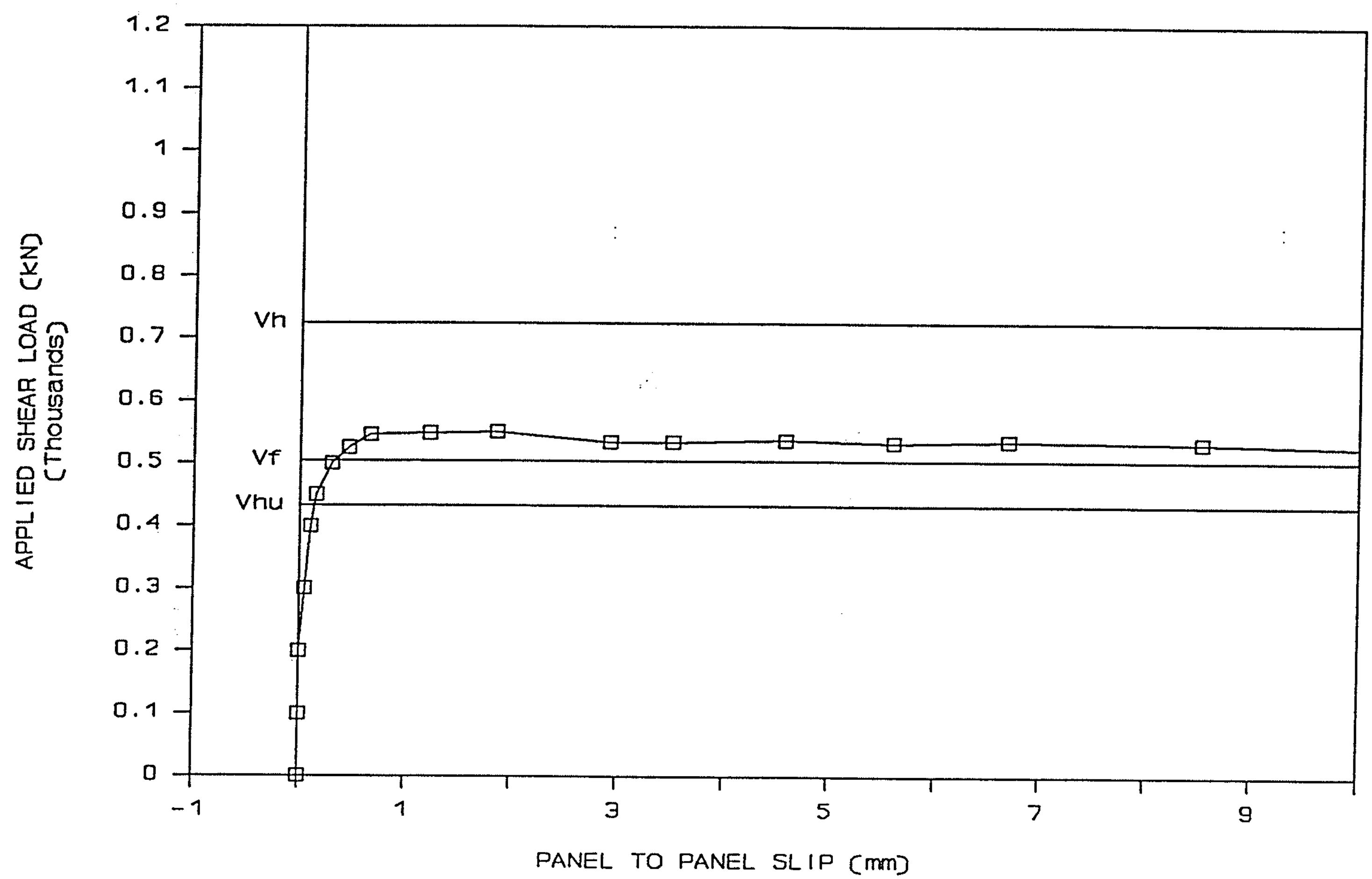

Figure 5.12 Specimen 1HD4 Model Predictions vs Test Results

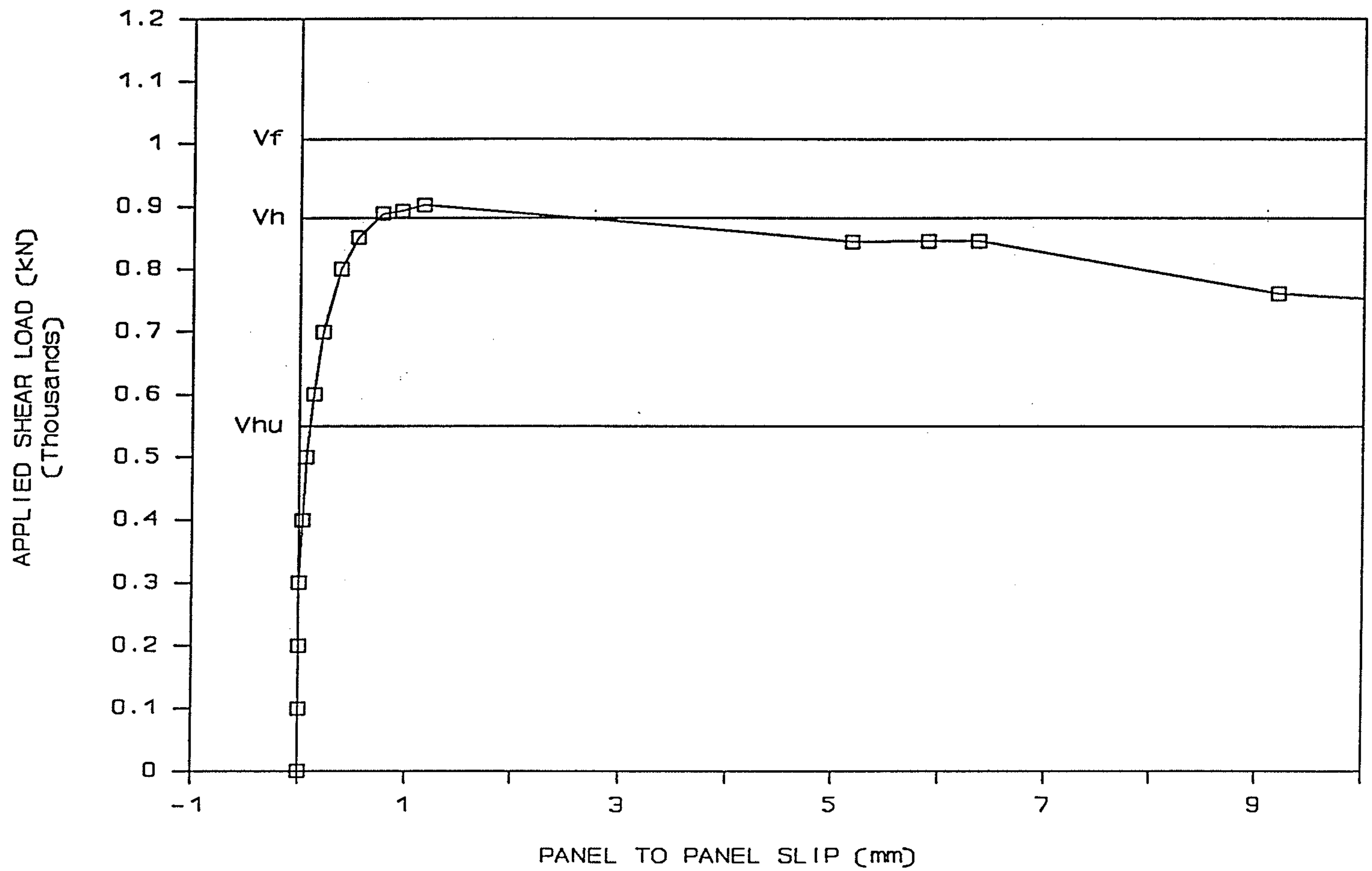

Figure 5.13 Specimen 2HD8 Model Predictions vs Test Results

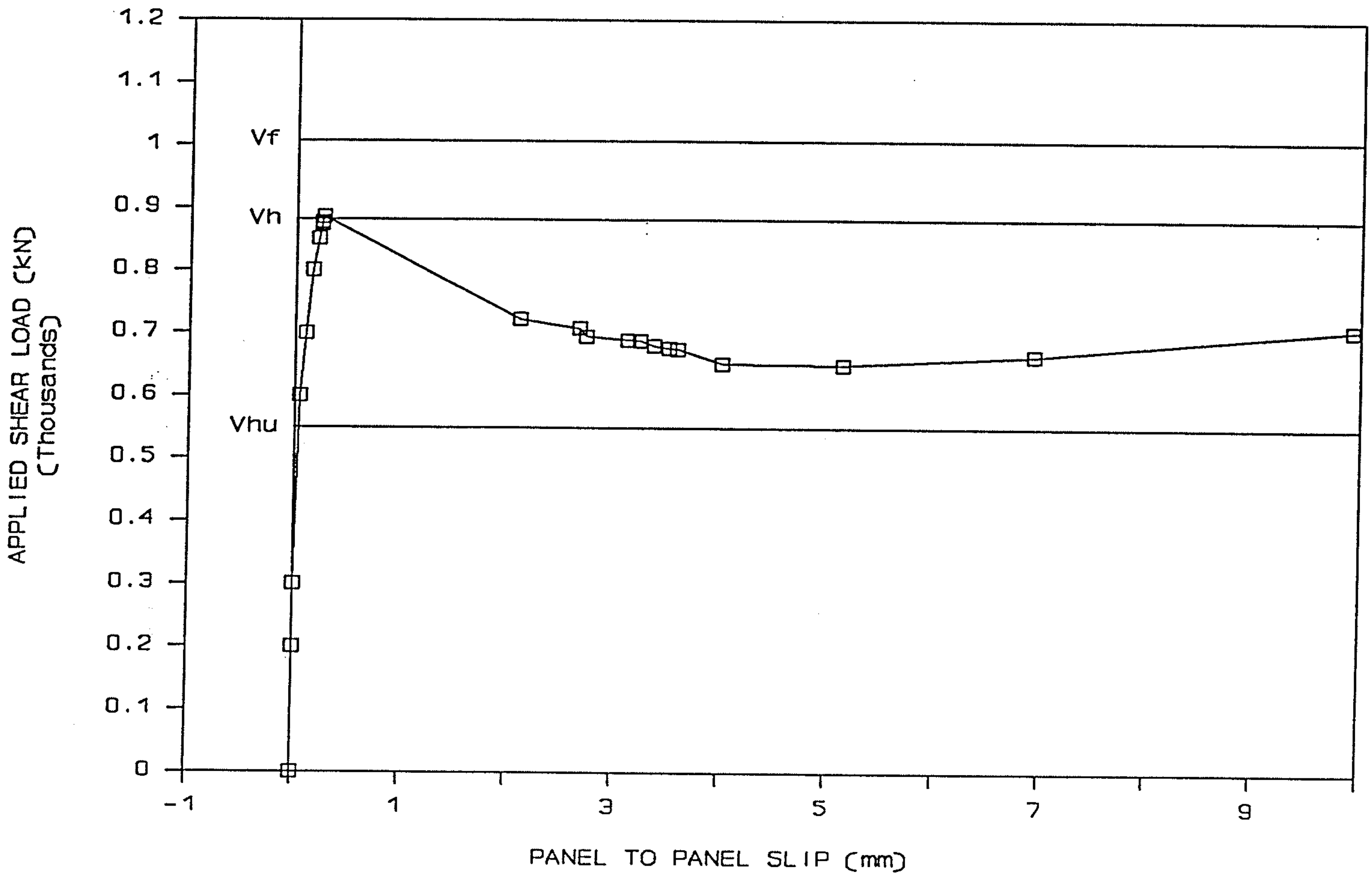

Figure 5.14 Specimen 3HD8 Model Predictions vs Test Results

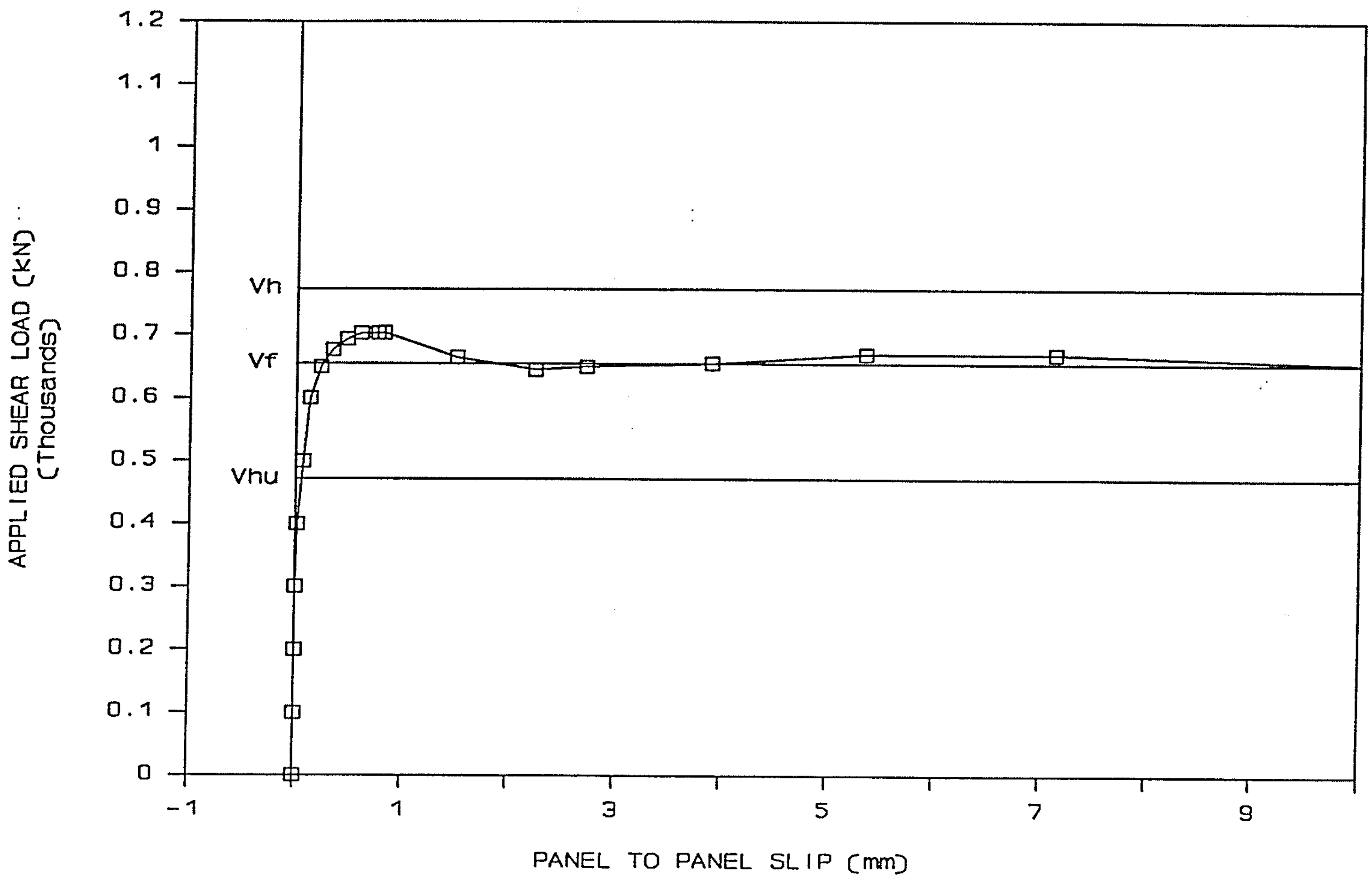

Figure 5.15 Specimen 4HP4 Model Predictions vs Test Results

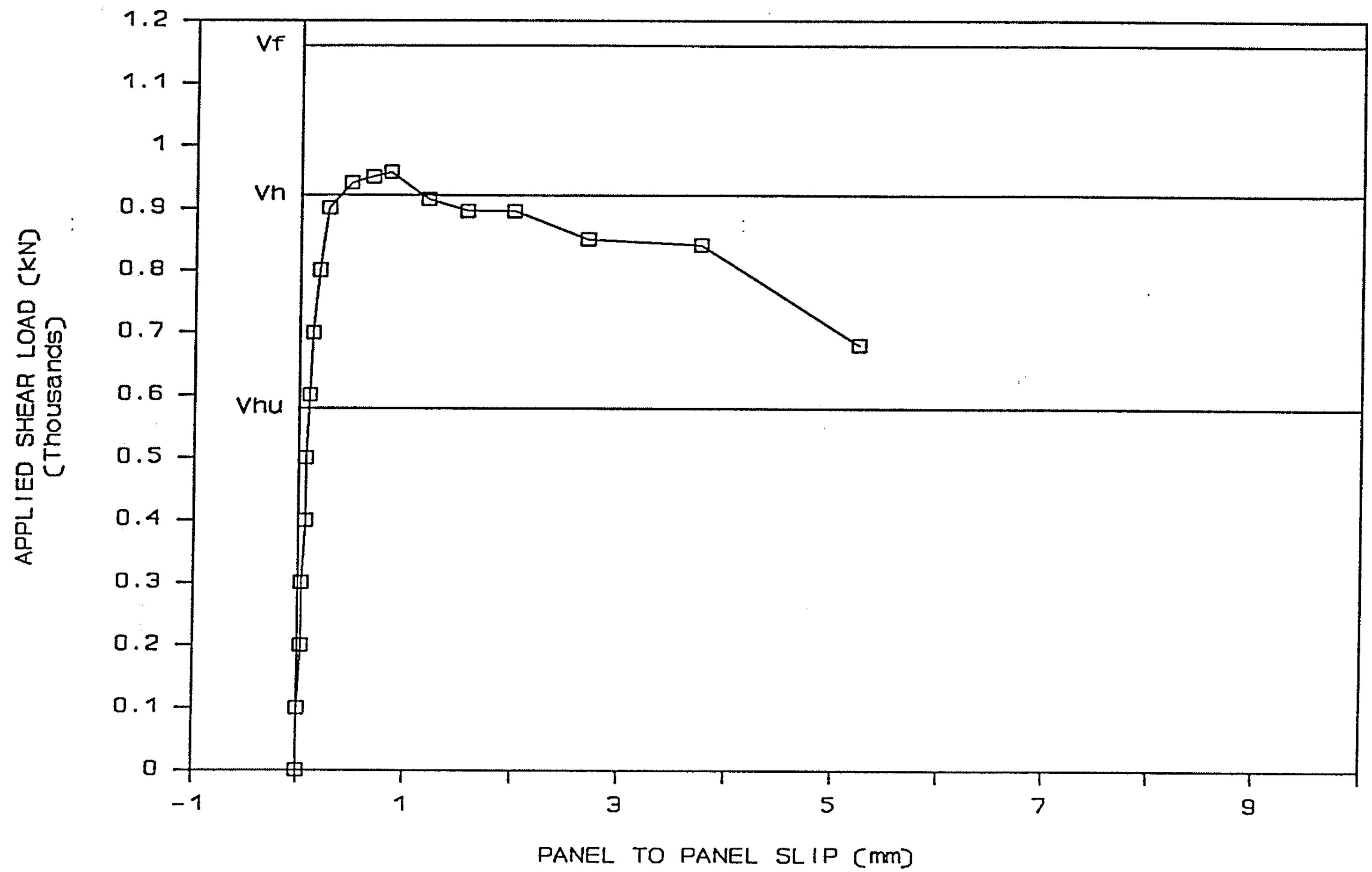

Figure 5.16 Specimen 5HP8 Model Predictions vs Test Results

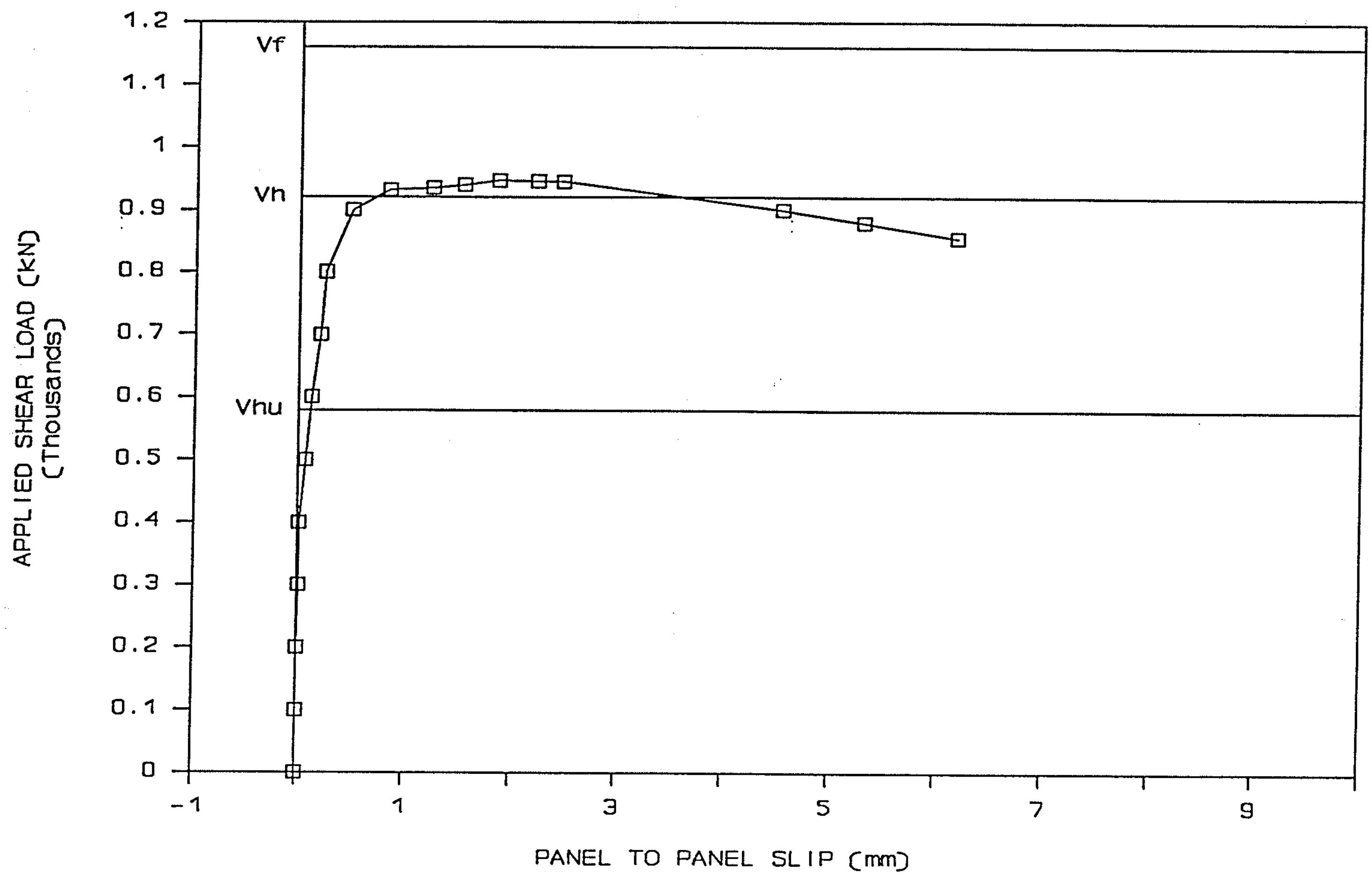

Figure 5.17 Specimen 6HP8 Model Predictions vs Test Results

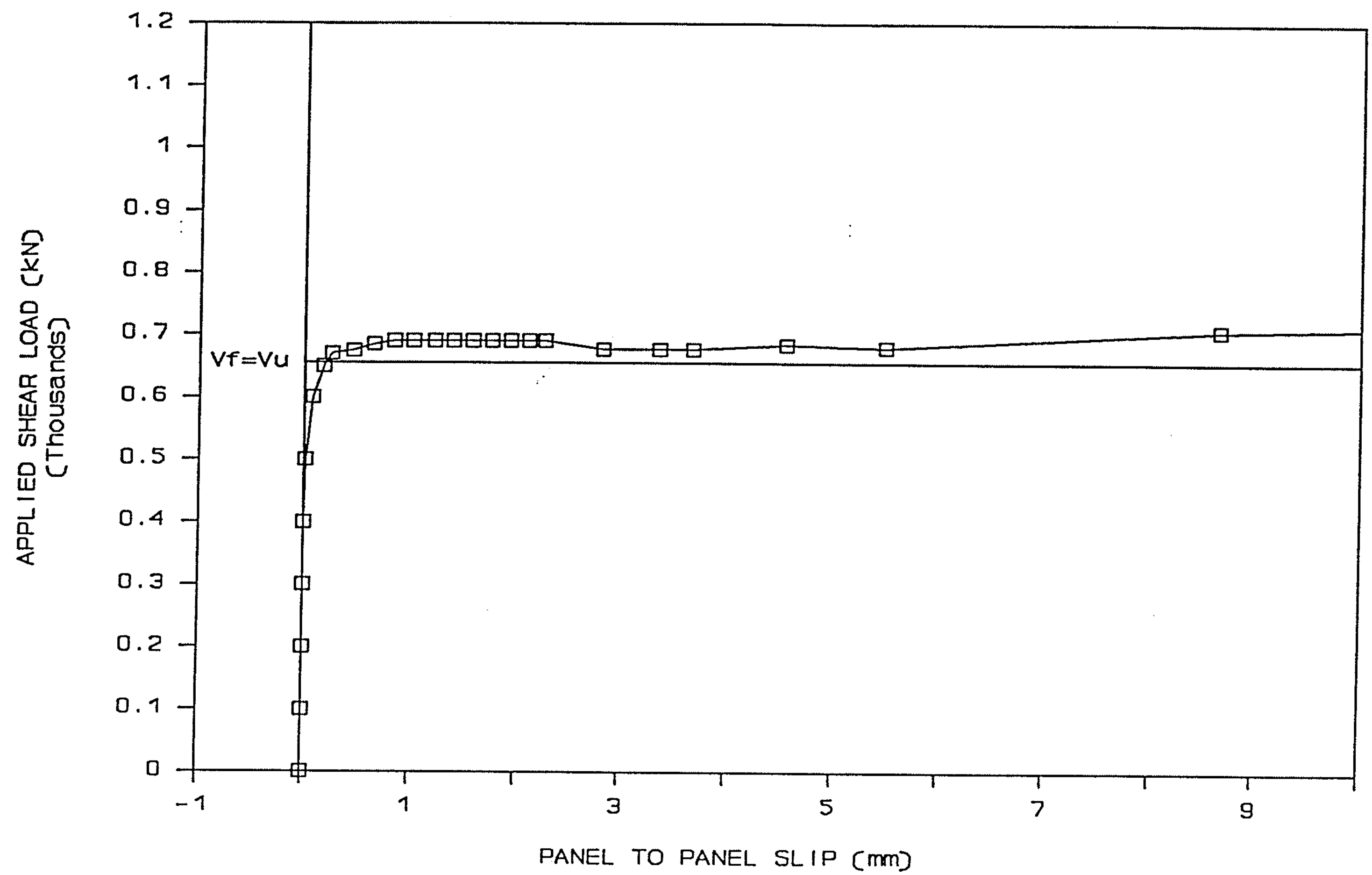

Figure 5.18 Specimen 7PD4 Model Predictions vs Test Results

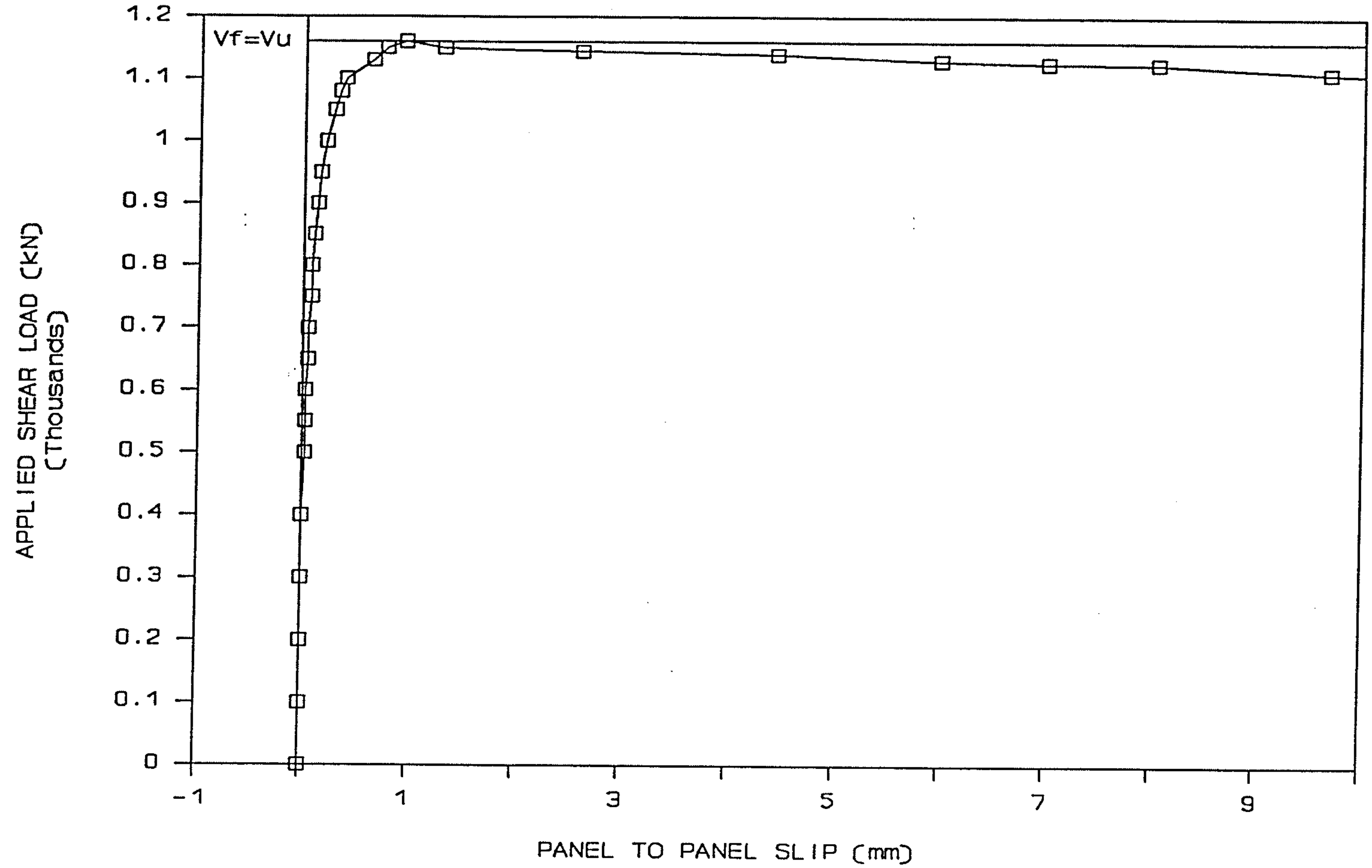

Figure 5.19 Specimen 8PD8 Model Predictions vs Test Results

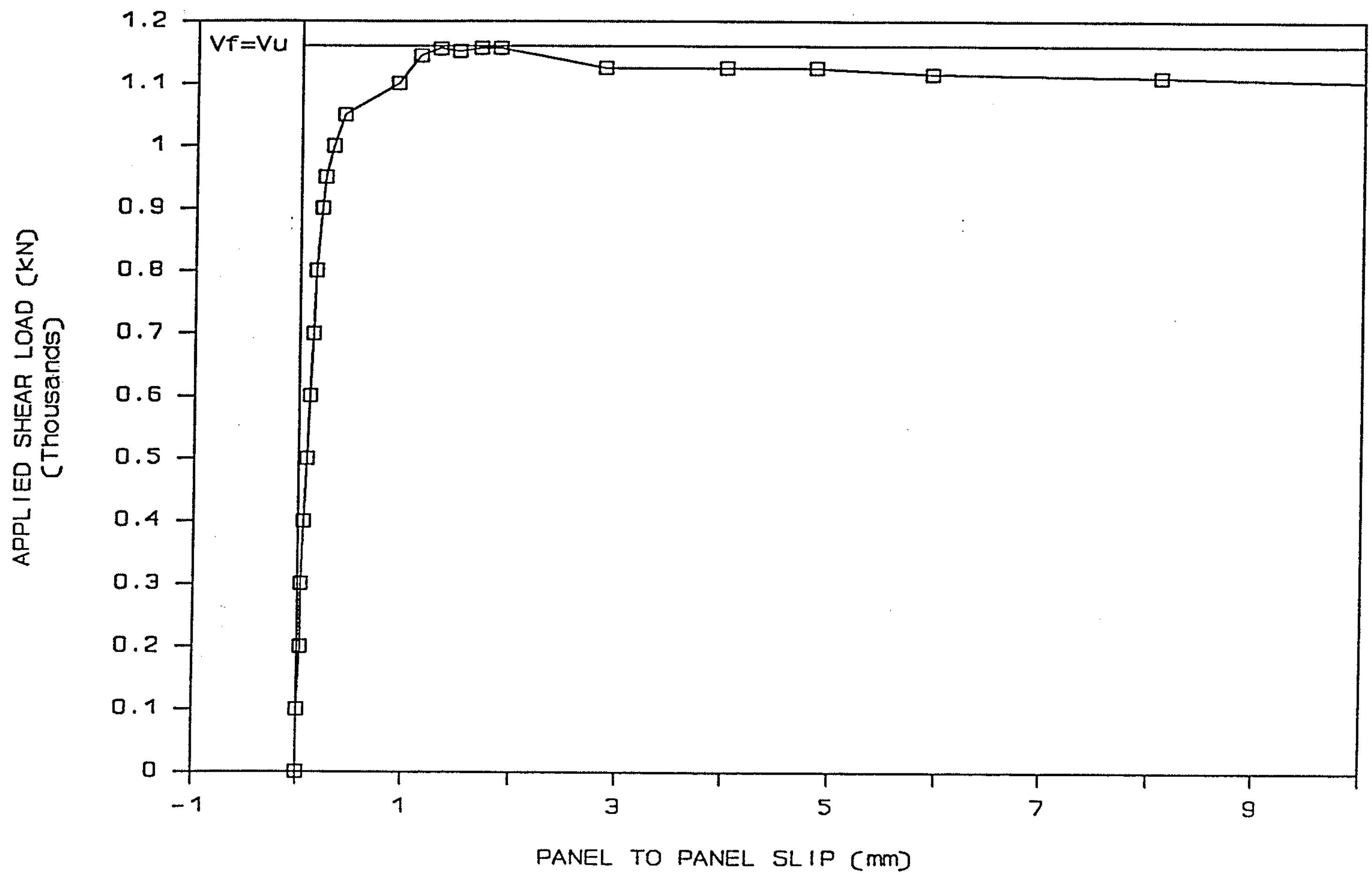

Figure 5.20 Specimen 9PD8 Model Predictions vs Test Results

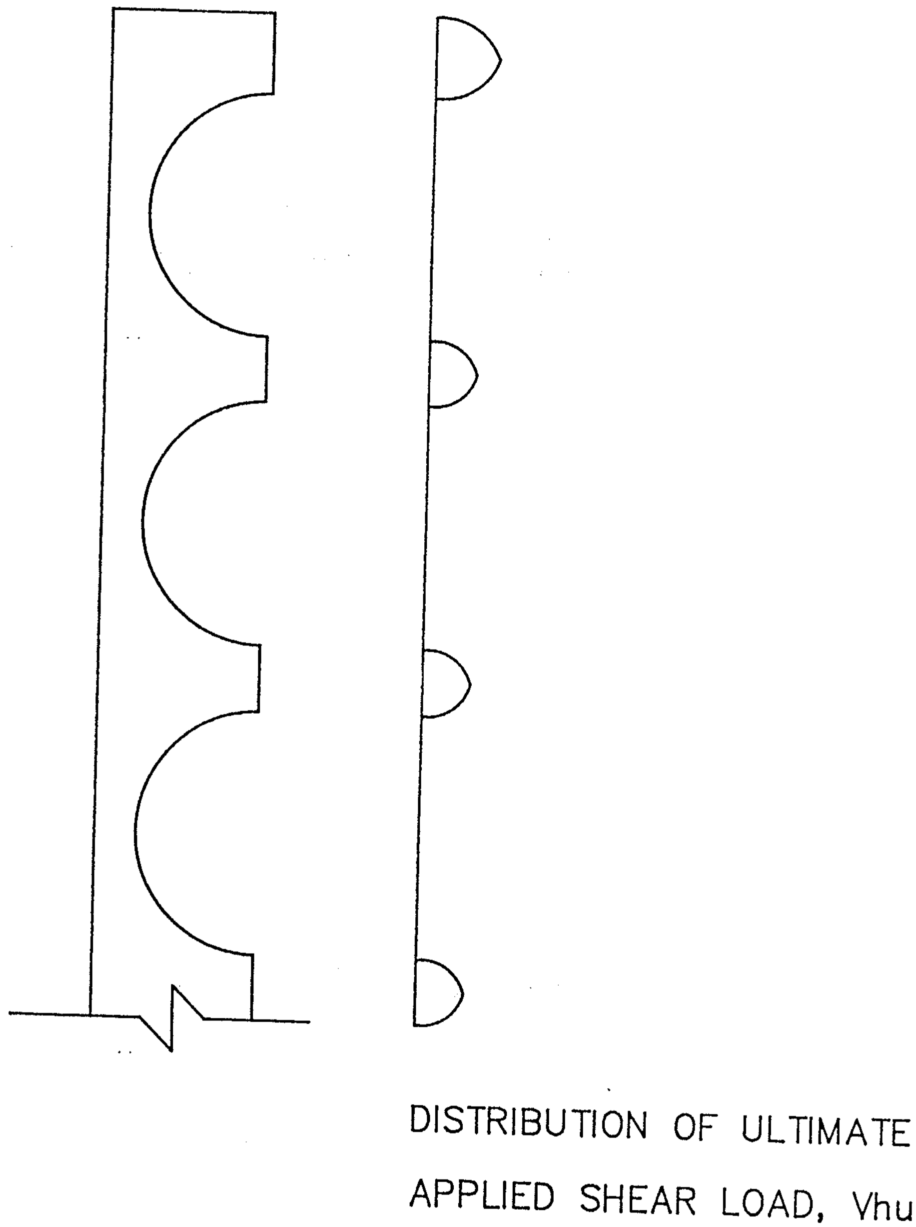

Figure 5.21 Distribution of Shear Stress on Unbonded Hollow-core Slab at Ultimate